The role of Na^+/Ca^{2+} exchanger in development of cardiac alternans

PhD Thesis

Jozefina Szlovák, MSc

Supervisor:

Dr. Norbert Nagy, PhD

Department of Pharmacology and Pharmacotherapy

Faculty of Medicine

University of Szeged

Szeged

Hungary

2021

TABLE OF CONTENTS

ABSTRACT

INTRODUCTION: Cardiac alternans refer beat-to-beat oscillation of the action potential duration (APD) and calcium transient and typically appear at rapid heart frequency. Cardiac alternans could provide repolarization heterogeneity leading to life-threating arrhythmias. The cellular mechanism of the development of alternans is not completely clarified, as well as there is no specific pharmacological intervention to treat alternans-mediated arrhythmias. The Na^+/Ca^{2+} exchanger is suggested to have important role in the underlying mechanism of alternans, therefore it may provide a novel promising pharmacological tool to attenuate alternans.

METHODS: The action potential (AP) sequences were measured by conventional microelectrode technique. The ion current were performed by whole-cell configuration of patch-clamp technique, and Ca^{2+} movements were monitored by fluorescent optical method with fluorescent dye.

KEY RESULTS: 1) Selective NCX inhibition significantly attenuated APD alternans and calcium transient amplitude alternans. 2) Application of 1μM ORM-10962 extended the postrepolarization refractoriness. 3) In isolated sinus node cells the Ca^{2+}-transient amplitude and diastolic Ca^{2+} increased after ORM-10962 treatment. 4) $I_{K\text{-}ATP}$ current was effectively activated by pinacidil and the subsequently applied carbachol significantly reduced the current.

CONCLUSION: These results indicate that NCX may have important role in the alternans mechanism, therefore, selective NCX inhibition could be a feasible antiarrhythmic strategy against alternans-based arrhythmias. However, our results support the Ca^{2+}-driven mechanism of alternans, it is feasible that different conditions, such as ischemia-reperfusion involves other currents ($I_{K\text{-}ATP}$) as underlying mechanism.

PUBLICATIONS RELATED TO THE THESIS

I. Szlovák J, Tomek J, Zhou X, Tóth N, Veress R, Horváth B, Szentandrássy N, Levijoki J, Papp JG, Herring N, Varró A, Eisner DA, Rodriguez B, Nagy N.
Blockade of sodium-calcium exchanger via ORM-10962 attenuates cardiac alternans.
J Mol Cell Cardiol. 2020 Dec 28; 153:111-122.

II. Kohajda Z, Tóth N, **Szlovák J**, Loewe A, Bitay G, Gazdag P, Prorok J, Jost N, Levijoki J,Pollesello P, Papp JG, Varró A, Nagy N.
Novel Na^{+}/Ca^{2+} Exchanger Inhibitor ORM-10962 Supports Coupled Function of Funny-Current and Na^{+}/Ca^{2+} Exchanger in Pacemaking of Rabbit Sinus Node Tissue
Front Pharmacol. 2020 Jan 29; 10:1632.

III. Magyar T, Árpádffy-Lovas T, Pászti B, Tóth N, **Szlovák J**, Gazdag P, Kohajda Z, Gyökeres A, Györe B, Gurabi Z, Jost N, Virág L, Papp JG, Nagy N, Koncz I.
Muscarinic agonists inhibit the ATP-dependent potassium current and suppress the ventricle-Purkinje action potential dispersion
Can J Physiol Pharmacol. 2020 Nov 26; 1-7.

FURTHER PUBLICATIONS

I. Pászti B, Prorok J, Magyar T, Árpádffy-Lovas T, Györe B, Topál L, Gazdag P, **Szlovák J**, Naveed M, Jost N, Nagy N, Varró A, Virág L, Koncz I.
Cardiac electrophysiological effects of ibuprofen in dog and rabbit ventricular preparations: possible implication to enhanced proarrhythmic risk
Can J Physiol Pharmacol 2021 Jan;99(1):102-109

II. Orvos P, Kohajda Z, **Szlovák J**, Gazdag P, Árpádffy-Lovas T, Tóth D, Geramipour A, Tálosi L, Jost N, Varró A, Virág L.
Evaluation of Possible Proarrhythmic Potency: Comparison of the Effect of Dofetilide, Cisapride, Sotalol, Terfenadine, and Verapamil on hERG and Native IKr Currents and on Cardiac Action Potential
Toxicol Sci.2019 Apr 1; 168 (2):365-380.

III. Gazdag P, Oravecz K, Acsai K, Demeter-Haludka V, Ördög B, **Szlovák J**, Kohajda Z, Polyák A, Barta BA, Oláh A, Radovits T, Merkely B, Papp JG, Baczkó I, Varró A, Nagy N, Prorok J.
Increased Ca^{2+} content of the sarcoplasmic reticulum provides arrhythmogenic trigger source in swimming-induced rat athlete's heart model.
Sci. Rep.2020 Nov11; 10 (1):19596.

ACRONONYMS AND ABREVIATIONS

AP: action potential

APD: action potential duration

ATP: adenosine-triphosphate

BCL: basic cycle length

CaM: calmodulin

cAMP: cyclic adenosine-monophosphate

CDI: Ca^{2+} dependent inactivation

CICR: Ca^{2+} induced Ca^{2+} release

CL: cycle length

CaT: Ca^{2+} transient

CS: Cell shortening

DAD: delayed afterdepolarizations

DD: diastolic depolarization

EAD: early afterdepolarizations

ECC: excitation-contraction coupling

$[Ca^{2+}]$ i : intracellular Ca^{2+}

I_{CaL}: L-type Ca^{2+} current

I_{CaT}: T-type Ca^{2+} current

$I_{K\text{-}ATP}$: ATP-dependent K^+ current

INa: Na^+ current

I_{NaL}: Late Na^+ current

I_{NaK}: Na^+ /K^+ pump current

LCR: Local Ca^{2+} releases

NCX: Na^+ /Ca^{2+} exchanger

NKA : Na^+ /K^+ ATPase

ORM-10103 : NCX inhibitor

ORM-10962: NCX inhibitor

PMCA: sarcolemmal Ca^{2+} ATPase

RyR: ryanodine receptor

SAN: sinoatrial-node

SERCA2a: myocardial sarcoplasmic reticulum Ca^{2+} ATPase

SL: Sarcolemma

SR: sarcoplasmic reticulum

TnC: Troponin C

TWA: T-wave alternans

VF: Ventricular fibrillation

Vm: Membrane voltage

1. Introduction

The cardiac AP is a characteristic, time-dependent voltage response of the membrane to an appropriate stimulus and formed by coordinated cooperation of various transmembrane ion channels. [1]. Several time-dependent Na^+, Ca^{2+}, and K^+ currents contribute to shaping the action potential and its contour is further modified by the effects of intracellular Ca-handling. This complex crosstalk provides that the AP is able to adapt in a wide range of physiological requirements (e.g.: APD shortening in tachycardia), at the same time, the intracellular Ca-mismanagement often causes abnormal action potential waveform that could lead to life-threating arrhythmias [2-4]. A typical cellular arrhythmia mechanism that involves both the Ca-handling and the transmembrane ionic currents of the AP is the so-called cardiac alternans.

1.1 Action potential and determining ionic currents

1.1.1 Fast inward sodium current (I_{NA})

In cardiomyocytes, the fast inward sodium current (I_{Na}) activated during the zero phase (phase 0) of the AP (**Figure 1**) [5]. When the membrane potential is -60 mV or more positive, the channels open temporarily for a short time (1-2ms), and sodium ions (Na^+) flow into the cell and depolarizing it [5]. The influx of Na^+ is provided by Nav1.5 channels [6]. The large number of channels on the surface membrane provides large current density ensuring fast AP depolarization and impulse conduction [7]. It is important to note that a small fraction of the channels remain opened during the plateau phase of the action potential (i.e. late Na^+ current) and substantially contribute to maintain the plateau phase [6]. The fast inward sodium current was an important pharmacological target earlier in the treatment of arrhythmias, by reducing the impulse propagation [7, 8].

1.1.2 Transient outward potassium current (I_{to})

The fast inward sodium channel inactivation and the transient outward potassium current activation jointly result the early repolarization (phase 1) (**Figure 1**) of the AP [9, 10]. The channel expression varies between tissues and species. The channels are characterized by rapid activation near to -30 mV and rapid inactivation [11]. Potassium ions (K^+) migrate into the extracellular space for a short time and it leads to a rapid repolarization [9]. I_{to} may have an important role in the development of arrhythmias such as Brugada-syndrome [12]. The inhibitors of the channels are mostly not specific like 4-aminopyridine, chromanol 293B, quinidine and phrixotoxin [11, 12].

1.1.3 Inward calcium current (I_{Ca})

Inward Ca^{2+} current has two main types (T and L type) in myocardium. The L-type ($I_{Ca,L}$) channel (Cav1.2) has more significance [13, 14] in the ventricular AP, while the T-type primarily operates in nodal tissue such as sinus-node and atrioventricular node where initializes the phase 0 depolarization [15] . The L-type Ca^{2+} channel function is characterized by rapid activation at -40 mV and a relatively slow inactivation which provides the plateau phase (**Figure 1**) of AP (phase 2) [16]. I_{CaL} has crucial importance in the Ca^{2+} cycle, since the Ca^{2+} influx through the channel triggers the ryanodine receptors providing Ca^{2+} release from the sarcoplasmic reticulum (SR) [17]. The operation of the channel is regulated by cAMP, extracellular Ca^{2+} and other factors [18]. In several arrhythmias Ca^{2+} channel blockers (nifedipine) and non-selective inhibitors (verapamil, diltiazem) are applied during clinical treatments [19, 20].

1.1.4 The rapid delayed rectifying potassium current (I_{Kr})

These channels (in human HERG) open during depolarization when the voltage reaches the -20 mV or more positive, and it deactivates relatively slowly [21, 22] which is important in maintaining the plateau phase (phase 3) of the AP (**Figure 1**) [23, 24]. It can be blocked by dofetilide leading to prolongation of the APD [25]. The I_{Kr} is considered as the most important repolarizing current and the primarily player of the repolarization reserve [22]. Selective inhibition of I_{Kr} represents one of the most important antiarrhythmic intervention to lengthen the ECG QT interval.

1.1.5 The slow delayed rectifying potassium current (I_{Ks})

The I_{Ks} current is provided by the Kv7.1 channel [26] but the β subunit shows interspecies variation [27]. I_{Ks} is activated slowly at a voltage near to -30 mV or more positive values and the current deactivates quickly [28, 29]. However, I_{Ks} contributes to the repolarization process under normal condition, its crucial importance is showed up in the repolarization reserve (**Figure 1**). This means that inhibition of this current attenuates the reserve capacity of the repolarization but does not result in excessive prolongation of the APD since other currents (such as I_{Kr} and I_{K1}) are able to compensate for the I_{Ks} reduction [30]. At the same time, when the I_{Ks} is inhibited, block of a further current may cause an excessive prolongation in the action potential and the ECG QT interval that can lead to life-threating arrhythmias such as Torsades-de-pointes arrhythmia [31].

1.1.6 Inward rectifier potassium current (I_{K1})

When the membrane potential is more negative than -40 mV the voltage-dependent I_{K1} (Kir2.1) channels open and play a crucial role in the terminal phase of repolarization (**Figure 1**) [32, 33]. The current exerts strong inward rectification caused by intracellular Mg^{2+} and polyamines [34]. It is important to note that I_{K1} remains active during the entire resting membrane potential therefore, it contributes to maintain the stable resting potential. It has crucial role in the counterbalance of the possible spontaneous delayed afterdepolarizations initiated by Ca^{2+}_i overload [1].

1.1.7 Sodium-calcium exchanger (NCX)

The NCX antiporter delivers Na^+ and Ca^{2+} ions between the intra- and extracellular space depending on the actual intracellular levels of these ions and the membrane voltage [35, 36]. Two main modes of operation are known: the forward mode transports 1 Ca^{2+} out and 3 Na^+ in the cell, in contrast, the reverse mode moves Ca^{2+} into the cell and 3 Na^+ out [37]. These ion movements can be measured as inward and outward currents (I_{NCX}) (**Figure 1**). The inward current may contribute to the formation of EADs and DADs, so selective inhibition of the current can reduce the development of this arrhythmias [38]. Recently, a novel selective inhibitor, ORM-10962 has been shown to effectively inhibit both modes of the NCX without influencing other currents [39].

1.1.8 Na^+/K^+-ATP-ase

Na^+/K^+-pump is involved in the restoration of normal intracellular Na^+ and K^+ levels after the AP [40]. As it works against the electrochemical gradient, its operation requires energy [41]. It pumps 3 Na^+ ions out and 2 K^+ in generating net outward current (**Figure 1**) that slightly contributes to the repolarization ($I_{Na/Kpump}$). The cardiac glycosides are effective inhibitors (such as digoxin or digitoxin) of the pump that increase the Na_i level and thus enhances the Ca^{2+}_i content through the NCX providing improved ventricular performance in heart failure [42].

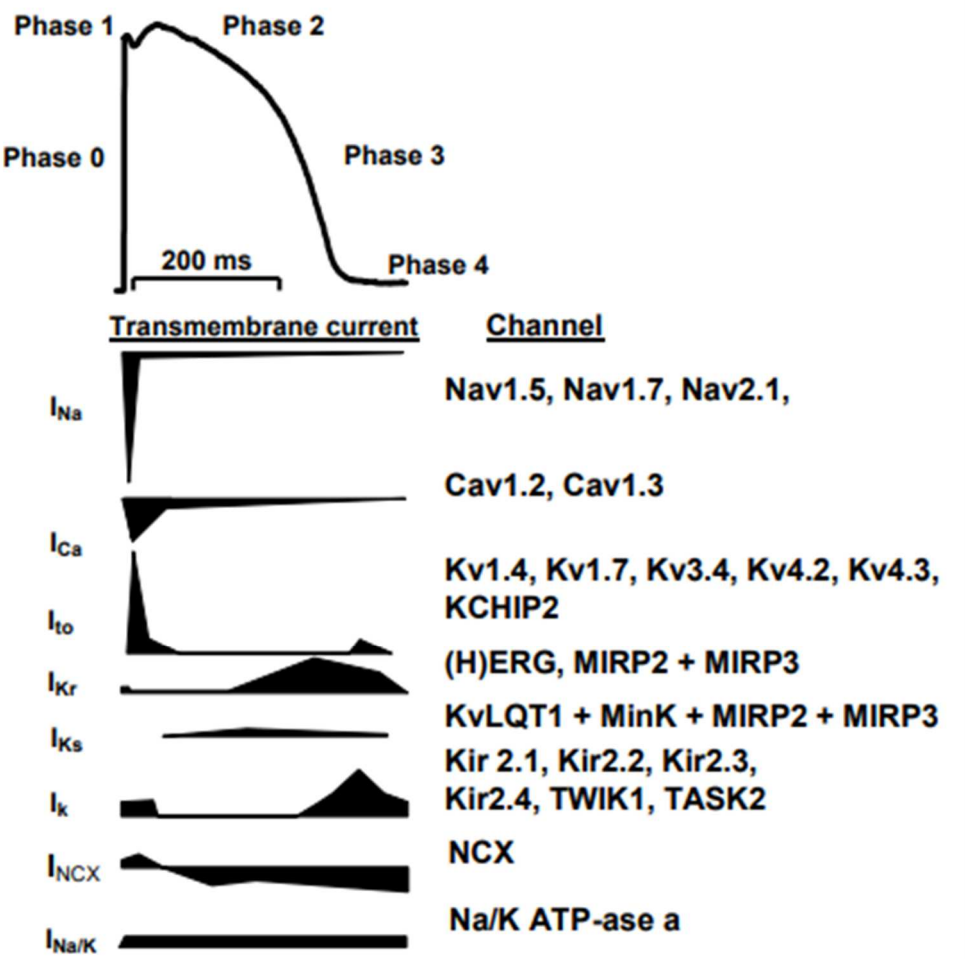

Figure.1. *The ventricular action potential and the major underlying ionic currents. Below the AP ion currents shown according to the corresponding phase. The channel proteins are shown on the right side of the panel (modified from Ravens et al.).* [43]

1.2 Cardiac intracellular Ca^{2+} homeostasis

Cardiac intracellular Ca^{2+} cycling provides stable and flexible Ca^{2+} balance for the cardiac muscle contraction. During the plateau phase of the AP the opening of the L-type Ca^{2+} channels provides Ca^{2+} influx that leads to release of Ca^{2+} from the SR. The Ca^{2+} release (Ca^{2+} transient (CaT)) provides available Ca^{2+} for the contraction machinery (**Figure 2**) [31]. Under physiological condition the Ca^{2+} balance requires that neither Ca^{2+} loss nor Ca^{2+} gain happen. In order to secure this, the Ca^{2+} influx must equal to the Ca^{2+} efflux and the Ca^{2+} release must be equal to the amount of Ca^{2+} sequestered back to the SR [44]. The intracellular Ca^{2+} handling is able to set its stable balance via the interactions of the Ca^{2+} fluxes, called autoregulation [17,

45]. The autoregulation works in each cardiac ventricular cell, and does not require autonomic control, or phosphorylation of the channels [46].

1.2.1 Ca^{2+} influx

The L-type Ca^{2+} current is activated when the AP reaches -40 mV. Ca^{2+} ions enter into the cell, and bound to the ryanodine receptors (RyR) triggering the Ca^{2+} release from the sarcoplasmic reticulum (SR). This process is called calcium induced calcium release (CICR) (**Figure 2**) [31]. The released calcium is proportional with the calcium influx, so the inflowing Ca^{2+} defines the calcium release and in line with this the Ca^{2+} content of the SR. Inactivation of the Ca^{2+} current occurs in two ways: the repolarization inactivates the channels in voltage dependent manner (voltage-dependent inactivation), and the other way is the calcium dependent inactivation (CDI) which is regulated by the released Ca^{2+} indirectly, through negative feedback mechanism via calmodulin (CaM) [17, 45].

1.2.2 Ca^{2+} release

Ryanodine receptors are located on the surface of the SR which. RyR has 3 isoforms, in myocardium RyR type 2 (RyR2) are expressed. The receptor has an N-terminal region, containing regulative domains to control opening and closing by phosphorylation spaces. The closed state of the receptor is stabilized by calstabin and it also controls the opening period [45]. During systole the RyR2 channels activated by the Ca-influx, thus the intracellular Ca^{2+} rapidly increases and activates adjacent are ryanodine channels, that results in a rapid rise of the $Ca^{2+}{}_i$ from the resting 100 nmol/l concentration to the 1 µmol/l maximum. (**Figure 2**). Under specific conditions, such as $Na^{+}{}_i$-overload, the reverse NCX-mediated Ca^{2+} inflow may also contributes to the Ca^{2+} influx [44].

1.2.3 Ca^{2+} reuptake and relaxation

In well-functioning myocardial cells, the proper relaxation requires fast dissociation of the Ca^{2+} from the TnC. During relaxation, sequestration of the intracellular Ca^{2+} occurs mainly through active Ca^{2+} uptake by the SR, through the sarcoplasmic reticulum Ca^{2+} ATPase (SERCA2a) [45] (**Figure 2**). SERCA function is regulated by phospholamban protein (PLN) which is activated by phosphorylation, leading to a decreased interaction between the PLN-SERCA2a and improved transport rate. Ca^{2+}, adenosine-triphosphate (ATP), Mg^{2+}, and optimal pH are required for normal SERCA2a function. About 70% of the released Ca^{2+} is taken back to the

SR. The remaining 30% is removed by the forward mode of the NCX however, the extent of the extruded Ca^{2+} is largely species-dependent, i.e. in rats it is only 7-8% [45]. The plasma membrane Ca^{2+} ATPase (PMCA), as an active transporter, removes Ca^{2+} from cytoplasmic space with a slow kinetics to provide fine balance of the diastolic Ca^{2+} [44, 47].

1.3 The control of intracellular Ca^{2+} fluxes

During the contraction-relaxation cycle of the heart the intracellular and transcellular Ca^{2+} changes are precisely regulated in order to avoid unintended intracellular Ca^{2+} gain or Ca^{2+} loss. The most important components of the regulation are the local feed-back mechanism of the trigger Ca^{2+} and the regulation of the SR Ca^{2+} content. Both mechanism is based on the dynamic balance of the sarcolemma (SL) and SR Ca^{2+} fluxes [45, 48].

1.3.1 Autoregulation of Ca^{2+} influx

In case of steady-state operation of the heart the Ca^{2+} influx and efflux are equal, the average Ca^{2+} content does not change. During systole, the amount of trigger Ca^{2+} depends on the activated Ca^{2+}channels and their duration of open state. The number of activated channels is determined by the transmembrane potential changes. In contrast, the duration of open state is sensitive to submembrane Ca^{2+} changes, so the Ca^{2+} influx is regulated by the local feed-back mechanism of the CaT. If the $Ca^{2+}{}_i$ decreases, the Ca^{2+} content of the SR will also be decreased due to decreased function of SERCA2a pump activity. Consequently, the amplitude of CaT as well as the submembrane Ca^{2+} level will be also smaller and in line with this the NCX function is reduced. The decreased submembrane Ca^{2+} level inhibits less the Ca-channels, therefore the CDI is reduced leading to longer opened state of the channel. The longer opening leads to an increase of the current integral providing intracellular Ca^{2+} accumulation that ultimately resets the normal amplitude of the Ca^{2+}-transients.

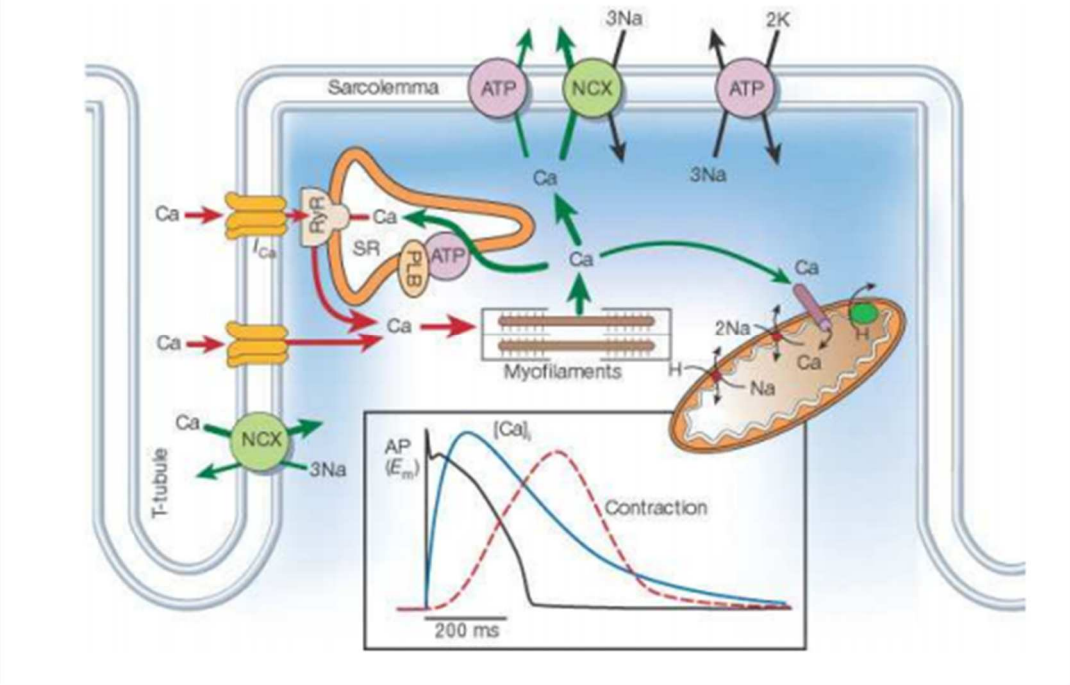

Figure2. *Cardiac intracellular Ca^{2+} cycling. The panel shows the main steps of the Ca^{2+} homeostasis main steps, including influx, release, reuptake and extrusion. The lower part of the panel introduces the electromechanical relationship between the action potential and the cardiac contraction [44].*

1.3.2 Role and regulation of sodium-calcium exchanger

The primary role of the Na^+/Ca^{2+} exchangers is to extrude intracellular Ca^{2+}. There are three isoforms (NCX1, NCX2, NCX3), however, the most important is the NCX1, expressed in the sarcolemma [37]. It has 10 transmembrane segments assembled in dimers. The regulatory function is provided by cytoplasmic loop between segment 5 and segment 6. It also contains two Ca^{2+} binding sites, CBD1 and CBD2. The increased extracellular Ca^{2+} binds to the CBD domains and activates the channel [49].

1.3.3 Pharmacology of the sodium-calcium exchanger

In the past decade, selective NCX inhibition emerged as a promising therapeutic tool for treatment of arrhythmias. So far, several pharmacological agents show various degree of NCX inhibition, however, other ion channels were also affected, thus the data interpretation was difficult. Amiloride analogues showed NCX inhibition, but in the same time these compounds blocked the voltage gated Ca^{2+} channels [50, 51]. Other agents, like bepridil and amiodarone are also capable of NCX inhibition but in a non-selective manner [51]. In numerous studies,

benzyloxyphenyl derivate inhibitors have been used as NCX inhibitors: KB-R7943, SEA0400, SN-6 [50]. KB-R7943 effectively blocked the reverse mode of the NCX in cardiac cells (EC_{50} : 0,3 μM on reverse mode and 17 μM on forward mode) [52]. SEA-0400 seemed to be a more effective inhibitor (EC_{50} of both forward and reverse mode was similar) although both these drugs had significant non-selective effects on other ion channels such as: I_{Na}, I_{CaL}, I_{K1} and delayed rectifier K^+ currents [53, 54]. SN-6 is also an effective inhibitor of NCX in turn, it has an inhibitory effect on I_{Na}, I_{CaL}, I_{Kr}, I_{Ks} I_{K1} currents [53, 54].

Recently, ORM-10103 and ORM-10962 appear to be promising NCX inhibitors. In dog preparations the ORM-10103 effectively inhibited both modes of NCX [55], however, the I_{Kr} was slightly inhibited. ORM-10962, a recently developed NCX inhibitor has promising selectivity and antiarrhythmic effect [56].

1.4 Cardiac alternans

Cardiac alternans develop at rapid heart rate showing beat-to-beat oscillation of the action potential duration, and calcium transient amplitude as well (**Figure 3**) [57]. At the same time typical T-wave alternans (TWAs) appeared on the ECG with microvolt deviations [58]. Alternans change the cardiac tissue repolarization pattern by influencing the AP duration and diastolic interval, therefore transform the physiological repolarization providing enhanced APD heterogeneity [58]. In the 1990s, clinical studies have been connected the TWAs with increased risk for arrhythmias [57]. However, the development of cardiac alternans is not fully clarified. The exact mechanism is still disputed but APD restitution and calcium handling have significant role in the process [58].

1.4.1 The role of cardiac alternans in arrhythmogenesis

Cardiac alternans have two important types at rapid heart rate. In spatially *concordant* case the AP and calcium transient alternate in the same phase in all regions of the heart. In that case, for a given beat the AP duration and calcium transient amplitude both large/long or small/short in the tissue (**Figure 3**) [57]. Since the effective refractory period alternates in synchronized way, the dispersion of refractoriness and repolarization is only slightly changed. Therefore, spatially concordant alternans less predispose to arrhythmias [57]. In contrast, *discordant* alternans has more importance in arrhythmogenesis (**Figure 3**). Concordant alternans can be transformed into discordant by the rising heart rate, premature beats or damaged tissue which provides a physical

barrier in conduction. During discordant alternans the action potential duration and calcium transient amplitude are out-of-phase in the neighboring tissues therefore it increases APD heterogeneity and predispose arrhythmias [57].

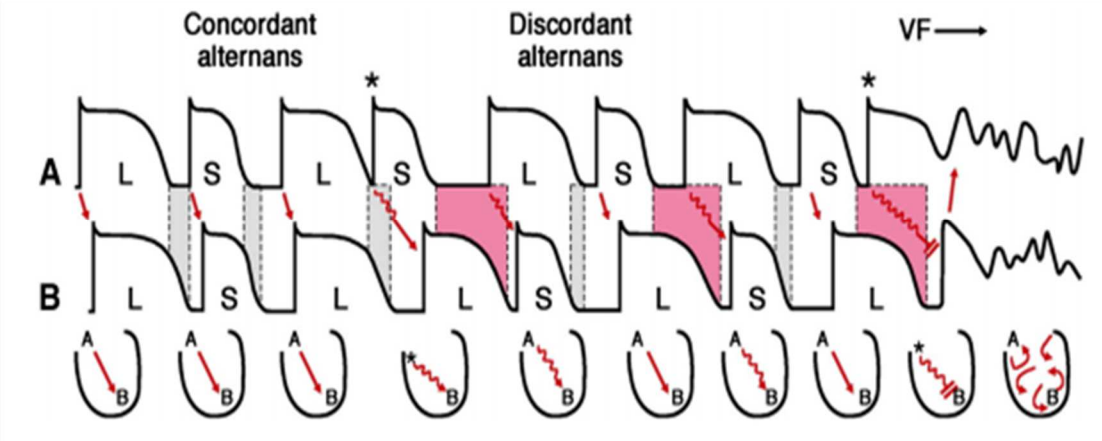

Figure 3.: *Action potential formation between 2 cardiac sites (A-B) during concordant alternans and discordant cardiac alternans. A premature beat (*) caused discordant alternans and induced ventricular fibrillation (VF). Grey areas of the panel introduce the dispersion of repolarization. L: long action potential duration S: short action potential duration [58].*

1.4.2 Cellular mechanism of cardiac alternans

There are two hypotheses regarding the underling mechanism of alternans. In 1968 Nolasco and Dhalen hypothesized that the development of APD alternans is governed by APD restitution [57]. APD restitution measures the changes of APD in the function of the previous diastolic interval (DI) [59]. The steepness of restitution curve is influenced by the recovery of all ion channels during the action potential [59]. The recovery kinetics of the ion channels may affect APD restitution via diastolic interval [59]. Nolasco and Dhalen observed that for a given cycle length (CL) APD alternans appear when the APD restitution curve is larger than 1 [57]. The second hypothesis claims that the calcium handling mismanagement can also induce APD alternans since the membrane potential and intracellular Ca^{2+} are coupled [59]. This theory is the so called Ca^{2+}-driven hypothesis. Alternating Ca^{2+} transients are able to cause APD alternans via enhancing the inward NCX current while it reduces the I_{CaL} due to Ca^{2+}-dependent inactivation. Furthermore, there are some Ca^{2+} sensitive currents (such as Ca^{2+} activated chloride current) that could also contribute to the underlying mechanism [57].

2 Materials and methods

2.1 Ethical statement

Every experiments were accomplished in compliance with the Guide for the Care and Use of Laboratory Animals (USA NIH publication No 85–23, revised 1996) and were confirmed by the Csongrád County Governmental Office for Food Safety and Animal Health, Hungary (approval No.: XIII/1211/2012). The ARRIVE guidelines were adhered to during the study, (NC3Rs Reporting Guidelines Working Group, 2010).

2.2 Standard microelectrode technique

For our experiments we used beagle dogs of either sex weighing 8 to 16 kg obtained from a licensed supplier. Sedation of the dogs occurred with xylazine (1 mg/kg, *i.v.)* and thiopental (30 mg/kg *i.v.*), after it, each heart was rapidly removed through a right lateral thoracotomy and immediately was placed into oxygenated Locke's solution. Action potentials were measured at 37 °C from dog right ventricular papillary muscles using conventional microelectrode technique. The preparations were mounted in a custom made plexiglass chamber, allowing continuous superfusion with O_2-CO_2 saturated Locke's solution (containing in mM: NaCl 120, KCl 4, $CaCl_2$ 1.0, $MgCl_2$ 1, $NaHCO_3$ 22, and glucose 11). The pH of this solution was set between 7.35 and 7.4 with a mixture of 95% O_2 and 5% CO_2 at 37 ºC. The tissue samples were stimulated with constant current pulses of 1 ms duration at a rate of 1 Hz through a pair of bipolar platinum electrodes using an electrostimulator (Hugo Sachs Elektronik, model 215/II). Tip resistance of sharp microelectrodes were 10-20 MΩ, filled with 3 M KCl, and were connected to an amplifier (Biologic Amplifier, model VF 102). Voltage output from the amplifier was sampled using an AD converter (NI 6025, Unisip Ltd). APD, determined at 80% level of repolarization (APD_{80}), was obtained using Evokewave v1.49 software (Unisip Ltd). Alternans were provoked by application of 20 beats in a cycle lengths of 250 ms to 160 ms. Efforts were made to maintain the same impalement throughout the whole experiment. When the impalement was dislodged, an adjustment was attempted. The measurements were only continued if the action potential characteristics of the re-established impalement deviated less than 5% from the previous one.

2.3 Cell isolation

Left ventricular cardiomyocytes were produced with enzymatic isolation from dog hearts. The prepared left ventricular segments were perfused through a coronary artery using a gravity flow at Langendorff apparatus. The perfused solution was a modified Tyrode (composition in mM: NaCl 144, NaH_2PO_4 0.4, KCl 4.0, $MgSO_4$ 0.53, glucose 5.5) supplemented with 1.2 mM $CaCl_2$, 10 mM HEPES, 20 mM taurine, and 1.6 mM Na-pyruvic acid (pH=7.2 with NaOH). At the beginning of isolation, we applied Ca^{2+} containing solution to remove the blood from the tissue. After it, the perfusate was switched for 10 minutes to Ca^{2+}-free Tyrode to wash out redundant Ca^{2+} and stop the contraction. Dissociation of tissues was achieved by application of 0.5 g/l collagenase (Sigma type II) for 50 minutes in the presence of 50 μM $CaCl_2$. During the isolation procedure the solutions were gassed with 100% oxygen and the temperature was maintained at 37°C. At the end of the isolation, the midmyocardial tissue was minced and suspended while the cells released from the tissue. One drop of cell suspension was placed in an inverted microscope (Olympus IX71, Olympus, Tokyo, Japan). Several living cells were visible with clear striations, and they were used for cell measurements. We applied HEPES-buffered Tyrode's solution as normal superfusate (for description please see chapter 2.5).

2.4 Calcium transient measurements

Calcium transients were measured by a Ca^{2+}-sensitive fluorescent dye, Fluo-4 AM. Cardiomyocytes were loaded with the fluorescent dye at room temperature in the dark for 20 minutes. Loaded cells were placed in a low volume imaging chamber (RC47FSLP, Warner Instruments) and used a pair of platinum electrodes for field stimulation. Frequency pattern was applied by using Evokewave v1.49 software. Fluorescence measurements were accomplished on the scene of an Olympus IX 71 inverted fluorescence microscope. The dye was induced at 480 nm and between 515-550 nm the emitted fluorescence was detected. Optical signals were collected at 1 kHz and assumed by a photon counting photomultiplier module (Hamamatsu, model H7828). Axon Digidata 1550B System was used to process and analysis data. In order to calibrate the records, $Ca^{2+}{}_i$ signals were calibrated after disrupting of the cells by the patch-pipette by using the following equation for Fluo-4:

$$Ca^{2+}{}_i = Kd*(F-F_{min})/(F_{max}-F)$$

2.5 Whole cell configuration of patch-clamp technique

From cell suspension one drop was placed in a transparent recording chamber mounted on the stage of an inverted microscope (Olympus IX51, Tokyo, Japan), and separate myocytes were visible. Superfusion was initiated and maintained by gravity flow after the cells rested 5–10 minutes. Only single, rod-shaped cells with clear striations were used. HEPES-buffered Tyrode's solution (composition in mM: NaCl 144, NaH2PO4 0.4, KCl 4.0, CaCl2 1.8, MgSO4 0.53, glucose 5.5 and HEPES 5.0, at pH of 7.4) was used for normal superfusion. During the measurements of $I_{K(ATP)}$, 1 μM nisoldipine was added to the extracellular solution to block I_{CaL}, 0.1 μM dofetilide to inhibit I_{Kr}, and 0.5 μM HMR-1556 to suppress I_{Ks}. Micropipettes were prepared from borosilicate glass capillaries (Science Products GmbH, Hofheim, Germany), using a P-97 Flaming/Brown micropipette puller (Sutter Co, Novato, CA, USA), and had a resistance of 1.5–2.5 MΩ when filled with pipette solution. The ionic currents were recorded with Axopatch-200B amplifiers (Molecular Devices, Sunnyvale, CA, USA) by whole-cell configuration of the patch-clamp technique. The membrane currents were digitized with 250 kHz analogue to digital converters (Digidata 1440A, Molecular Devices, Sunnyvale, CA, USA) under software control (pClamp 8 and pClamp 10, Molecular Devices, Sunnyvale, CA, USA). The compounds of the pipette solution (in mM) was the following: KOH 110, KCl 40, K_2ATP 5, MgCl2 5, EGTA 5, HEPES 10 and GTP 0.1 (pH was adjusted to 7.2 by aspartic acid).

2.6 Signal analysis

APD alternans were extracted based on 6 consecutive APs as the difference between average APDs of even and odd APs. During signal analysis, the APD_{25} (25% repolarization, i.e., mainly plateau duration) and APD_{80} (80% repolarization) were evaluated. The diastolic intervals were calculated as the time difference between the previous APD_{80} and the next AP upstroke. The first and last diastolic intervals were discarded as they are typically incomplete.

Calcium alternans was based on six consecutive CaTs, where the average CaT amplitude was computed for even and odd beats. The amplitude of a single CaT was estimated as the difference between the peak and the minimum directly preceding the given CaT (i.e., it is the CaT upstroke amplitude). CaT alternans is expressed as the ratio of the amplitudes of the larger to the smaller CaT.

3 Results

3.1 APD and CaT alternans are attenuated via ORM-10962

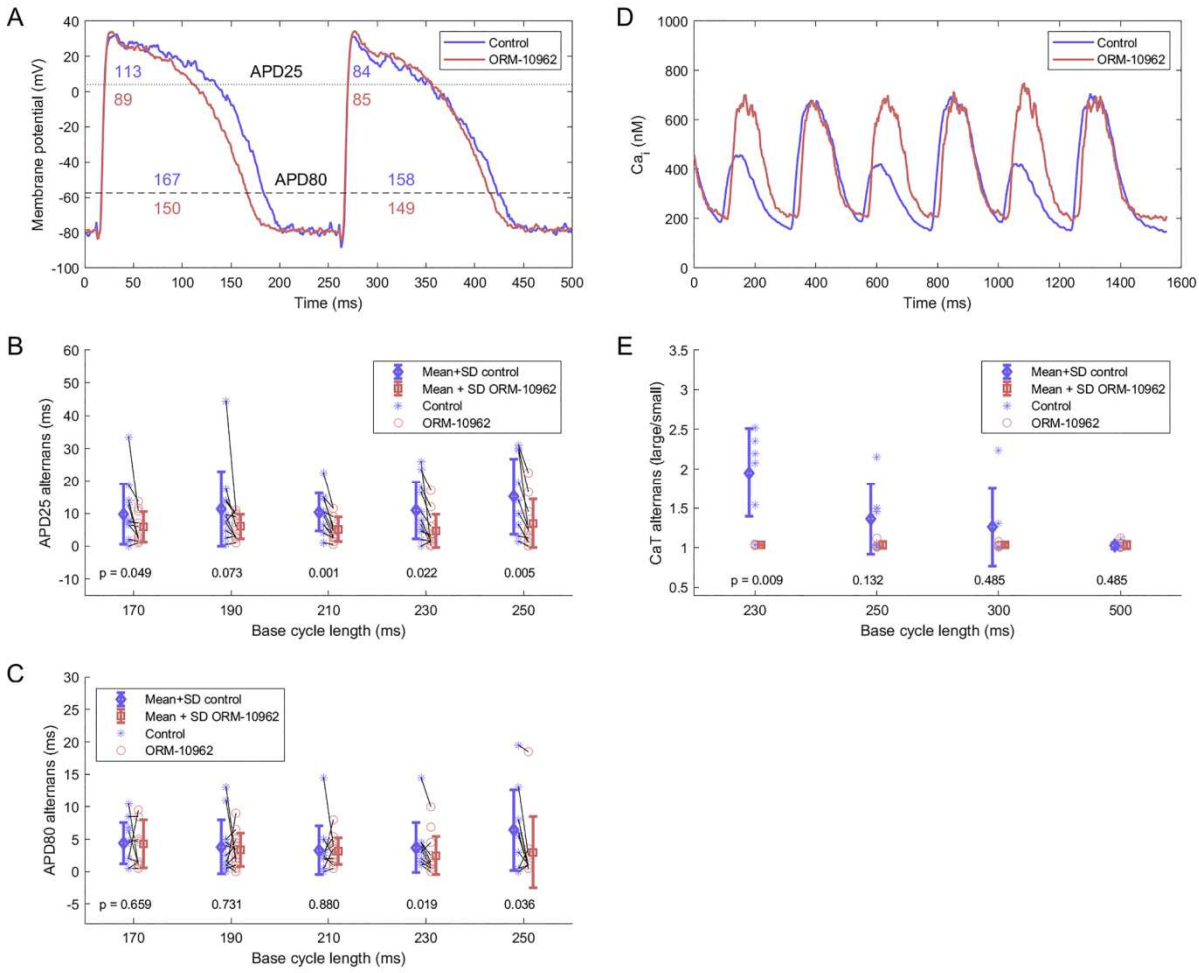

Figure 4.: *Attenuation of alternans via ORM-10962. A) APD alternans at two repolarization levels (APD_{25} and APD_{80}) in control conditions and after selective NCX inhibition in canine muscle preparations. B) APD_{25} alternans at different pacing rates (n=13). C) APD_{80} alternans at different pacing rates (n=13). D) Reduction of CaT alternans in isolated canine cells via ORM-10962. E) Quantitative summary of CaT alternans in control (n=6) and with ORM-10962 (n=6). Unpaired rank sum test was used in E and different variance between control and ORM-10962.*

In canine ventricular papillary muscle APD alternans were measured at two repolarization levels: APD_{25} and APD_{80} (**Figure 4A**). Under control conditions APD alternans are clearly visible at rapid frequency. Application of 1µM ORM-10962 significantly attenuated APD_{25}

alternans at all basic cycle length (**Figure 4B**). APD_{80} level alternans were also decreased at basic cycle length of 250 ms and 230 ms (**Figure 4C**).

In order to supplement the electrophysiological recordings of alternans, calcium movements were additionally measured in isolated cells. It was found that transient amplitude alternans were potently and significantly attenuated after selective NCX inhibition by using ORM-10962 at BCL of 230 ms with a trend towards significance at 250 ms bcl (**Figure 4D,E**).

3.2 Alternans attenuation via ORM-10962 is independent from APD restitution

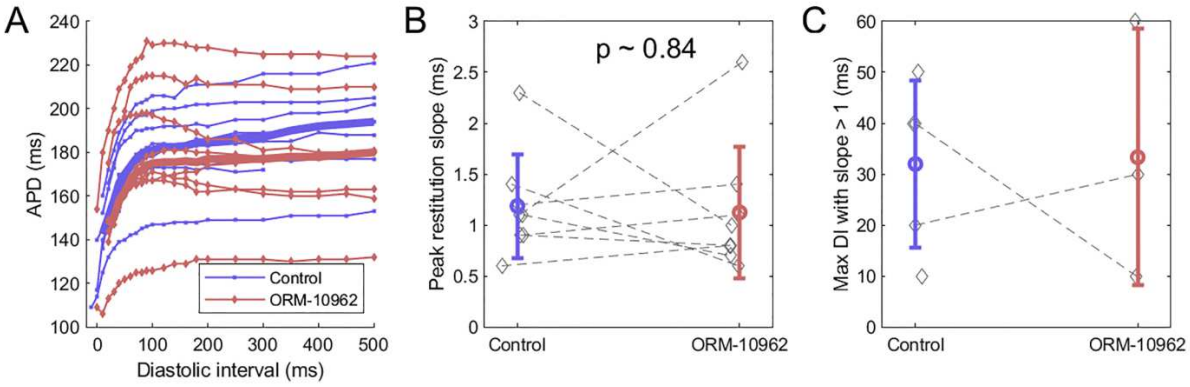

Figure 5.: *Cardiac alternans attenuation via ORM-10962. A) Restitution curves measured in control conditions and after application of ORM-10962 in canine tissue samples (n=8). B) Paired measurements of maximum slope of the restitution curve before and after selective NCX inhibition; the overlay gives mean±SD. 3 restitution curves following ORM-10962 application did not have any interval of slope > 1 C) Longest diastolic interval before which the slope of restitution curve is larger than 1; the overlay gives mean±SD. The pair [40, 50] is present twice in the data and these are overlapping in the plot.*

In the next experimental set, we investigated the possible role of APD restitution in alternans development. APD restitution was measured by using the classic S1-S2 protocol (**Figure 5A**). Under control condition, all hearts exerted restitution slope larger than >1 and there was a non-significant trend towards restitution flattening with ORM-10962 (**Figure 5B**, p = 0.25). The longest diastolic interval with slope >1 was excerpted in each recording (**Figure 5C**), with the hypothesis that if diastolic intervals observed during alternans fall within the zone of restitution slope >1, the restitution is a potential explanation of APD alternans. Based on the results, there

is no recording in the zone of slope >1 extended beyond DI = 50 ms, essentially excludes the restitution-based mechanism as the driver of alternans in our data given that DI < 50 ms were generally observed rarely in our data (e.g., only 2 in 68 recordings of bcl ≥210 ms had the shorter DI below 50 ms). At the same time, APD alternans were present even at 250 ms bcl pacing, where the DIs are typically close to 100 ms, i.e., both short and long DI were outside the zone of steep restitution. Ultimately, the fact that the value of the longest DI with slope >1 is not significantly changed by ORM-10962 (**Figure 5C**) suggests that the alternans attenuation is also not linked to restitution properties. Together, these observations indicate that alternans we observed are not driven by APD restitution, rather by calcium oscillations.

3.3 ORM-10962 extends postrepolarization refractoriness

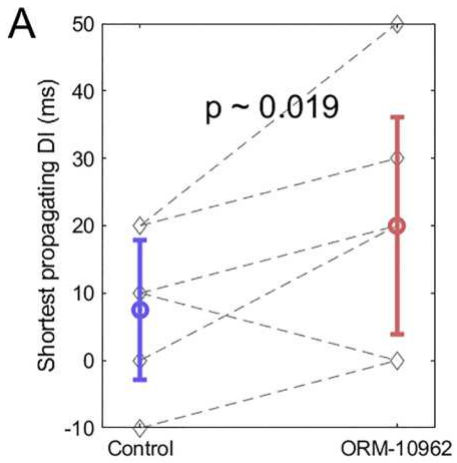

Figure 6.: *Experimental data from tissue samples of the shortest DI which led to formation of an action potential in the S1-S2 protocol.*

In the results of S1-S2 protocol, ORM-10962 extended the duration of postrepolarization refractoriness (PRR), i.e., the interval following APD_{80} where the tissue is still refractory (**Figure 6**).

3.4 Na^+/Ca^{2+}exchanger inhibition reduces spontaneous sinus-node automaticity and increases Ca^{2+}i level

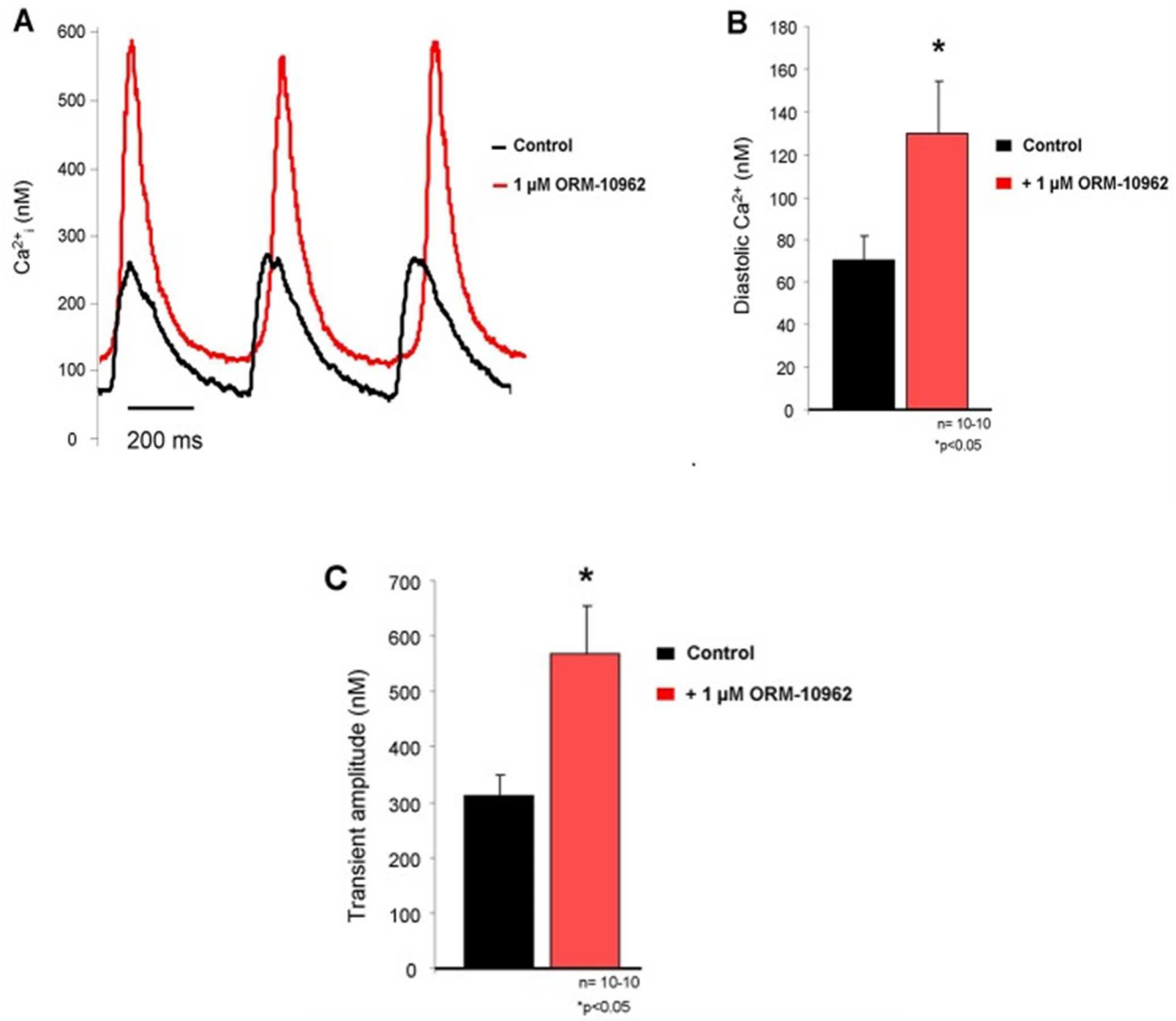

Figure 7.: (A) *Representative Ca^{2+} transient traces under control conditions (black trace) and after 1 µM ORM-10962 (ORM) application (red trace) from spontaneously contracting isolated sinus node (SAN) cells. After selective NCX block a slight but significant increase of the diastolic Ca^{2+} level* (B) *with increased transient amplitude* (C) *was observed [56]* .

Literature data [57] and our experiments demonstrate that cardiac alternans are in intimate relationship with pacing frequency. Since it is well-known that the inward NCX current has a crucial role in the diastolic depolarization of the sinus-node cells [60] one can speculate that a possible reduction in the sinus frequency may indirectly facilitate the "anti-alternans" effect of

selective NCX inhibition. This possibility was investigated in spontaneously beating isolated sinus-node cells from rabbit right atrium.

In isolated SAN cells the spontaneous frequency of the sinus node cells decreased (CL: 455.6 ± 32 ms *vs.* 493.0 ± 38 ms; Δ = 8.1 ± 1.8% $p < 0.05$) while the diastolic Ca^{2+} level increased after ORM-10962 treatment (70±11 nM *vs.* 130±24 nM; $p<0.05$, n = 10; (**Figure 7A**,**B**)). Furthermore, considerable increase in the transient amplitude (312 ± 37 nM *vs.* 568 ± 85 nM; $p < 0.05$, n = 10 (**Figure 7C**)) was observed, which was nearly doubled (82.1 ± 22%) in response to ORM-10962 application compared to the control value.

3.5 Carbachol decreased the pinacidil-induced current activation

Beyond the Ca^{2+}-dependent currents (such as I_{CaL}, I_{NCX}), the role of other currents in the APD alternans development cannot be ruled out. It is known that glycolytic inhibition [61] or myocardial infarction [62] promotes the development of cardiac alternans. Under this condition the normal ATP formation is decreased due to tissue hypoxia, therefore the activation of the ATP-dependent K-channels could markedly contribute to the action potential shortening and repolarization heterogeneity.

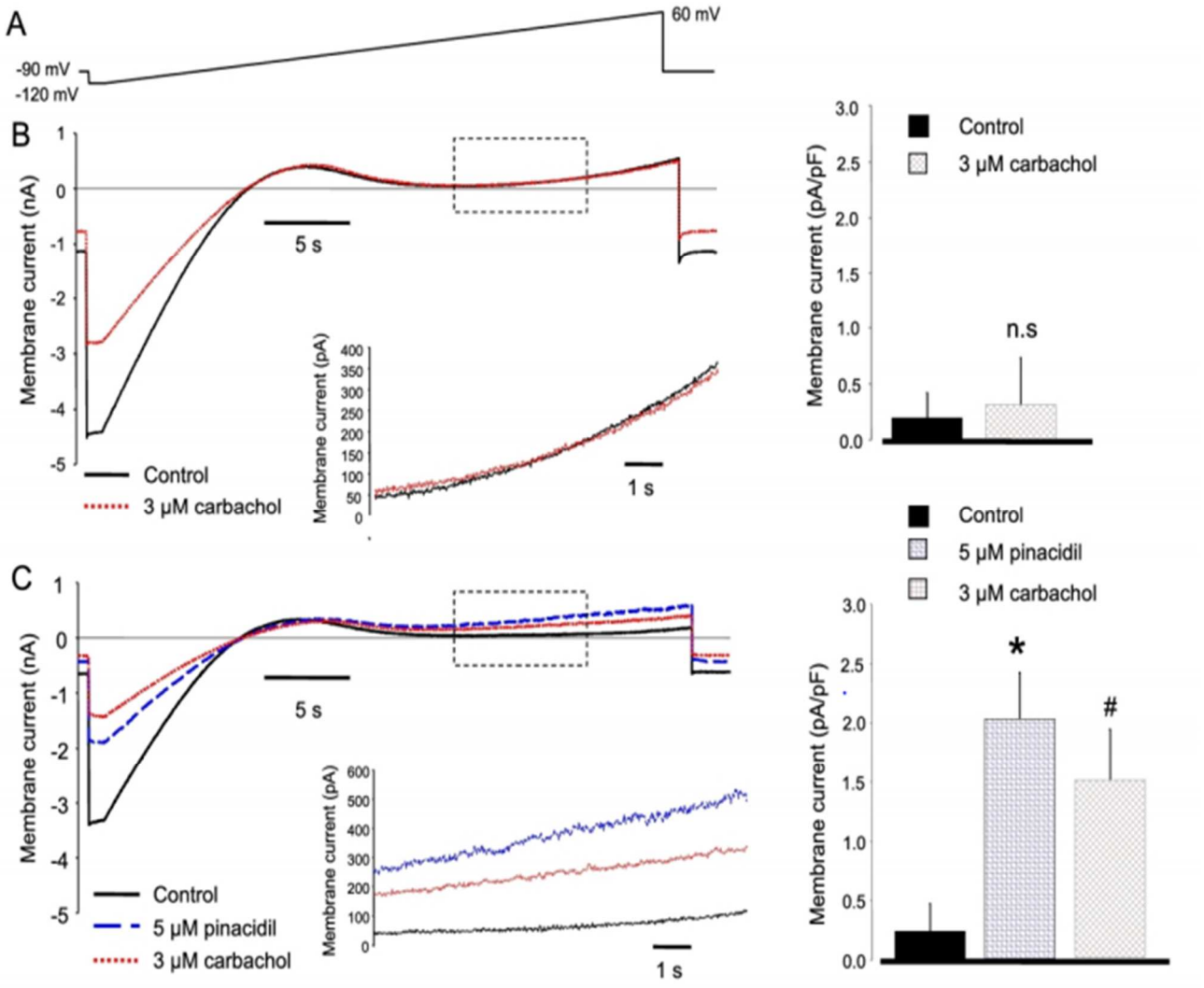

Figure 8.: *Effect of pinacidil and carbachol on IK-ATP. Ionic currents were measured between -120 mV and 60 mV under a slow voltage ramp protocol* ***(panel A)****. The currents were analyzed at 0 and 30 mV.* ***Panel B*** *shows original representative current traces (left) and bar graphs (right) where 3 μM carbachol (dotted line) failed to influence the control current analyzed at 0 mV. Inset shows identical current fractions between –3 mV and 45 mV (indicated by dashed rectangle). Current traces in* ***panel C*** *as well as in the inset, illustrate large increase of the membrane current after application of 5 μM pinacidil (blue dashed line) that was inhibited by the later applied 3 μM carbachol (red dotted line). In bar graphs (right), asterisk denotes significant change between control (left column) and pinacidil (middle column), while hash tag indicates significant change between pinacidil (middle column) and carbachol (right column) [63].*

In our ionic current measurements, voltage ramps were used from a holding potential of -90 mV. Membrane potential was hyperpolarized to -120 mV, and then was slowly (over 36 s) depolarized to 60 mV (**Figure 8 panel A**). Ionic currents were analyzed and compared at 0 and +30 mV [63]. Carbachol did not change the control current when it was applied without

pinacidil (**Figure 8 panel B**) (0 mV - control: 0.20±0.2 pA/pF vs 3 μM carbachol: 0.32±0.2 pA/pF, n=6 and +30 mV - control: 0.55±0.4 pA/pF vs 3 μM carbachol: 0.74±0.3 pA/pF, n=6). In contrast, when 5 μM pinacidil was applied first, subsequently employed carbachol significantly reduced the current at both voltages (**Figure 8 panel C**). (0 mV – control: 0.24±0.2 pA/pF 5 μM pinacidil: 2.03±0.3 pA/pF 3 μM carbachol: 1.51±0.4 pA/pF, n=8, $p < 0.05$) [63].

4 Discussion

Main findings of the thesis:

1) Selective NCX inhibition by 1 μM ORM-10962 attenuates AP alternans primarily at APD_{25} levels.

2) Selective NCX inhibition suppresses the alternans of CaT amplitude

3) Selective NCX inhibition extends postrepolarization refractoriness but does not influence the restitution steepness

4) Selective NCX inhibition increases the intracellular Ca^{2+} level in spontaneously beating sinus node cells

5) The muscarinerg antagonist carbachol inhibits the activated IK_{ATP} current.

4.1 Selective NCX blockade attenuates cardiac alternans

Cardiac alternans have been shown to have significant role in the onset of ventricular fibrillation. The underlying mechanism, however, is not fully clarified so far. The first proposed mechanism was based on the restitution steepness [57]. The authors claimed that alternans will develop when the APD restitution steepness is larger than 1. This theory was termed as voltage-driven mechanism. Later, the voltage-driven mechanism was criticized by several laboratories, and the underlying mechanism was suggested to be rather Ca^{2+}-driven.
The NCX has crucial importance in the normal Ca^{2+}-cycling, due to extrusion of intracellular Ca^{2+} equal to Ca influx. During Ca-efflux a net inward current is generating, therefore the NCX represents a link between intracellular Ca^{2+}-movements and membrane voltage. Considering this dual nature of NCX, it was suggested that NCX may have an important role in the alternans development. The first proposed mechanism of NCX in alternans development was introduced by Eisner et al [35]. They suggested when Ca-release-efflux ratio is steep, Ca alternans development is largely facilitated. In this case, NCX inhibition may flatten the release-efflux ratio and a decrease in the Ca^{2+}-alternans is expected.

The second proposed mechanism is based on the Ca^{2+}-mediated shifts of I_{CaL} and I_{NCX}. When a large Ca^{2+} release influences more the I_{CaL} than NCX, it will facilitate the Ca^{2+}-dependent inactivation of the I_{CaL}. As a consequence, the I_{CaL} integral decreases and the AP is shortened. In this case, the large Ca^{2+} releases will be coupled with short APs (negative Ca-to-Vm

coupling). In the case of Ca^{2+} release has larger impact on NCX, the large Ca^{2+} release will drive large Ca^{2+} efflux and concomitant large inward NCX current that prolongs the AP (positive Ca-to-Vm coupling). A previous paper experimentally demonstrated that NCX is the most plausible candidate for alternans development since was found positive Ca-to-Vm coupling in all cases [64].

In line with previous results, in our experiments we found that selective NCX inhibition by ORM-10962 markedly reduces both APD and CaT alternans (**Figure 4**). At the same time, ORM did not influence the restitution curve of the action potential (**Figure 5)** that suggests that the anti-alternans effect of selective NCX inhibition could be independent from the restitution properties of the heart. The underlying mechanism of CaT alternans suppression was assessed by computer simulations. The NCX-inhibition increases the Ca^{2+}-content and indirectly reduces the I_{CaL} magnitude via enhanced CDI. When NCX is inhibited, the Ca^{2+} efflux is suppressed, and the SERCA becomes a better competitor during Ca^{2+} removal leading to enhanced SR Ca^{2+} content [65]. The enhanced SR reuptake could reduce the refractoriness of Ca^{2+} release [66]. Since refractoriness of SR Ca^{2+} release was demonstrated as a potential Ca^{2+}-driven mechanism for alternans [67] [68], it is feasible that selective NCX inhibition-mediated alternans attenuation based on reduced SR Ca^{2+} refractoriness as a direct underlying mechanism.

It was also found that selective NCX inhibition extends post-repolarization refractoriness. Computer simulations revealed that indirect suppression of I_{CaL} upon NCX inhibition could be an underlying mechanism. A further, alternative mechanism could be a calcium-induced inactivation of the fast-sodium current [69]. The gain in the Ca^{2+} upon NCX inhibition may inhibit I_{Na} and prolongs refractoriness.

4.2 Na^+/Ca^{2+} exchanger inhibition markedly increases the Ca^{2+}_I level

The sinus-node pacemaking has one of the most interesting history in the cardiac electrophysiology. The exact mechanism of the spontaneous automaticity was matter of debate for 25 years. Initial concepts claimed that activation of the principal K-current I_{Kr} provides the repolarization and maximal diastolic depolarization and its deactivation provides possibility to the slow depolarization achieved by slow inward leakage currents [70]. This theory was replaced after the discovery of the pacemaker current (funny-current, I_f) [71]. The concept announced that the I_f is the primary drive of the spontaneous diastolic depolarization, as having a hyperpolarization-activated kinetics, and shows strong cAMP-dependence to respond to adrenergic stimulation. The I_f-driven pacemaking had dominant role in sinus-node automaticity

until the late 90's when the importance of the intracellular Ca^{2+} handling was supported by an increasing number of publications. These reports focused to the role of inward (forward) NCX as an essential player transforming Ca^{2+}-changes to membrane potential depolarization. A break-through discovery was published in 2004 when spontaneous, rhythmic, local-Ca^{2+} releases were found preceding the "normal" Ca^{2+} release from the SR. These local events (LCR) generate NCX current to contribute to the diastolic depolarization. Since the rhythmicity of the LCRs may provide rhythmic sinus-node pacemaking, it was termed 'Ca-clock'. This theory could be considered as a counterpoint of the I_f-based pacemaking, where the automaticity was completely based on the LCRs [72].

At the same time, it was indisputable that selective inhibition of various transmembrane ionic currents (I_f, I_{Kr}, I_{CaL}, I_{CaT}) substantially influence pacemaking. Several publications were released demonstrating coupling between surface membrane ion channels and Ca^{2+} handling, leading to the current, widely accepted theory: 'coupled-clock' mechanism [71]. The coupled-clock concept claims that that surface membrane ion channels as well as intracellular Ca^{2+}-handling work together, neither is dominant, but provides a redundant, fail-safe, complex mechanism.

Our previous results indicated that selective NCX inhibition decreases the alternans magnitude that could be associated to a shift in the Ca^{2+}-handling. However, based on the coupled-clock mechanism, it is feasible that selective NCX inhibition may decrease the spontaneous sinus-node frequency as well. In this case a bradycardic effect of ORM-10962 could indirectly facilitate the alternans attenuation of selective NCX block.

In our experiments, we found a slight but statistically significant (~8%) decrease in the cycle length of sinus node cells [73]. This effect, however lower than was expected, it was coupled with an increase of the diastolic Ca^{2+} and the transient amplitude. The selective NCX inhibition caused similar diastolic Ca^{2+} changes compared to the Yaniv model[72] predicted, however, in contrast with modeling, we found markedly increased Ca^{2+} transient amplitude which is generally expected after decreased rate of Ca^{2+} extrusion. The observed quantitative discrepancy between experiments and modeling may indicate that the extent of NCX inhibition in the experiments could be larger than 41%.

We can speculate that the increasing intracellular Ca^{2+} is known to facilitate the inactivation of the L-type Ca^{2+} current as a part of the autoregulation. The gain of the $[Ca^{2+}]_i$ may indirectly shortens the CL which means two parallel, counteracting effect of selective NCX inhibition:

the inhibition of the inward NCX current may reduce the actual frequency by suppressing its contribution to the DD, however it is partially compensated for the CL abbreviating effect of increased $[Ca^{2+}]_i$. Furthermore, the I_f may also contribute in the limitation of the ORM effect: i) a theoretical possibility exists that ORM-induced Ca^{2+} elevation may increase the I_f, however this was ruled out by a previous work [74] (ii) It was reported that SAN myocytes express Ca^{2+}-activated adenylate cyclase isoform, which might raise cAMP (and I_f) in response to NCX blockade [74]. Furthermore, a possible Ca^{2+}-mediated increase of the $I_{K(Ca)}$ is also feasible [75].

Taking together these results, it is feasible that selective NCX inhibition may cause several concomitant and counterintuitive changes in the sinus node cells, because NCX inhibition not only inhibits the NCX current during the DD, but modulates the Ca^{2+} levels of the cells. Ultimately, it results marginal decrease in sinus-node frequency, but it may have potential significance in the alternans-attenuation effect of selective NCX inhibition. In our AP alternans experiments we have never observed APD alternans at BCL of 300 ms, in contrast, alternans were always found at 250 ms. This may indicate a very narrow frequency border between normal and alternating AP behavior. In this case, a mild bradycardic effect may have important role in attenuation of alternans.

4.3 Acetylcholine inhibits the IK-ATP in canine ventricular myocytes

It was reported that alternans are often developed in ischemia-reperfusion injury [63]. This finding raises the possibility that $I_{K\text{-}ATP}$ that exerts a well-known activation in ischemia, may contribute to the alternans mechanism, at least via increasing the APD heterogeneity. In contrast, the direct role of the $I_{K\text{-}ATP}$ in the development of alternans is controversial. It was reported that $I_{K\text{-}ATP}$ expression exerts down-regulation during myocardial infarction. Nicorandil (an $I_{K\text{-}ATP}$ opener) restored the APD and flattened the restitution curve and suppressed the spatially discordant arrhythmias [62]. In contrast, *in-silico* simulations indicate that any intervention that widen the alternans vulnerable window including altered Ca^{2+} cycling and enhanced K^+-currents promotes alternans. This study claims that $I_{K\text{-}ATP}$ agonists facilitate the alternans development [76].

In line with this, it was showed by early studies, that increased parasympathetic tone is able to reduce ischemia-related arrhythmias [77] [78]. In our experiments, as was expected, we found significant increase of $I_{K\text{-}ATP}$ after application of pinacidil (almost 10-fold increase). It was also demonstrated that this large increase of the current abbreviates the ventricular action potential [63]. Interestingly, our novel finding is that muscarinergic-agonist carbachol is able to reduce

the previously activated the $I_{K\text{-}ATP}$ current. The underlying mechanism could be related to the change of intracellular signaling pathways such as PKC [63] however, it requires further experiments. These interesting results may provide a further aspect of antiarrhythmic effect of increased parasympathetic tone in ischemia [79]. This effect of parasympathetic tone could be achieved, at least partially, via attenuation the $I_{K\text{-}ATP}$-mediated increased alternans propensity. However, this question requires further experiments.

4.4 Further currents in alternans development: the role of late-Na current and Ca^{2+}-current

Late Na^+-current is developed after rapid opening and inactivation of the peak Na^+-current. After activation, a small (1%) portion of the current remains active contributing in the maintenance of the plateau phase of the action potential. However, I_{NaL} is relatively small current under normal condition, it is known that its amplitude is increased during heart failure [80]. The increased I_{NaL} contributes to prolong the action potential duration and thus, facilitates transmural APD heterogeneity, and the development of EADs. Furthermore, it is important to note that the extra Na-influx through I_{NaL} increases the intracellular Na^+_i level and therefore facilitates the Ca^{2+}-uptake of the cell due to reverse NCX function. This Ca^{2+} entry promotes SR Ca^{2+} overloads, spontaneous Ca-releases and arrhythmias, such as DAD. I_{NaL} was suggested to having important role in the alternans development [80], therefore its inhibition could be also a promising tool against alternans. It was demonstrated that the I_{NaL} inhibitor ranolazine suppresses spatially discordant APD alternans, and normalizes the Ca-impairment in dog rapid-pacing induced heart failure model [80]. Therefore, I_{NaL} inhibition could also be a feasible tool to reduce and prevent alternans-based arrhythmias [80].

The L-type Ca^{2+}-current has prominent role in the phase 2 action potential by maintaining the plateau phase furthermore the Ca-influx through I_{CaL} has key role in the ignition of the intracellular Ca-cycling. The I_{CaL} has well proven role in the EAD generation, however its role in the alternans development is controversial.

Several studies reported that I_{CaL} is able to induce alternans via incomplete time-dependent recovery [81] [82] [83] [84]. In contrast, numerous papers provided evidence that alternans can occur while the peak I_{CaL} remained unchanged [85] [86] [87] [65] [88]. Additionally, several reports were published claiming that CaT alternans can be found in the absence of AP alternans [85] [86] [87] [89] [90].

5 Conclusion

Our results indicate that NCX has an important direct and indirect role in the mechanism of the development of the alternans, consequently, selective NCX inhibition could be a feasible therapeutic strategy to suppress cardiac alternans. The cellular effect of ORM-10962 against alternans resulted in independence from the restitution properties therefore our results support the Ca^{2+}-driven mechanism of alternans.

However, literature data indicate that alternans could not be defined as a result of a single underlying mechanism. Various ionic currents could contribute to the underlying mechanism therefore several approaches seem to be feasible to use in alternans based arrhythmia prevention.

6 Study limitations

Our study has the following:

(i) The action potential measurements were carried out on tissue while CaTs were recorded from isolated cells. This may indicate that the magnitude and kinetics of action potential alternans could not be directly related to CaT alternans.

(ii) The action potential measurements were performed on intact ventricular tissue to avoid shortcomings arising from repolarization attenuation caused by enzymatic dissociation. Due to the stable repolarization, the alternans could be evoked with 100% probability and small APD changes could be detected with high fidelity. At the same time, it also means that our action potential measurements represent only the endocardial tissue. Other cell layers (such as epicardial cells) may have different characteristic during alternans.

7 REFERENCES

[1] Varró A, Tomek J, Nagy N, Virag L, Passini E, Rodriguez B, et al. Cardiac Transmembrane Ion Channels and Action Potentials: Cellular Physiology and Arrhythmogenic Behavior. Physiological Reviews. 2020.
[2] Bartos DC, Grandi E, Ripplinger CM. Ion Channels in the Heart. Comprehensive Physiology. 2015;5 3:1423-64.
[3] Bendahhou S, Marionneau C, Haurogne K, Larroque M-M, Derand R, Szuts V, et al. In vitro molecular interactions and distribution of KCNE family with KCNQ1 in the human heart. Cardiovascular research. 2005;67:529-38.
[4] Sekiya S, Ichikawa S, Tsutsumi T, Harumi K. Nonuniform action potential durations at different sites in canine left ventricle. Japanese heart journal. 1983;24:935-45.
[5] Fozzard HA, January CT, Makielski JC. New studies of the excitatory sodium currents in heart muscle. Circulation research. 1985;56:475-85.
[6] Rook MB, Evers MM, Vos MA, Bierhuizen MF. Biology of cardiac sodium channel Nav1.5 expression. Cardiovascular research. 2012;93:12-23.
[7] Roden DM. Pharmacology and Toxicology of Nav1.5-Class 1 anti-arrhythmic drugs. Cardiac electrophysiology clinics. 2014;6:695-704.
[8] Lei M, Wu L, Terrar DA, Huang CL. Modernized Classification of Cardiac Antiarrhythmic Drugs. Circulation. 2018;138:1879-96.
[9] Patel SP, Campbell DL. Transient outward potassium current, 'Ito', phenotypes in the mammalian left ventricle: underlying molecular, cellular and biophysical mechanisms. The Journal of physiology. 2005;569:7-39.
[10] Chiamvimonvat N, Chen-Izu Y, Clancy CE, Deschenes I, Dobrev D, Heijman J. Potassium currents in the heart: functional roles in repolarization, arrhythmia and therapeutics. 2017;595:2229-52.
[11] Virág L, Jost N, Papp R, Koncz I, Kristóf A, Kohajda Z, et al. Analysis of the contribution of I(to) to repolarization in canine ventricular myocardium. British journal of pharmacology. 2011;164:93-105.
[12] Wang Z, Fermini B, Nattel S. Effects of flecainide, quinidine, and 4-aminopyridine on transient outward and ultrarapid delayed rectifier currents in human atrial myocytes. The Journal of pharmacology and experimental therapeutics. 1995;272:184-96.
[13] Hirano Y, Fozzard HA, January CT. Characteristics of L- and T-type Ca2+ currents in canine cardiac Purkinje cells. The American journal of physiology. 1989;256:H1478-92.
[14] Mitra R, Morad M. Two types of calcium channels in guinea pig ventricular myocytes. Proceedings of the National Academy of Sciences of the United States of America. 1986;83:5340-4.
[15] Zhou Z, Lipsius SL. T-type calcium current in latent pacemaker cells isolated from cat right atrium. Journal of molecular and cellular cardiology. 1994;26:1211-9.
[16] Isenberg G, Klöckner U. Calcium currents of isolated bovine ventricular myocytes are fast and of large amplitude. Pflugers Archiv : European journal of physiology. 1982;395:30-41.
[17] Dibb KM, Eisner DA, Trafford AW. Regulation of systolic [Ca2+]i and cellular Ca2+ flux balance in rat ventricular myocytes by SR Ca2+, L-type Ca2+ current and diastolic [Ca2+]i. The Journal of physiology. 2007;585:579-92.
[18] Kokubun S, Irisawa H. Effects of various intracellular Ca ion concentrations on the calcium current of guinea-pig single ventricular cells. The Japanese journal of physiology. 1984;34:599-611.
[19] Hondeghem LM, Carlsson L, Duker G. Instability and triangulation of the action potential predict serious proarrhythmia, but action potential duration prolongation is antiarrhythmic. Circulation. 2001;103:2004-13.
[20] Suenari K, Chen YC, Kao YH, Cheng CC, Lin YK, Chen YJ, et al. Discrepant electrophysiological characteristics and calcium homeostasis of left atrial anterior and posterior myocytes. Basic research in cardiology. 2011;106:65-74.
[21] Smith PL, Baukrowitz T, Yellen G. The inward rectification mechanism of the HERG cardiac potassium channel. Nature. 1996;379:833-6.
[22] Spector PS, Curran ME, Zou A, Keating MT, Sanguinetti MC. Fast inactivation causes rectification of the IKr channel. The Journal of general physiology. 1996;107:611-9.
[23] Iost N, Virág L, Opincariu M, Szécsi J, Varró A, Papp JG. Delayed rectifier potassium current in undiseased human ventricular myocytes. Cardiovascular research. 1998;40:508-15.
[24] Jost N, Virág L, Bitay M, Takács J, Lengyel C, Biliczki P, et al. Restricting excessive cardiac action potential and QT prolongation: a vital role for IKs in human ventricular muscle. Circulation. 2005;112:1392-9.
[25] Jurkiewicz NK, Sanguinetti MC. Rate-dependent prolongation of cardiac action potentials by a methanesulfonanilide class III antiarrhythmic agent. Specific block of rapidly activating delayed rectifier K+ current by dofetilide. Circulation research. 1993;72:75-83.

[26] Nerbonne JM, Kass RS. Molecular physiology of cardiac repolarization. Physiol Rev. 2005;85:1205-53.
[27] Lundquist AL, Manderfield LJ, Vanoye CG, Rogers CS, Donahue BS, Chang PA, et al. Expression of multiple KCNE genes in human heart may enable variable modulation of I(Ks). Journal of molecular and cellular cardiology. 2005;38:277-87.
[28] Virág L, Iost N, Opincariu M, Szolnoky J, Szécsi J, Bogáts G, et al. The slow component of the delayed rectifier potassium current in undiseased human ventricular myocytes. Cardiovascular research. 2001;49:790-7.
[29] Volders PG, Stengl M, van Opstal JM, Gerlach U, Spätjens RL, Beekman JD, et al. Probing the contribution of IKs to canine ventricular repolarization: key role for beta-adrenergic receptor stimulation. Circulation. 2003;107:2753-60.
[30] Varkevisser R, Wijers SC, van der Heyden MA, Beekman JD, Meine M, Vos MA. Beat-to-beat variability of repolarization as a new biomarker for proarrhythmia in vivo. Heart rhythm. 2012;9:1718-26.
[31] Roden DM. Taking the "idio" out of "idiosyncratic": predicting torsades de pointes. Pacing and clinical electrophysiology : PACE. 1998;21:1029-34.
[32] Matsuda H. Effects of external and internal K+ ions on magnesium block of inwardly rectifying K+ channels in guinea-pig heart cells. The Journal of physiology. 1991;435:83-99.
[33] Martin RL, Koumi S, Ten Eick RE. Comparison of the effects of internal [Mg2+] on IK1 in cat and guinea-pig cardiac ventricular myocytes. Journal of molecular and cellular cardiology. 1995;27:673-91.
[34] Weiss JN, Qu Z, Shivkumar K. Electrophysiology of Hypokalemia and Hyperkalemia. Circulation Arrhythmia and electrophysiology. 2017;10.
[35] Eisner DA, Caldwell JL, Kistamás K, Trafford AW. Calcium and Excitation-Contraction Coupling in the Heart. Circulation research. 2017;121:181-95.
[36] Hurtado C, Prociuk M, Maddaford TG, Dibrov E, Mesaeli N, Hryshko LV, et al. Cells expressing unique Na+/Ca2+ exchange (NCX1) splice variants exhibit different susceptibilities to Ca2+ overload. American journal of physiology Heart and circulatory physiology. 2006;290:H2155-62.
[37] Sher AA, Noble PJ, Hinch R, Gavaghan DJ, Noble D. The role of the Na+/Ca2+ exchangers in Ca2+ dynamics in ventricular myocytes. Progress in biophysics and molecular biology. 2008;96:377-98.
[38] Jost N, Nagy N, Corici C, Kohajda Z, Horváth A, Acsai K, et al. ORM-10103, a novel specific inhibitor of the Na+/Ca2+ exchanger, decreases early and delayed afterdepolarizations in the canine heart. British journal of pharmacology. 2013;170:768-78.
[39] Kohajda Z, Farkas-Morvay N, Jost N, Nagy N, Geramipour A, Horváth A, et al. The Effect of a Novel Highly Selective Inhibitor of the Sodium/Calcium Exchanger (NCX) on Cardiac Arrhythmias in In Vitro and In Vivo Experiments. PloS one. 2016;11:e0166041.
[40] Gadsby DC. Influence of Na/K pump current on action potentials in Purkinje fibers. Advances in myocardiology. 1985;5:279-94.
[41] Shattock MJ, Ottolia M, Bers DM, Blaustein MP, Boguslavskyi A, Bossuyt J, et al. Na+/Ca2+ exchange and Na+/K+-ATPase in the heart. The Journal of physiology. 2015;593:1361-82.
[42] Glitsch HG. Electrophysiology of the sodium-potassium-ATPase in cardiac cells. Physiol Rev. 2001;81:1791-826.
[43] Ravens U, Cerbai E. Role of potassium currents in cardiac arrhythmias. Europace : European pacing, arrhythmias, and cardiac electrophysiology : journal of the working groups on cardiac pacing, arrhythmias, and cardiac cellular electrophysiology of the European Society of Cardiology. 2008;10:1133-7.
[44] Bers DM. Cardiac excitation-contraction coupling. Nature. 2002;415:198-205.
[45] Eisner DA, Choi HS, Díaz ME, O'Neill SC, Trafford AW. Integrative analysis of calcium cycling in cardiac muscle. Circulation research. 2000;87:1087-94.
[46] Bers DM, Ginsburg KS. Na:Ca stoichiometry and cytosolic Ca-dependent activation of NCX in intact cardiomyocytes. Annals of the New York Academy of Sciences. 2007;1099:326-38.
[47] Choi HS, Eisner DA. The role of sarcolemmal Ca2+-ATPase in the regulation of resting calcium concentration in rat ventricular myocytes. The Journal of physiology. 1999;515 (Pt 1):109-18.
[48] Díaz ME, Graham HK, O'Neill S C, Trafford AW, Eisner DA. The control of sarcoplasmic reticulum Ca content in cardiac muscle. Cell calcium. 2005;38:391-6.
[49] Nicoll DA, Longoni S, Philipson KD. Molecular cloning and functional expression of the cardiac sarcolemmal Na(+)-Ca2+ exchanger. Science (New York, NY). 1990;250:562-5.
[50] Antoons G, Willems R, Sipido KR. Alternative strategies in arrhythmia therapy: Evaluation of Na/Ca exchange as an anti-arrhythmic target. Pharmacology & Therapeutics. 2012;134:26-42.
[51] Iwamoto T, Watanabe Y, Kita S, Blaustein MP. Na+/Ca2+ exchange inhibitors: a new class of calcium regulators. Cardiovascular & hematological disorders drug targets. 2007;7:188-98.
[52] Watano T, Kimura J, Morita T, Nakanishi H. A novel antagonist, No. 7943, of the Na+/Ca2+ exchange current in guinea-pig cardiac ventricular cells. British journal of pharmacology. 1996;119:555-63.
[53] Matsuda T, Arakawa N, Takuma K, Kishida Y, Kawasaki Y, Sakaue M, et al. SEA0400, a Novel and Selective Inhibitor of the Na⁺-Ca²⁺ Exchanger, Attenuates Reperfusion

Injury in the in Vitro and in Vivo Cerebral Ischemic Models. Journal of Pharmacology and Experimental Therapeutics. 2001;298:249.
[54] Matsuda T, Koyama Y, Baba A. Functional Proteins Involved in Regulation of Intracellular Ca2+ for Drug Development: Pharmacology of SEA0400, a Specific Inhibitor of the Na+-Ca2+ Exchanger. Journal of Pharmacological Sciences. 2005;97:339-43.
[55] Jost N, Nagy N, Corici C, Kohajda Z, Horváth A, Acsai K, et al. ORM-10103, a novel specific inhibitor of the Na+/Ca2+ exchanger, decreases early and delayed afterdepolarizations in the canine heart. British journal of pharmacology. 2013;170:768-78.
[56] Kohajda Z, Farkas-Morvay N, Jost N, Nagy N, Geramipour A, Horvath A, et al. The Effect of a Novel Highly Selective Inhibitor of the Sodium/Calcium Exchanger (NCX) on Cardiac Arrhythmias in In Vitro and In Vivo Experiments. PloS one. 2016;11:e0166041.
[57] Weiss JN, Karma A, Shiferaw Y, Chen PS, Garfinkel A, Qu Z. From pulsus to pulseless: the saga of cardiac alternans. Circulation research. 2006;98:1244-53.
[58] Verrier RL, Malik M. Electrophysiology of T-wave alternans: Mechanisms and pharmacologic influences. Journal of electrocardiology. 2013;46:580-4.
[59] Tse G, Wong ST, Tse V, Lee YT, Lin HY, Yeo JM. Cardiac dynamics: Alternans and arrhythmogenesis. Journal of arrhythmia. 2016;32:411-7.
[60] Kohajda Z, Tóth N, Szlovák J, Loewe A, Bitay G, Gazdag P, et al. Novel Na(+)/Ca(2+) Exchanger Inhibitor ORM-10962 Supports Coupled Function of Funny-Current and Na(+)/Ca(2+) Exchanger in Pacemaking of Rabbit Sinus Node Tissue. Frontiers in pharmacology. 2019;10:1632.
[61] Morita N, Lee JH, Bapat A, Fishbein MC, Mandel WJ, Chen PS, et al. Glycolytic inhibition causes spontaneous ventricular fibrillation in aged hearts. American journal of physiology Heart and circulatory physiology. 2011;301:H180-91.
[62] Lee HL, Chang PC, Chou CC, Wo HT, Chu Y, Wen MS, et al. Blunted proarrhythmic effect of nicorandil in a Langendorff-perfused phase-2 myocardial infarction rabbit model. Pacing and clinical electrophysiology : PACE. 2013;36:142-51.
[63] Magyar T, Árpádffy-Lovas T, Pászti B, Tóth N, Szlovák J, Gazdag P, et al. Muscarinic agonists inhibit the ATP-dependent potassium current and suppress the ventricle-Purkinje action potential dispersion. Canadian journal of physiology and pharmacology. 2021;99:247-53.
[64] Wan X, Cutler M, Song Z, Karma A, Matsuda T, Baba A, et al. New experimental evidence for mechanism of arrhythmogenic membrane potential alternans based on balance of electrogenic I(NCX)/I(Ca) currents. Heart rhythm. 2012;9:1698-705.
[65] Diaz ME, O'Neill SC, Eisner DA. Sarcoplasmic reticulum calcium content fluctuation is the key to cardiac alternans. Circulation research. 2004;94:650-6.
[66] Ramay HR, Liu OZ, Sobie EA. Recovery of cardiac calcium release is controlled by sarcoplasmic reticulum refilling and ryanodine receptor sensitivity. Cardiovascular research. 2011;91:598-605.
[67] Tomek J, Tomkova M, Zhou X, Bub G, Rodriguez B. Modulation of Cardiac Alternans by Altered Sarcoplasmic Reticulum Calcium Release: A Simulation Study. Frontiers in physiology. 2018;9:1306.
[68] Wang L, Myles RC, De Jesus NM, Ohlendorf AK, Bers DM, Ripplinger CM. Optical mapping of sarcoplasmic reticulum Ca2+ in the intact heart: ryanodine receptor refractoriness during alternans and fibrillation. Circulation research. 2014;114:1410-21.
[69] Casini S, Verkerk AO, van Borren MM, van Ginneken AC, Veldkamp MW, de Bakker JM, et al. Intracellular calcium modulation of voltage-gated sodium channels in ventricular myocytes. Cardiovascular research. 2009;81:72-81.
[70] Zhang H, Vassalle M. Role of dual pacemaker mechanisms in sinoatrial node discharge. Journal of biomedical science. 2000;7:100-13.
[71] DiFrancesco D, Noble D. The funny current has a major pacemaking role in the sinus node. Heart rhythm. 2012;9:299-301.
[72] Yaniv Y, Lakatta EG, Maltsev VA. From two competing oscillators to one coupled-clock pacemaker cell system. Frontiers in physiology. 2015;6:28.
[73] Kohajda Z, Tóth N, Szlovák J, Loewe A, Bitay G, Gazdag P, et al. Novel Na(+)/Ca(2+) Exchanger Inhibitor ORM-10962 Supports Coupled Function of Funny-Current and Na(+)/Ca(2+) Exchanger in Pacemaking of Rabbit Sinus Node Tissue. Frontiers in pharmacology. 2020;10:1632-.
[74] Kohajda Z, Loewe A, Tóth N, Varró A, Nagy N. The Cardiac Pacemaker Story-Fundamental Role of the Na(+)/Ca(2+) Exchanger in Spontaneous Automaticity. Frontiers in pharmacology. 2020;11:516.
[75] Torrente AG, Zhang R, Wang H, Zaini A, Kim B, Yue X, et al. Contribution of small conductance K(+) channels to sinoatrial node pacemaker activity: insights from atrial-specific Na(+) /Ca(2+) exchange knockout mice. 2017;595:3847-65.
[76] Weinberg S, Malhotra N, Tung L. Vulnerable windows define susceptibility to alternans and spatial discordance. American journal of physiology Heart and circulatory physiology. 2010;298:H1727-37.

[77] Zuanetti G, De Ferrari GM, Priori SG, Schwartz PJ. Protective effect of vagal stimulation on reperfusion arrhythmias in cats. Circulation research. 1987;61:429-35.
[78] Collins MN, Billman GE. Autonomic response to coronary occlusion in animals susceptible to ventricular fibrillation. The American journal of physiology. 1989;257:H1886-94.
[79] Song Y, Thedford S, Lerman BB, Belardinelli L. Adenosine-sensitive afterdepolarizations and triggered activity in guinea pig ventricular myocytes. Circulation research. 1992;70:743-53.
[80] Fukaya H, Plummer BN, Piktel JS, Wan X, Rosenbaum DS, Laurita KR, et al. Arrhythmogenic cardiac alternans in heart failure is suppressed by late sodium current blockade by ranolazine. Heart rhythm. 2019;16:281-9.
[81] Fox JJ, McHarg JL, Gilmour RF, Jr. Ionic mechanism of electrical alternans. American journal of physiology Heart and circulatory physiology. 2002;282:H516-30.
[82] Shiferaw Y, Watanabe MA, Garfinkel A, Weiss JN, Karma A. Model of intracellular calcium cycling in ventricular myocytes. Biophysical journal. 2003;85:3666-86.
[83] Li Y, Díaz ME, Eisner DA, O'Neill S. The effects of membrane potential, SR Ca2+ content and RyR responsiveness on systolic Ca2+ alternans in rat ventricular myocytes. The Journal of physiology. 2009;587:1283-92.
[84] Kanaporis G, Blatter LA. Membrane potential determines calcium alternans through modulation of SR Ca(2+) load and L-type Ca(2+) current. Journal of molecular and cellular cardiology. 2017;105:49-58.
[85] Hüser J, Wang YG, Sheehan KA, Cifuentes F, Lipsius SL, Blatter LA. Functional coupling between glycolysis and excitation-contraction coupling underlies alternans in cat heart cells. The Journal of physiology. 2000;524 Pt 3:795-806.
[86] Shkryl VM, Maxwell JT, Domeier TL, Blatter LA. Refractoriness of sarcoplasmic reticulum Ca2+ release determines Ca2+ alternans in atrial myocytes. American journal of physiology Heart and circulatory physiology. 2012;302:H2310-20.
[87] Díaz ME, Eisner DA, O'Neill SC. Depressed ryanodine receptor activity increases variability and duration of the systolic Ca2+ transient in rat ventricular myocytes. Circulation research. 2002;91:585-93.
[88] Belevych AE, Terentyev D, Viatchenko-Karpinski S, Terentyeva R, Sridhar A, Nishijima Y, et al. Redox modification of ryanodine receptors underlies calcium alternans in a canine model of sudden cardiac death. Cardiovascular research. 2009;84:387-95.
[89] Chudin E, Goldhaber J, Garfinkel A, Weiss J, Kogan B. Intracellular Ca(2+) dynamics and the stability of ventricular tachycardia. Biophysical journal. 1999;77:2930-41.
[90] Wan X, Laurita KR, Pruvot EJ, Rosenbaum DS. Molecular correlates of repolarization alternans in cardiac myocytes. Journal of molecular and cellular cardiology. 2005;39:419-28.

8 ACKNOWLEDGEMENT

I would like to express my sincere thanks to my PhD supervisor **Dr. Norbert Nagy**, for his professional advice, continuous support of my work and for introducing me to the research field of cardiac cellular electrophysiology.

I appreciate very highly the advice, comments and support of **Professor Julius Gy. Papp** MD, DSc, academician.

I am also grateful to **Professor András Varró** MD, DSc and **Dr. István Baczkó** for providing me the opportunity for conducting research as PhD student at the Department of Pharmacology and Pharmacotherapy, University of Szeged.

I would like to thank **Dr. Zsófia Nagy** for her work and personal guidance. I also thank **Dr. Noémi Tóth** and **Péter Gazdag**, MSc for their work and for their support during my PhD studies.

Journal of Molecular and Cellular Cardiology 153 (2021) 111–122

Contents lists available at ScienceDirect

Journal of Molecular and Cellular Cardiology

journal homepage: www.elsevier.com/locate/yjmcc

Original article

Blockade of sodium-calcium exchanger via ORM-10962 attenuates cardiac alternans

Jozefina Szlovák [a,1], Jakub Tomek [b,c,*,1], Xin Zhou [c], Noémi Tóth [a], Roland Veress [d], Balázs Horváth [d,e], Norbert Szentandrássy [d], Jouko Levijoki [f], Julius Gy. Papp [a,g], Neil Herring [b], András Varró [a,g], David A. Eisner [h], Blanca Rodriguez [c], Norbert Nagy [a,g]

[a] Department of Pharmacology and Pharmacotherapy, Faculty of Medicine, University of Szeged, Hungary
[b] Department of Physiology, Anatomy, and Genetics, University of Oxford, United Kingdom
[c] Department of Computer Science, University of Oxford, United Kingdom
[d] Department of Physiology, Faculty of Medicine, University of Debrecen, Hungary
[e] Faculty of Pharmacy, University of Debrecen, Hungary
[f] Orion Pharma, Espoo, Finland
[g] MTA-SZTE Research Group of Cardiovascular Pharmacology, Hungarian Academy of Sciences, Szeged, Hungary
[h] Unit of Cardiac Physiology, Manchester Academic Health Science Centre, University of Manchester, Core Technology Facility, Manchester, UK

ARTICLE INFO

Keywords:
Alternans
Sodium-calcium exchanger
Sodium-calcium exchanger inhibition
Canine myocytes
Cardiac simulation

ABSTRACT

Repolarization alternans, a periodic oscillation of long-short action potential duration, is an important source of arrhythmogenic substrate, although the mechanisms driving it are insufficiently understood. Despite its relevance as an arrhythmia precursor, there are no successful therapies able to target it specifically. We hypothesized that blockade of the sodium-calcium exchanger (NCX) could inhibit alternans. The effects of the selective NCX blocker ORM-10962 were evaluated on action potentials measured with microelectrodes from canine papillary muscle preparations, and calcium transients measured using Fluo4-AM from isolated ventricular myocytes paced to evoke alternans. Computer simulations were used to obtain insight into the drug's mechanisms of action. ORM-10962 attenuated cardiac alternans, both in action potential duration and calcium transient amplitude. Three morphological types of alternans were observed, with differential response to ORM-10962 with regards to APD alternans attenuation. Analysis of APD restitution indicates that calcium oscillations underlie alternans formation. Furthermore, ORM-10962 did not markedly alter APD restitution, but increased post-repolarization refractoriness, which may be mediated by indirectly reduced L-type calcium current. Computer simulations reproduced alternans attenuation via ORM-10962, suggesting that it is acts by reducing sarcoplasmic reticulum release refractoriness. This results from the ORM-10962-induced sodium-calcium exchanger block accompanied by an indirect reduction in L-type calcium current. Using a computer model of a heart failure cell, we furthermore demonstrate that the anti-alternans effect holds also for this disease, in which the risk of alternans is elevated. Targeting NCX may therefore be a useful anti-arrhythmic strategy to specifically prevent calcium driven alternans.

1. Introduction

The cardiac sodium-calcium exchanger (NCX) exchanges a single calcium ion for three sodium and is therefore electrogenic [1]. It links cardiac electrophysiology with cellular calcium handling as NCX is the primary path of calcium efflux from the cell [2]. The exchange may proceed in either direction, depending on ionic concentrations and membrane potential: *forward* mode (calcium efflux) or *reverse* mode (calcium influx). Given its central role in cellular function, it is not surprising that NCX is implicated in multiple arrhythmogenic phenomena, such as early afterdepolarizations [3], delayed afterdepolarizations [4], and alternans [5]. Experimental research of NCX was until recently complicated by a lack of specific NCX blockers [6]. However, the NCX blocker ORM-10962 has been shown to be a useful tool for the study of

* Corresponding author at: Department of Physiology, Anatomy, and Genetics, University of Oxford, United Kingdom.
E-mail address: jakub.tomek.mff@gmail.com (J. Tomek).
[1] Shared first authors.

https://doi.org/10.1016/j.yjmcc.2020.12.015
Received 1 February 2020; Received in revised form 8 December 2020; Accepted 21 December 2020
Available online 28 December 2020

NCX, given its selectivity and lack of strong preference to either mode of NCX [6]. While this drug does not block the L-type calcium current (I_{CaL}), it was nevertheless observed to reduce it indirectly, likely via calcium-driven inactivation [7]. ORM-10962 has been applied to the study of afterdepolarizations [6], but not cardiac alternans, which is the focus of this study.

Action potential duration (APD) alternans is the oscillation of long and short APD at rapid heart rates, and has been shown to precede the formation of arrhythmia in the heart [8,9]. Multiple studies suggest that the mechanisms of arrhythmia induction following alternans are linked to increased dispersion of repolarization [10–12]. The vulnerability of hearts to alternans considerably increases in many heart diseases, such as heart failure [13], hypertrophic cardiomyopathy [14], or myocardial infarction [12,15,16]. APD alternans typically occurs concurrently with oscillation of calcium transient (CaT) amplitude [17,18], presenting the question which of these two is the main driver. It is possible that steep restitution of APD drives alternans [19]. However, further studies suggested that CaT oscillations are the primary driver [20], subsequently translated into APD alternans by NCX and other calcium-sensitive currents [21].

Given the possible involvement of NCX in alternans, ORM-10962 may be a promising antiarrhythmic strategy, particularly in cardiac diseases with elevated risk of alternans. However, the precise effect of NCX blockade on alternans is not necessarily straightforward. If we assumed a constant level of CaT alternans, NCX blockade would clearly reduce APD alternans. However, the assumption of constant CaT alternans following NCX blockade may not hold. On the one hand, it has been suggested that CaT alternans occurs if there is a steep dependence of calcium efflux from the cell on the SR calcium content [22]. Inhibition of NCX will make this dependence less steep and might therefore decrease alternans. On the other hand, CaT alternans is mostly thought to arise from increased sarcoplasmic reticulum release and CaT amplitude [11,23]. Therefore, the effect of NCX block, reducing efflux and locking more calcium in the cell, could be an increase in SR loading and thus release, increasing alternans. This could subsequently negate the reduction in APD alternans, or even extend the presence of alternans to slower pacing rates, which would be proarrhythmic. The aim of this study was therefore to characterize the effect of NCX blockade on both APD and CaT alternans and provide insight into the mechanisms involved.

2. Materials and methods

2.1. Experimental methods

2.1.1. Ethical statement

All experiments were carried out in compliance with the Guide for the Care and Use of Laboratory Animals (USA NIH publication No 85–23, revised 1996) and were approved by the Csongrád County Governmental Office for Food Safety and Animal Health, Hungary (approval No.: XIII/1211/2012). The ARRIVE guidelines were adhered to during the study, (NC3Rs Reporting Guidelines Working Group, 2010).

2.1.2. Standard microelectrode technique

Beagle dogs of either sex weighing 8 to 16 kg obtained from a licensed supplier were used for the study. Following sedation of the dogs with xylazine (1 mg/kg, *i.v.)* and thiopental (30 mg/kg *i.v.*), each heart was rapidly removed through a right lateral thoracotomy and immediately rinsed in oxygenated Locke's solution. Action potentials were recorded at 37 °C from the surface of dog right ventricular papillary muscles using conventional microelectrode technique. A total of $n = 13$ preparations were recorded from $n = 9$ hearts, and clustering analysis was carried out to ascertain that pseudoreplication did not occur when more than one preparation per heart was measured (Appendix F). The preparations were mounted in a custom made plexiglass chamber, allowing continuous superfusion with O_2-CO_2 saturated Locke's solution (containing in mM: NaCl 120, KCl 4, $CaCl_2$ 1.0, $MgCl_2$ 1, $NaHCO_3$ 22, and glucose 11). The pH of this solution was set between 7.35 and 7.4 when saturated with a mixture of 95% O_2 and 5% CO_2 at 37 °C. The tissue samples were stimulated with constant current pulses of 1 ms duration at a rate of 1 Hz through a pair of bipolar platinum electrodes using an electrostimulator (Hugo Sachs Elektronik, model 215/II). The stimulus electrode was placed at the proximal site of the papillary muscle providing impulse propagation towards the tendons. Sharp microelectrodes with tip resistance of 10–20 MΩ, when filled with 3 M KCl, were connected to an amplifier (Biologic Amplifier, model VF 102). Voltage output from the amplifier was sampled using an AD converter (NI 6025, Unisip Ltd). Alternans was evoked by application of 20 beats at cycle lengths of 250 ms to 160 ms. Efforts were made to maintain the same impalement throughout the whole experiment. When the impalement was dislodged, an adjustment was attempted. The measurements were only continued if the action potential characteristics of the re-established impalement deviated less than 5% from the previous one. APD alternans were measured at a following pre-defined pacing cycle lengths: 250, 230, 210, 190 and 170 ms. After recording the control pacing protocol, 1 μM ORM-10962 was employed and alternans protocol was repeated.

2.1.3. Cell isolation

Ventricular myocytes were enzymatically dissociated from dog hearts. The excised left ventricular segments were perfused through the left anterior descending coronary artery using a gravity flow Langendorff apparatus. The perfusate was a modified Tyrode solution (composition in mM: NaCl 144, NaH_2PO_4 0.4, KCl 4.0, $MgSO_4$ 0.53, glucose 5.5) supplemented with 1.2 mM $CaCl_2$, 10 mM HEPES, 20 mM taurine, and 1.6 mM Na-pyruvic acid (pH = 7.2 with NaOH). After removal of the blood the perfusate was switched for 10 min to nominally Ca^{2+}-free Tyrode. Dispersion of cells was achieved by application of 0.5 g/l collagenase (Sigma type I) for 40 min in the presence of 50 μM $CaCl_2$. During the isolation procedure the solutions were gassed with 100% oxygen and the temperature was maintained at 35 °C. Finally, the tissue was minced and gently agitated. The cells, freshly released from the tissue, were stored at room temperature before use. At least 60% of the cells were rod-shaped and showed clear striation when the external Ca^{2+} was restored. One drop of cell suspension was placed in a transparent recording chamber mounted on the stage of an inverted microscope (Olympus IX71, Olympus, Tokyo, Japan), and individual myocytes were allowed to settle and adhere to the chamber bottom for at least 5–10 min before superfusion was initiated and maintained by gravity. Only rod-shaped cells with clear striations were used. HEPES-buffered Tyrode's solution served as the normal superfusate.

2.1.4. S1S2 restitution

In order to determine the recovery kinetics of APD_{80} extra test action potentials were elicited by using single test pulses (S2) in a preparation constantly paced in a basic cycle length of 1000 ms. The S1-S2 interval was increased progressively from $APD_{80} - 50$ ms to $APD_{80} + 500$ ms. The effective refractory period was defined as the longest S2 coupling interval that did not lead to an action potential developing in the tissue sample. In addition, postrepolarization refractoriness (PRR) was inferred from the S1S2 restitution protocol. PRR was defined as the shortest diastolic interval between the S1 and S2 stimuli that led to a propagation of an action potential (this corresponds to ERP - APD(S1), where APD (S1) is the APD80 of the S1 stimulus and ERP is the effective refractory period).

2.1.5. Calcium transient measurements

CaTs were recorded using a Ca^{2+}-sensitive fluorescent dye, Fluo-4 AM simultaneously with ionic current measurements. Cardiomyocytes isolated from the left ventricle were loaded with 5 μM Fluo 4-AM for 15 min at room temperature in the dark. Loaded cells were mounted in a

low volume imaging chamber (RC47FSLP, Warner Instruments) and field stimulated with a pair of platinum electrode. Frequency pattern was applied by using Evokewave v1.49 software. Fluorescence measurements were performed on the stage of an Olympus IX 71 inverted fluorescence microscope. The dye was excited at 480 nm and the emitted fluorescence is detected between 515 and 550 nm. Optical signals were sampled at 1 kHz and recorded by a photon counting photomultiplier module (Hamamatsu, model H7828). Data acquisition and analysis were performed using Axon Digidata 1550B System. All CaTs were measured at 37C°. In order to calibrate the records, alterations in $Ca^{2+}{}_i$ were calibrated after disruption of the cells by a patch pipette, by using the following equation for Fluo-4:

$$Ca^{2+}{}_i = Kd^*(F - F_{min})/(F_{max} - F)$$

2.2. Signal analysis

APD alternans was extracted based on four consecutive action potentials as the difference between average APDs of even and odd AP. The electrophysiological measurements were at most 1 s long, yielding four action potentials at the longest cycle length of 250 ms. A custom-written Matlab script was used for this purpose. The four beats were smoothed via zero-phase digital filtering (@filtfilt in Matlab) with diameter of 10 ms. The baseline of such signal was taken as the 2.5-percentile of the signal, and the peak as the 99.5-percentile. Based on this, the thresholds (membrane potential levels at which APD is measured) for APD25 (25% repolarization, i.e., mainly plateau duration) and APD80 (80% repolarization) were computed. Each threshold was applied to the whole 4-beat recording, rather than being estimated from each AP separately. This is to avoid "threshold alternans" where alternation of AP peak potential induces alternation of the thresholds, which taints the estimation of the degree of alternans. In the majority of recordings of APD alternans, the basic cycle lengths used were 170, 190, 210, 230, and 250 ms. In several preparations, slightly different basic cycle lengths were used – in such a case, the alternans at the above-mentioned basic cycle lengths was obtained interpolation (e.g., *alternans* at 170 ms basic cycle length would be obtained as the average of alternans at 160 and 180 ms if these two were available). When diastolic intervals were measured, they were taken as the periods between segments corresponding to APD80 of action potentials. The first and last such diastolic intervals were discarded as they are typically incomplete.

Calcium alternans in the experiments was based on six consecutive CaTs, where the average CaT amplitude was computed for even and odd beats. The signal was separated into CaTs using the 'comb' algorithm for fixed-rate pacing [24]. The amplitude of a single CaT was estimated as the difference between the peak and the minimum directly preceding the given CaT (i.e., it is the CaT upstroke amplitude). CaT alternans is expressed as the ratio of the amplitudes of the larger to the smaller CaT.

Three subtypes of APD alternans were defined based on the phase of alternans at the levels of 25% and 80% repolarization:

- Recordings of the '++' alternans type manifest concurrent prolongation (or concurrent shortening) by at least 3 ms both at the 25% and 80% repolarization level. I.e., oscillations of APD at the 25% and 80% levels are in phase.
- Recordings of the '+−' alternans manifest concurrent prolongation by at least 3 ms at the 25% repolarization level and shortening by at least 3 ms at the 80% repolarization level (or vice versa). I.e., oscillations of APD at the 25% and 80% levels are in the opposing phase.
- Recordings of the '+0' are recordings manifesting shortening or prolongation by at least 3 ms at the 25% repolarization level, while the prolongation or shortening at the 80% level is less than 3 ms. I.e., there is clear APD25 alternans, but not APD80 alternans.

When analysing experimental S1S2 restitution protocol, the APD was measured at 80% level of repolarization using Evokewave v1.49 software (Unisip Ltd).

2.3. Computer simulations

ToR-ORd, a recent robustly validated human ventricular myocyte model, was used throughout this study [25], being selected for its improved representation of L-type calcium current and sodium and calcium balance compared to its predecessors. This model is capable of reproducing calcium-driven alternans stemming from refractoriness of Ca^{2+} cycling in the sarcoplasmic reticulum; the mechanism is described in detail in [23]. It is therefore more suitable for this study than other human ventricular models, such as Grandi et al. [26], which does not manifest alternans, or Ten Tusscher et al. [27], which manifests alternans, but one that is driven by APD restitution (which is shown not to be the key cause of alternans in the experiments in this study). Simulations using a human model provide a bridge for the interpretation and translation of the findings obtained using animal experiments towards clinically-relevant outcomes. The effect of ORM-10962 on ionic dynamics was modelled as reducing NCX availability to 50% and reducing I_{CaL} availability to 65% as observed experimentally [7]. Additional experiments were carried out to verify that even at rapid pacing used in this study, the NCX block achieved with the given ORM-10962 concentration is close to 50% (Appendix G).

Originally, we also considered the most up-to-date canine model of the Rudy family [28]. However, when simulating the effect of ORM-10962, the canine model predicted a substantial APD prolongation not seen in our experimental data (see Fig. 3; mean APD at DI of 500 ms is 183 ± 31 ms for ORM-10962, and 198 ± 23 ms for control; $p = 0.28$) or that of others [6]. Subsequent analysis revealed that the APD prolongation in the canine model is linked to artefactual lack of I_{Kr} activation following AP plateau lowering (which follows from I_{CaL} reduction). This is a manifestation of a problem which warranted the replacement of the I_{Kr} model in development of ToR-ORd [25]. For this reason, and given that there are no known differences between canine and human calcium handling pertaining to the phenomena studied there, we believe that ToR-ORd is the best model choice.

The S1-S2 protocol was simulated by first prepacing the cell during 1000 beats at 1 Hz (S1), followed by a single S2 stimulus at varying S1-S2 intervals = 150, 152, 154, …350, and then 400, 500, 600, …, 1000. For this protocol, the I_{Na} conductance was reduced to 25% to more clearly demonstrate the role of I_{CaL} in cellular excitability (see Section 3.4 for more details). The reaction to S2 stimulus was classified as an action potential if the peak membrane potential exceeded 10 mV.

When evaluating ERP in single cell for the investigation of post-repolarization refractoriness, this was defined as the longest S2 coupling interval that did not trigger a S2 AP.

2.3.1. Population of models construction

A population of ToR-Ord models was created by simulating 5000 models with perturbation of conductances of the following ionic currents: I_{Na}, I_{NaL}, I_{CaL}, I_{to}, I_{NaK}, I_{NaCa}, I_{Kr}, I_{Ks}, I_{K1}. Each current in each model was sampled in the 50–200% range (corresponding to a multiplier of 0.5–2), using symmetric sampling where the probability of x is the same as 1/x. The formula used to obtain each multiplier is $e^{(U(0,1)-0.5)\cdot\frac{\log(2)}{0.5}}$, where U(0,1) is random number uniformly sampled between 0 and 1. It can be seen that e.g. for the random number being 0 and 1, the resulting values of multiplier are 0.5 and 2 respectively. This approach ensures that approximately half of multipliers is below 1 and a half is above 1 (as opposed to uniformly sampling between 0.5 and 2 straight away, which will assign only a third of generated values below 1, and two thirds above 1, overrepresenting current conductance increase on average).

A calibration to human experimental data was carried out using the

following criteria:

- APD40, APD50, APD90, triangulation (APD90-APD40), peak upstroke velocity, and resting potential within experimental range, as in population of models construction in [29].
- Calcium transient duration is within standard deviation of the data in [30].
- The model manifests alternans at at least one of the tested basic cycle lengths (240, 250, …, 340 ms).

A total of 684 models fulfilled all the criteria, and these were subsequently used to compare alternans onset between the model and four simulated versions of NCX blockade (50% NCX availability + 50, 65, 70, and 80% I_{CaL} availability respectively).

2.3.2. Heart failure simulations

Heart failure remodelling was introduced in the ToR-ORd model, mainly based on studies summarized and used in [31]. Similarly to their study, we increased the conductances of I_{NaL} by 80%, I_{NaCa} by 50%, I_{Cab} by 53%, and reduced the conductance of I_{to} by 60%, I_{K1} by 32%, and I_{NaK} by 30%. In addition, the time constant of I_{NaL} inactivation τ_{hL} was increased by 80%, CaMKII autophosporylation rate was increased by 50%, and J_{leak} (leak from NSR to main cytosolic compartment) by 30%. The rate of SR reuptake via SERCA pumps J_{up} was reduced by 30% and SR release was made 20% more sensitive to calcium in the junctional SR.

In addition, we added an explicit leak flux $J_{leak,JSR}$ to the ryanodine receptor to represent increased ryanodine receptor leakiness present in heart failure [32]. The formulation is based on the $J_{leak,JSR}$ in [28]:

$$e^{\frac{Ca_{JSR}}{20}} \cdot (Ca_{JSR} - Ca_{SS})$$

Ca_{JSR} is the calcium concentration in the junctional SR, and Ca_{SS} is the calcium concentration in the junctional subspace.

Furthermore, the time constant of SR release was increased six-fold to represent the phenotype of SR release present in heart failure, where calcium sparks have markedly longer time to peak and duration [33,34]. Its precise magnitude is however not known. This change is very important for the increased vulnerability of the simulated heart failure cell to alternans by mechanism described in [23].

Ultimately, the sensitivity of SR uptake to intracellular calcium concentration was reduced, as this was also observed in heart failure [35]. This was achieved by shifting the half-activation of the SERCA reuptake as follows (for nonphosphorylated and phosphorylated reuptake):

$$J_{up,NP} = 0.005425 \cdot \frac{Ca_i}{Ca_i + 0.00092 + \mathbf{0003}}$$

$$J_{up,P} = 2.75 \cdot 0.005425 \cdot \frac{Ca_i}{Ca_i + 0.00075 + \mathbf{0003}}$$

The elements in bold were added to achieve the desensitization.

2.3.3. S1S2 in simulated cardiac fibre

The 1D fibre tissue simulations were conducted using the open-source software CHASTE [36]. The homogeneous monodomain 1D endocardial fibres had a length of 4 cm consisting of 200 nodes, with a conductivity of 1.64mS/cm to achieve a diffusion coefficient of 1.171 cm2/s [37]. The 1D fibres were paced under an S1-S2 protocol: regular S1 stimulus was applied with a cycle length of 1000 ms for 20 beats, followed by a single S2 stimulus; the coupling intervals simulated were 150, 152, 154, …, 450, and then 500, 600, …, 1000. Restitution curves were measured at the centre of the fibre. As in single cell restitution, I_{Na} conductance was reduced to 25%.

When evaluating ERP in a fibre for the investigation of post-repolarization refractoriness, this was defined as the longest S2 coupling interval that did not trigger a S2 AP in the cell at position x = 2 cm.

2.4. Statistical methods

Paired *t*-test was used for paired comparisons (Figs. 1B,C, 3B,C, 6A). Wilcoxon rank-sum test was used for unpaired comparisons (Fig. 1E), used over unpaired t-test given markedly different variance between the groups. The statistical significance level used was $\alpha = 0.05$.

3. Results

3.1. NCX blockade via ORM-10962 inhibits alternans of APD and CaTA

APD alternans was measured in canine papillary muscle preparations at two repolarization levels (25% and 80%), both in control conditions and after the application of ORM-10962 (Fig. 1A). ORM-10962 significantly attenuated APD25 at most basic cycle lengths (Fig. 1B). Alternans of APD80 was significantly attenuated only at the slowest pacing (basic cycle lengths 230 and 250) (Fig. 1C). To complement the electrophysiological recordings of alternans, calcium imaging measurements were additionally taken in isolated cells. These recordings confirmed that calcium transient amplitude alternans was also potently and significantly attenuated by ORM-10962 at 230 ms bcl (Fig. 1D,E).

Investigating the relationship between APD25 and APD80 alternans, we observed three types of behaviour. In the '++' type, the APD is prolonged/shortened at both levels of repolarization, at the same time between subsequent action potentials (Fig. 2A). In type '+−', the APD is prolonged at one level, but shortened at the other one (Fig. 2B). Ultimately, in type '+0', there is visible alternans at the APD25 level, but none at APD80 (Fig. 2C). All three types were present in control and ORM-10962 conditions, with ORM-10962-treated cells showing fewer recordings of the '++' type and more of the '+−' type (Fig. 2D,E). The analysis of transitions of alternans types before and after ORM-10962 treatment shows that many '++' recordings changed into the '+0' type with ORM10962, while '+0' recordings either stayed in the same class or transitioned towards the '+− ' type (Fig. 2F). We can thus see a pattern where a given APD25 prolongation during alternans is associated with less APD80 prolongation or even with its shortening following ORM-10962 treatment.

We carried out additional exploration of the effect of ORM-10962 on the three different alternans types reported above (Appendix B). Consistent with near-universal alternans attenuation observed for APD25 (Fig. 1B), alternans was generally attenuated by ORM-10962 for all alternans types (Appendix A, Supplementary Fig. 1A). However, the situation is different for alternans of APD80, where there was a marked difference in response of preparations manifesting '++' and '+0' alternans before the drug treatment (the number of cases of '+−' alternans is too low to allow drawing conclusions). Whereas alternans was attenuated in the vast majority of cases of '++' alternans (18 attenuated, 1 unchanged, 1 promoted; mean response is attenuation by 4.9 ms), the situation is much less clear for the '+0' type (8 attenuated, 3 unchanged, 9 promoted; mean response is promotion by 1.47 ms) (Appendix A, Supplementary Fig. 1B). In addition, the '++' type was prevalent for the slower pacing rates (basic cycle length of 230 or 250), but not for the faster ones (Appendix A, Supplementary Fig. 1C), which helps to explain why APD80 alternans attenuation was observed only for the slower pacing rates in Fig. 1C. In terms of absolute magnitude, APD80 alternans was the greatest in the '++' type, while being by definition minimal in the '+0' type (Appendix A, Supplementary Fig. 1D).

3.2. Alternans attenuation via ORM-10962 is not due to restitution of APD

We subsequently sought to determine the mechanism of alternans formation and its attenuation. We first explored the restitution-driven mechanism of APD alternans [19]. There the alternans arises from the slope of the restitution curve exceeding 1 for diastolic intervals (DI)

between the alternating beats. We measured restitution curves using the S1-S2 protocol in canine ventricular muscle preparations (Fig. 3A). Before ORM-10962 application, 5 out of 8 hearts did contain an interval of the restitution curve with slope > 1 and 3 out of 8 contained such an interval after ORM-10962 application. The change in the peak slope after the application of ORM-10962 was not statistically significant (Fig. 3B, p = 0.84). The longest diastolic interval with slope > 1 was extracted in each recording (Fig. 3C), with the hypothesis that if diastolic intervals observed during alternans fall within the zone of restitution slope > 1, the restitution is a plausible explanation of APD alternans. The fact that in no recording the zone of slope > 1 extended beyond DI = 60 ms essentially excludes the restitution-based mechanism as the driver of alternans in our data, given that DI < 60 ms were rarely observed in alternans recordings. Only 4 out of 68 recordings of bcl ≥ 210 ms had the shorter DI below the observed maximum of 60 ms, and none had the shorter DI below 35 (median of points shown in Fig. 3C; both groups pooled). APD alternans was also present at 250 ms bcl pacing, where the shorter DIs are typically close to 100 ms, i.e., both short and long DI were outside the zone of steep restitution. Together, these observations indicate that alternans we observed is not driven by APD restitution, but potentially by calcium oscillations.

3.3. Computational simulations illuminate the role of altered balance of calcium handling in alternans attenuation

Using the human ventricular myocyte ToR-ORd model [25], we then ran simulations of the action of ORM-10962 on calcium-driven alternans to gain further mechanistic understanding into the attenuation of calcium-driven alternans. The control ToR-ORd model manifests calcium-driven alternans for base cycle length of 280 ms and faster (Fig. 4A). The mechanism is linked to refractoriness of SR calcium cycling: following a large release at rapid pacing, the junctional SR is not replenished fully before the next beat, leading to CaT amplitude oscillations [23]. ORM-10962 was represented as a combined reduction of NCX and I_{CaL} (Methods 1.3). To gain a broader picture of the role of I_{CaL} reduction, we simulated five different levels of I_{CaL} availability (50%, 65%, 70%, 80%, and 100%) in addition to a 50% reduction of NCX. Interestingly, all studied combinations of NCX and reduced I_{CaL}

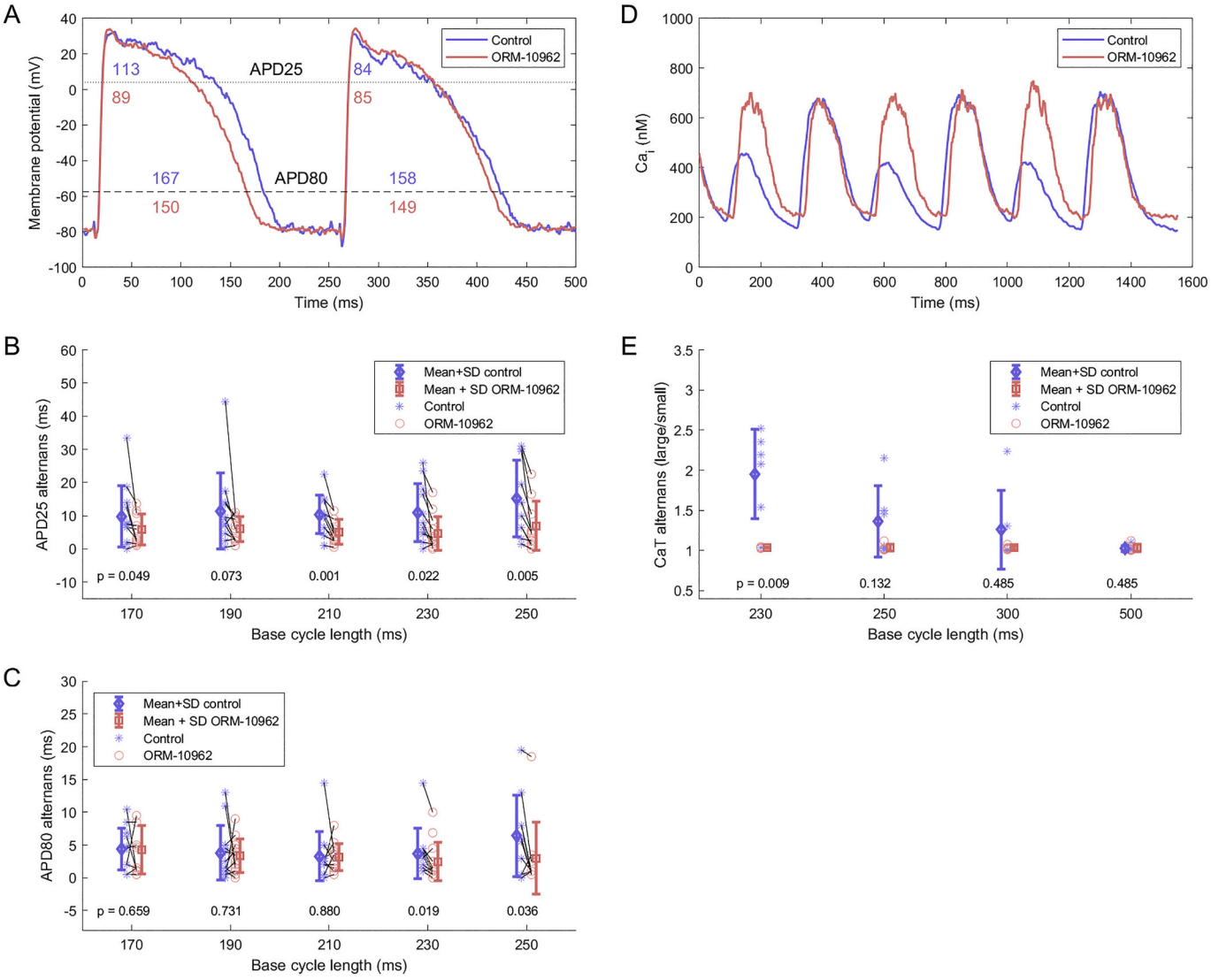

Fig. 1. Alternans attenuation via ORM-10962. A) Example of APD alternans at two levels (APD25 and APD80) in control condition and following ORM-10962 exposure in muscle preparations. B) APD25 alternans at a range of pacing rates (n = 13). C) APD80 alternans at a range of pacing rates (n = 13). In B,C, paired t-test was used to compute the p-values. D) Example of reduction in CaT alternans in isolated cells via ORM-10962. E) Quantitative summary of CaT alternans (expressed as the ratio between the amplitude of the larger versus smaller CaT) without (n = 6) and with (n = 6) ORM-10962. Unpaired rank-sum test was used in E given different variance between control and ORM-10962.

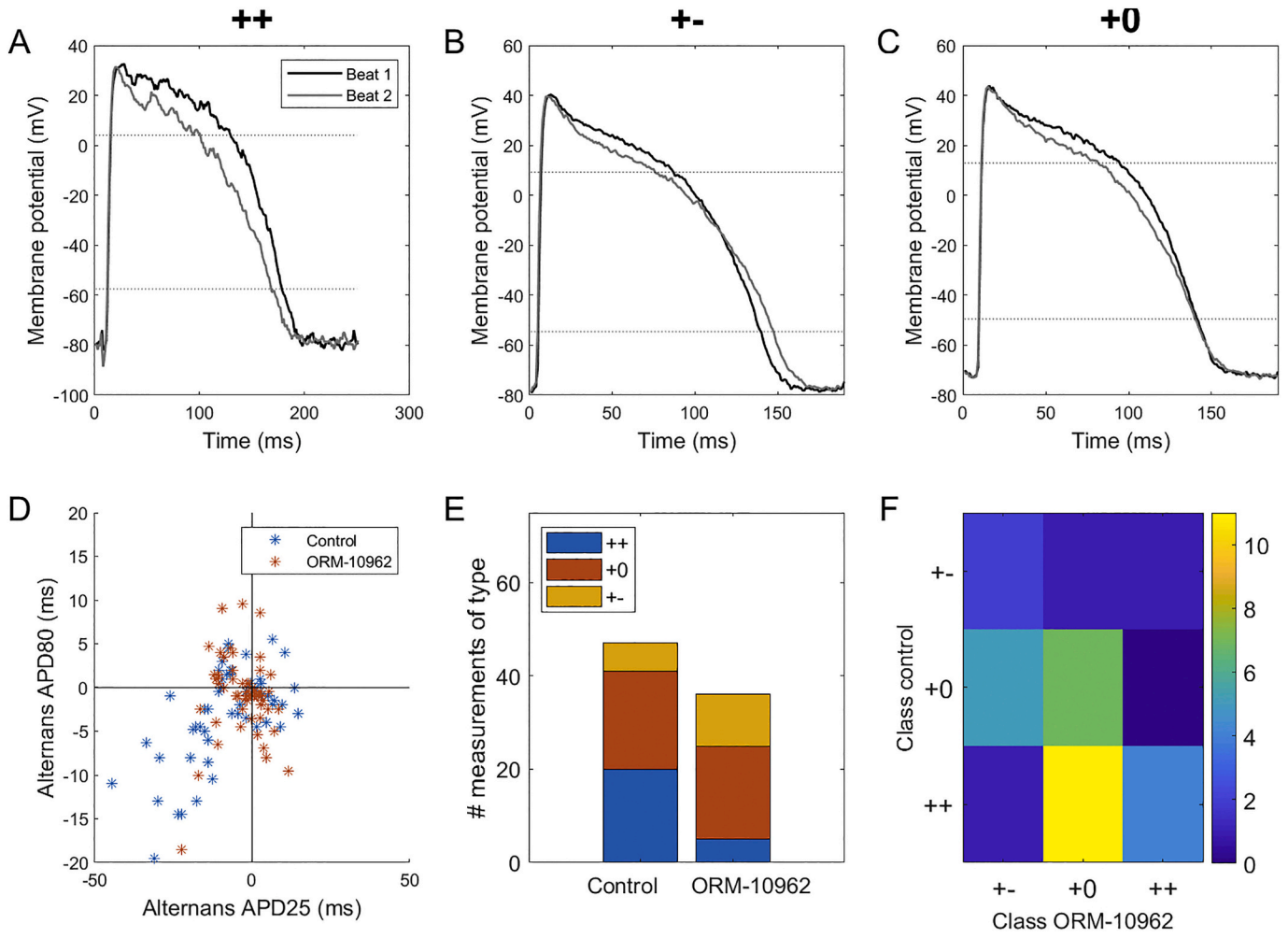

Fig. 2. Distinct patterns of alternans at two repolarization levels. A-C) Examples of '++', '+−', and '+0' types of alternans respectively (i.e., shortening plateau corresponds to prolonged, shortened, or unchanged APD at 80% level of repolarization). The three recordings shown were obtained at bcls of 250, 190, and 190 ms respectively. D) Correlation of the difference in consecutive APDs at repolarization levels of 25% and 80%; all tested bcls were pooled together in this plot. E) Composition of the three alternans types in the control condition and following ORM-10962 treatment. The lower total number of entries following ORM-10962 stems from alternans attenuation by the compound: a recording has to manifest alternans of at least 3 ms at the APD25 level in order to be classified as one of the three types. F) A transition matrix encoding the change in alternans type upon ORM-10962 application. Each matrix element colour-codes the number of preparations manifesting a given type of alternans in the control condition (y-axis) that transitioned into a given type of alternans after ORM-10962 application (x-axis).

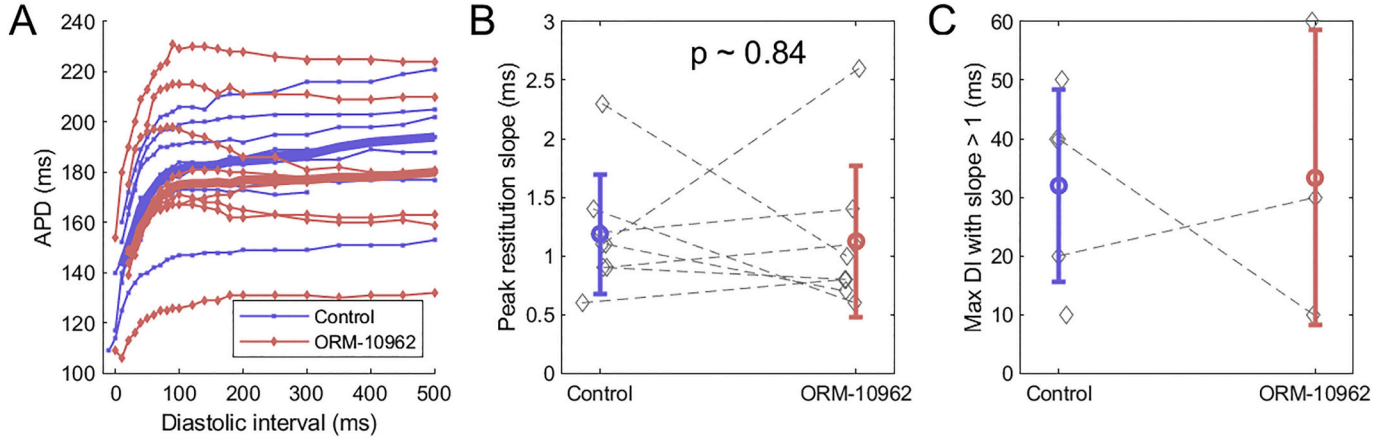

Fig. 3. ORM-10962 and restitution properties. A) Restitution curves measured before and after application of ORM-10962 to canine tissue samples ($n = 8$). Thick lines give the median S2 APD (computed where at least 3 data points are available for the given diastolic interval). B) Paired measurements of maximum slope of the restitution curve before and after ORM-10962; the overlay gives mean ± SD. C) Longest diastolic interval before which the slope of restitution curve is greater than 1; the overlay gives mean ± SD.

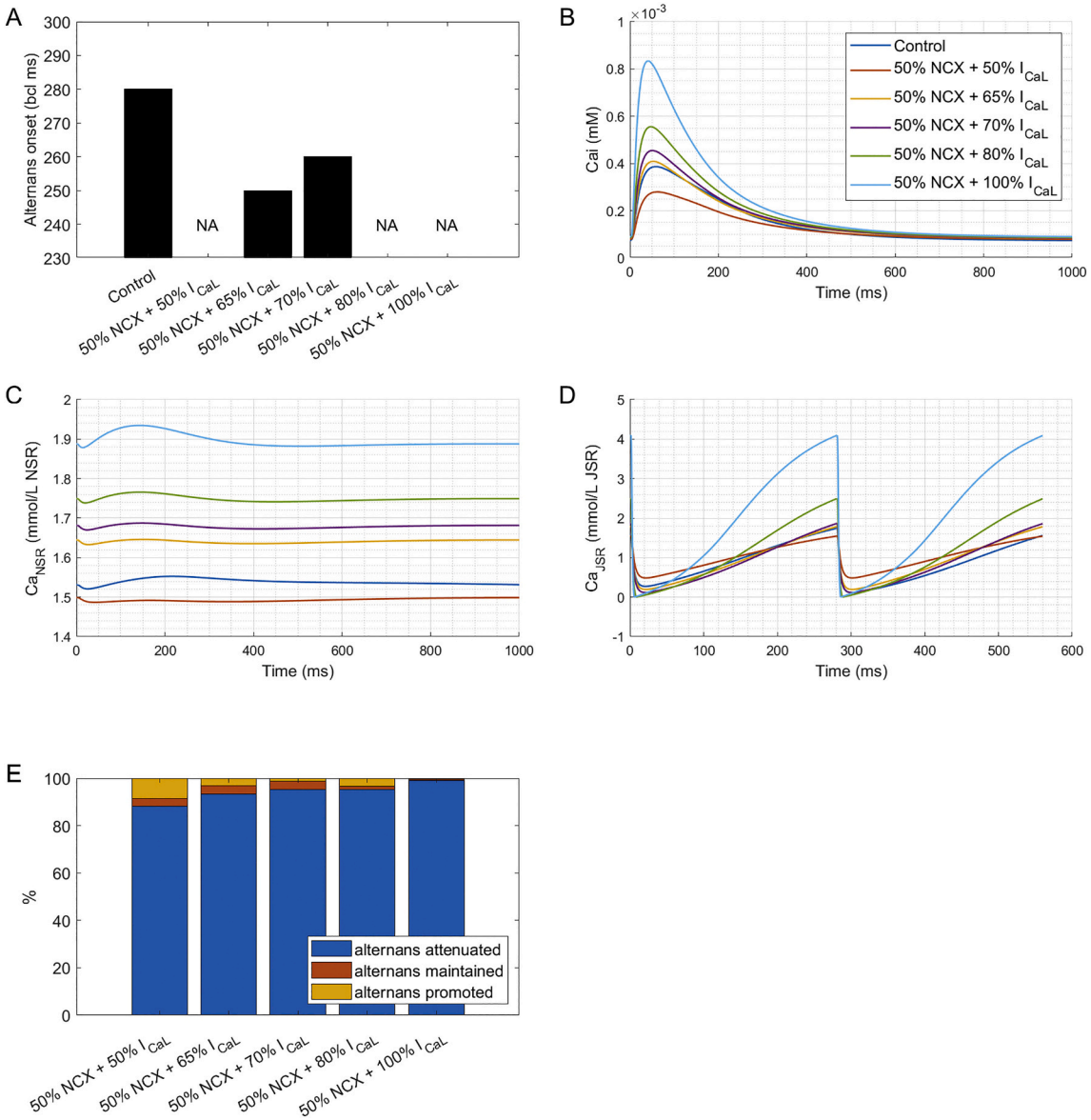

Fig. 4. Simulations of alternans and ORM-10962. A) The longest basic cycle length at which was alternans detected in control condition and several combinations of NCX and I_{CaL} availability representing simulated ORM-10962 (NA = not available = no alternans). See Appendix C for a full frequency-alternans relationship at all the studied conditions. B) Calcium transient at 1000 ms bcl pacing. C) Calcium concentration in the network SR at 1000 ms bcl pacing. D) Calcium concentration in the junctional SR at 280 ms bcl pacing. E) A breakdown of the effect of five treatments simulating ORM-10962 (50% NCX availability and the five listed availabilities of I_{CaL}) compared to the baseline model using a population of models approach. For each of 684 tested models in the population and for each treatment, a simulation was classified as 'alternans attenuated' if the treatment shifted alternans onset to shorter basic cycle length, 'alternans promoted' if alternans onset was shifted to longer basic cycle lengths, and 'alternans maintained' if alternans first appeared at the same basic cycle length. See Appendix D for a breakdown of how much was alternans promoted or attenuated in each condition.

availability led to alternans attenuation as assessed by moving alternans onset to faster frequencies, or abolishing alternans altogether (Fig. 4A); however, the mechanisms are distinct.

The case closest to experimental measurements is 50% NCX reduction and 65–70% I_{CaL} availability, which exerts a small or moderate increase in CaT amplitude compared to control ToR-ORd cell at 1 Hz pacing (Fig. 4B). This agrees with a previous study on ORM-10962 showing only a minor increase in calcium transient amplitude [6] and experimentally observed 65% I_{CaL} availability for 50% NCX availability after ORM-10962 treatment [7], Appendix G. The mechanism of alternans attenuation in such a setting is best illustrated on the case of 65% I_{CaL} availability: even though the CaT amplitude is almost identical to the control cell, the calcium loading of the network sarcoplasmic reticulum is increased at all tested pacing rates (example at 1 Hz in Fig. 4C). Consequently, the gradient between the network and junctional SR is increased, allowing faster refilling of the junctional SR, reducing SR refractoriness, inhibiting alternans [23].

A substantial increase in CaT amplitude compared to control cell is observed when I_{CaL} availability is 80% or 100% (Fig. 4B), and in these cases, no alternans is found (Fig. 4A). Inspection of the contents of junctional SR at base cycle length 280 (where the control model already shows alternans) reveals that the junctional SR is fully depleted in both beats in such conditions (Fig. 4D). The phenomenon of full SR depletion and consequent alternans abolishment in simulations was characterised previously [23], but its physiological relevance is debatable. Importantly, we note that in the cases of 65% and 70% I_{CaL} availability described above, the junctional SR is clearly not fully depleted at 280 ms bcl (Fig. 4D), verifying that the full depletion of junctional SR is not the

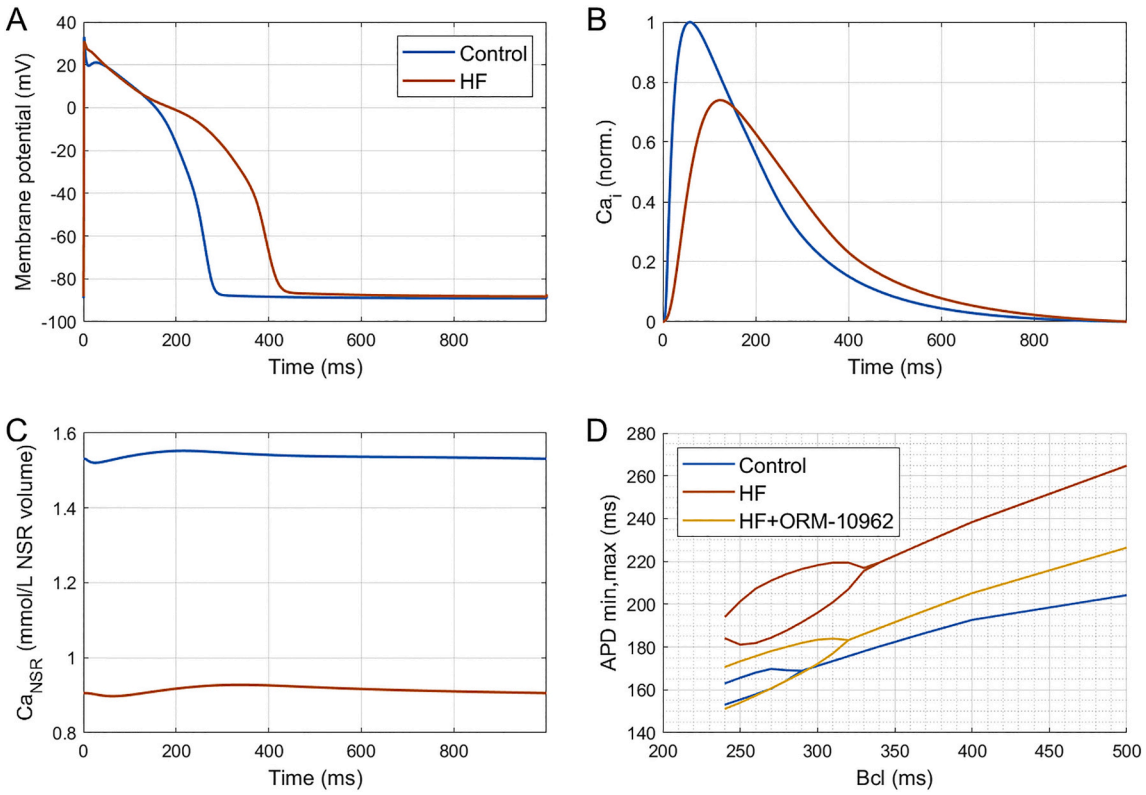

Fig. 5. Simulations of heart failure remodelling and alternans. A) Action potential in control and heart failure (HF) condition at 1 Hz pacing, showing APD prolongation and loss of notch following the peak in HF. B) Calcium transient in control and HF, showing its prolongation, prolonged time to peak, and reduced amplitude. The calcium transient was normalised between 0 and 1 to facilitate comparison: first, the minimum was subtracted from both calcium transients; second, both calcium transients were divided by the maximum of the control trace, preserving the ratio of amplitude between control and HF. C) Calcium concentration in the network SR showing reduced SR loading in HF. D) Simulation of the effect of heart failure (HF) remodelling and HF + ORM-10962 treatment (50% NCX + 65% I_{CaL}) on alternans development. For each model, the minimum and maximum APD90 achieved over two subsequent beats at the given basic cycle length is given, with bifurcations indicating alternans. Small-amplitude alternans in the HF condition developed already at bcl of 330 ms.

mechanism of alternans attenuation in these cases.

When the availability of I_{CaL} is low (50%), alternans is also never present (Fig. 4A). Given the CaT amplitude is considerably diminished (Fig. 4B), the lack of alternans is clear: calcium alternans stems from a greater calcium release, and when the release is not sufficiently large, there is no alternans. However, no such reduction in CaT amplitude was observed upon ORM-10962 application [6], and so this explanation can be excluded.

In order to assess the sensitivity of the results to specific parameter values in the ToR-ORd model, we further investigated the impact of simulated ORM-10962 on alternans using the population of models approach [29,38]. A population of 684 simulated cells calibrated to human experimental data was used (see Methods for details), and each cell was simulated in normal conditions and with five levels of I_{CaL} availability accompanying a 50% NCX block as above. In all five conditions, the vast majority of models showed alternans attenuation compared to the control model (over 88%, Fig. 4E), supporting the relevance of the anti-alternans effect of ORM-10962. Furthermore, additional analyses revealed that the mechanism underlying a substantial part of the cases of alternans promotion (including all the cases of alternans promotion at 50% or 65% I_{CaL}) has debatable relevance (Appendix B).

3.4. Validation of the anti-alternans effect of ORM-10962 in simulated heart failure

Even though alternans can usually arise even in healthy myocardium, its importance is even greater in cardiac diseases such as heart failure with reduced ejection fraction, where it manifests at slower pacing rates, often preceding the formation of ventricular fibrillation [8,13]. To assess the anti-alternans potential of ORM-10962 in heart failure, we incorporated a broad range of experimental data on heart failure remodelling in the baseline ToR-ORd model (see Methods). The resulting model replicates key hallmarks of human heart failure, such as APD prolongation and loss of spike-and-dome morphology (Fig. 5A) [39], reduced amplitude of calcium transient, along with the prolongation of its duration and time to peak (Fig. 5B) [40], and reduced calcium loading of the sarcoplasmic reticulum (Fig. 5C) [39].

Importantly, the onset of alternans in the control model (280 ms bcl) is shifted by heart failure remodelling to slower frequencies (330 ms bcl) (Fig. 5D), consistent with experimental observations [8,13]. The amplitude of repolarization alternans is also increased by the heart failure remodelling, leading to potentially greater dispersion of repolarization induced by alternans and thus a higher arrhythmic risk. Crucially, simulated ORM-10962 (using the data-driven version of 50% NCX and 65% I_{CaL} availability) attenuated alternans in the failing cell, both with regards to the alternans onset (310 versus 330 ms) and amplitude at most basic cycle lengths (Fig. 5D).

3.5. ORM-10962 extends post-repolarization refractoriness

Using the S1-S2 protocol, we observed that ORM-10962 extended the duration of post-repolarization refractoriness (PRR; see Methods 1.1.4 for the exact definition) (Fig. 6A). We hypothesized that this could be

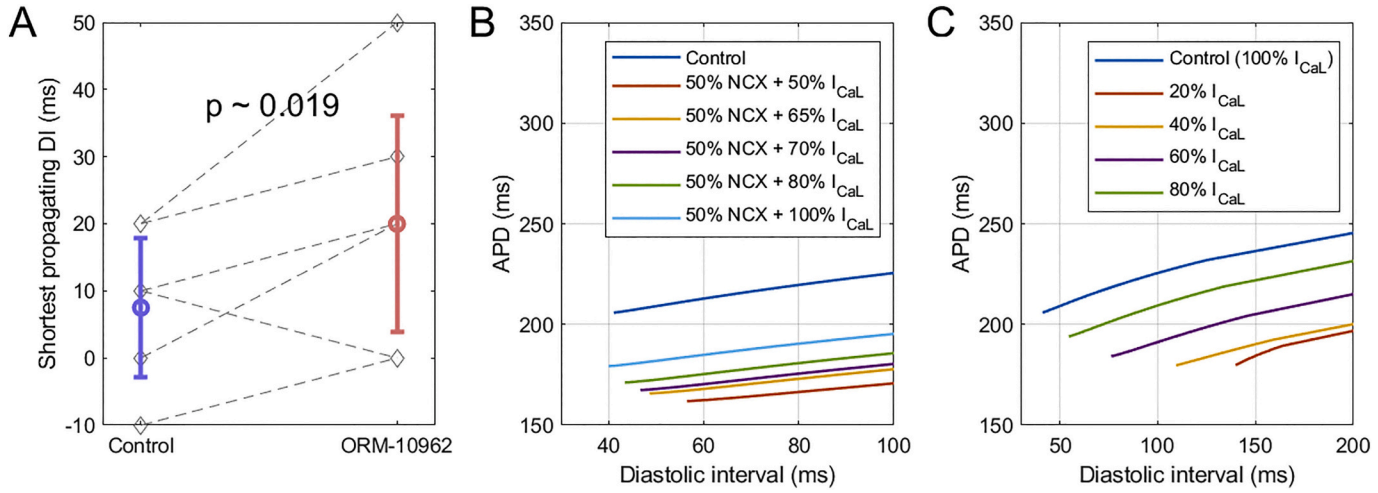

Fig. 6. ORM-10962 extends PRR. A) Experimental data from papillary muscle preparations of the shortest DI which led to formation of an action potential in the S1-S2 protocol ($n = 6$). B) Simulations of S1-S2 protocol under NCX block and I_{CaL} reduction. The leftmost point on each curve determines the PRR in the given condition. C) Simulations of S1-S2 protocol where the S1 phase was carried out using control model without any perturbation of NCX and I_{CaL}, with the I_{CaL} reduction being introduced only for the S2 beat.

mediated by an indirect reduction of I_{CaL} via ORM-10962, given the current's involvement in cellular excitability [41–43]. The hypothesis was tested using the ToR-ORd model with an increased role of I_{CaL} in excitability (Methods 2.3).

The S1-S2 protocol was simulated using single cells with a 50% block of NCX and several possible values of reduced I_{CaL} availability. We observed that the lower the I_{CaL} availability, the longer the PRR (Fig. 6B); this result was also confirmed in a fibre simulation (Appendix E). To exclude the possibility that this is due to a chronic effect following from pre-pacing in different conditions (e.g. APD change or a change in ionic concentrations), an additional modified S1-S2 protocol was simulated. There, S1 pacing was carried out in a control ToR-ORd model, with I_{CaL} availability changed only for the S2 stimulus. Again, cells with reduced I_{CaL} manifested extended PRR (Fig. 6C). In both scenarios, this is due to the fact that for a short coupling interval, I_{Na} is reduced due to partial refractoriness, giving greater importance to I_{CaL} in triggering an action potential. When I_{CaL} is reduced, so is the cellular excitability. Together, these results demonstrate that the experimentally observed extension of PRR under ORM-10962 can stem from an indirect reduction of I_{CaL}.

4. Discussion

The main findings of this combined experimental and computational work are: 1) ORM-10962 attenuates alternans of both action potential duration and calcium transient amplitude; however, the protective effect is not observed for APD80 alternans at very fast pacing rates. 2) Three distinct types of APD alternans are observed, revealing type-specific response to ORM-10962 with regards to APD80 alternans attenuation. 3) ORM-10962 does not markedly change APD restitution, and analysis of diastolic intervals suggests that calcium oscillations drive alternans in the experiments. 4) the suggested mechanism of calcium alternans inhibition by ORM-10962 is via reduced refractoriness of sarcoplasmic reticulum release. 5) ORM-10962 increases post-repolarization refractoriness, and this may be mediated by indirect L-type calcium current reduction following NCX blockade.

Cardiac alternans is an important arrhythmogenic phenomenon, which can be evoked in healthy hearts [44], but is particularly exacerbated in heart disease [12–14]. Alternans attenuation is consequently an important aim of antiarrhythmic medication, previously targeted mainly by SERCA pump overexpression [45]. Here, we demonstrate that the NCX blocker ORM-10962 has the potential to attenuate both alternans of APD and of calcium transient amplitude, with the alternans being calcium-driven. Importantly, our simulations suggest that ORM-10962 alternans attenuation could be effective also in the setting of heart failure remodelling.

In this study, we observed three types of APD alternans with regards to action potential morphology: '++' (APD25 prolongation during alternans occurs in the same beats as APD80 prolongation), '+−' (APD25 prolongation occurs in the same beats as APD80 shortening), and '+0' (APD25 alternans occurs in presence of negligible APD80 alternans). The fact that three distinct morphological patterns of alternans were observed in a single batch of experiments (in a single species and a single experimental protocol) suggests at relatively high and perhaps surprising intra-species phenotypic heterogeneity. ORM-10962 showed a tendency towards shifting alternans type to more negative type ('++' to '+0' and '+0' to '+−') compared to control. Response to ORM-10962 with regards to APD80 alternans differed by the type of alternans. While APD80 attenuation occurred for the vast majority of '++' alternans recordings, '+0' recordings have shown minimal attenuation or even alternans promotion (there was not enough data on '+−' type to draw any conclusions). Lack of alternans attenuation at APD80 for '+0' alternans is not surprising, given that the '+0' type is defined as type with little to no alternans at APD80. Consequently, a shift towards the '+−' type means that alternans at APD80 can be paradoxically promoted by ORM-10962. On the other hand, the negative-shifting effect of ORM-10962 on the alternans type means that the drug can be especially potent for '++' alternans, given that it can attenuate underlying calcium alternans, as well as shift the APD80 alternans type towards '+0', reducing dispersion of repolarization. The '++' type of alternans is possibly the most frequently reported type of alternans, observed in human [44], guinea pig [46,47], cat [48], or rabbit [17,49], supporting the relevance of alternans attenuation in this type. Finally, the fact that the '++' type manifested the greatest absolute amplitude of APD80 (with the amplitude being small or minimal for '+−' and '+0' types) means that clinical testing based on T-wave alternans is likely to detect precisely the patients who will benefit the most from hypothetical treatment based on NCX blockade. However, further research is needed to better characterize and understand the mechanisms (e.g. balance of ionic currents or regional differences) underlying the different types of alternans observed in this study.

The experimental results presented in this study suggest that ORM-10962 attenuates CaT alternans (as evidenced by measurements in isolated myocytes and by attenuation of APD25 alternans, which is very

likely to be tightly associated with CaT alternans). This is an important result, given that analysis of diastolic intervals and restitution suggest that APD alternans in the presented experiments is not driven by restitution, but rather by alternans of CaT. The most likely explanation of calcium alternans attenuation suggested by computer simulations is the altered balance of two factors contributing to the amplitude of the calcium transient: the L-type calcium current and the SR calcium loading. While I_{CaL} is indirectly reduced by the NCX blockade [7], our simulations suggest that the SR loading is, in turn, increased. This prediction is supported by the fact that ORM-10962 reduces I_{CaL}, but increases the calcium transient amplitude [6]. Therefore, there must be an additional contributor to the calcium transient amplitude which outweighs I_{CaL} reduction, and the increased SR loading is the most likely candidate. Such an effect is to be expected from an NCX blocker; the NCX and SERCA pumps in the SR are dominant mechanisms of removal of calcium from cytosol [2], and when NCX is inhibited, a greater relative role is given to SERCA pumps (Diaz et al., 2004), enhancing the reuptake into SR (provided the influx via I_{CaL} is not reduced excessively). Enhanced SR reuptake was then shown to reduce the refractoriness of calcium release from the SR [50]. Given that the refractoriness of release was shown to be a potential driver of alternans both experimentally and computationally [23,51], this could explain experimental observation of alternans inhibition following enhancement of SR reuptake [45,52].

Alternans attenuation via NCX inhibition may, in future, be an easier avenue towards alternans-aimed antiarrhythmics compared to previously considered SERCA overexpression. The NCX inhibition can be mediated by a channel-blocking drug such as ORM-10962, which can be administered or withdrawn as needed, unlike the manipulation of protein expression. In addition, NCX inhibition may also be anti-arrhythmic by preventing triggered activity due to delayed and early afterdepolarisations where NCX is thought to play an important role in their initiation [53]. Furthermore, under normal condition, the NCX inhibition has negligible proarrhythmic effects since it did not or marginally influence the ECG, the shape of the action potential and the kinetics of the Ca^{2+} transient [6,54,55].

The S1-S2 protocol has revealed that the ORM-10962 extends post-repolarization refractoriness (PRR). Computer simulations suggest the reduction in L-type calcium current following ORM-10962 exposure as a potential contributor, particularly in the setting when I_{Na} is reduced. An alternative explanation lies in the calcium-based inactivation of fast sodium current [56]: it is to be expected that following NCX blockade, sub-sarcolemmal calcium concentration would rise due to reduced calcium efflux, inhibiting fast sodium current and trivially extending PRR. Future quantitative studies may elucidate the relative contribution of these two mechanisms. Localized prolongation of PRR is known to be arrhythmogenic in the setting of acute ischemia; however, it was suggested that if PRR extension is global and without a major elevation of resting potential, it is antiarrhythmic instead, protecting the heart from re-entry [57]. PRR extension could therefore be an additional beneficial anti-arrhythmic effect of ORM-10962.

One interesting aspect of the simulation part of this study is the fact that an explicit reduction in I_{CaL} was required to manifest the experimentally observed reduction in I_{CaL} following ORM-10962 treatment. The indirect I_{CaL} reduction observed in experiments appears to stem from calcium-dependent inactivation of I_{CaL}, given that the effect is abolished by the fast buffer BAPTA, or by depletion of SR [7]. At the same time, the ToR-ORd showed only a negligible reduction in peak I_{CaL} in response to pure NCX block, similarly to other models we tried this treatment on (not shown) [27,58,59]. As all these models do represent experimental data on calcium-dependent inactivation, the discrepancy between experimental results and simulations suggests a gap in our understanding of calcium-dependent inactivation of I_{CaL}.

5. Study limitations

Our study has the following limitations:

(i) The action potential measurements were carried out on tissue while CaTs were recorded from isolated cells. This may indicate that the magnitude and kinetics of action potential alternans could not be directly related to CaT alternans. An alternative approach would be to use dual calcium-voltage imaging, but this approach would have a different set of limitations arising from the use of mechanical uncouplers such as blebbistatin [60].

(ii) The action potential measurements were performed on intact ventricular tissue to avoid shortcomings arising from repolarization attenuation caused by enzymatic dissociation. Due to the stable repolarization, the alternans could be evoked with 100% probability and small APD changes could be detected with high fidelity. At the same time, it also means that our action potential measurements represent only the endocardial tissue. Other cell layers (such as epicardial cells) may have different characteristics during alternans. Furthermore, the range of basic cycle lengths for the microelectrode measurements in ventricular tissue was determined based on pilot data suggesting that alternans will not be present at bcl of 250 ms; however, in data collected for the study, alternans was also present at bcl of 250 ms. It is consequently impossible to precisely determine the effect of ORM-10962 on alternans onset (the slowest frequency at which alternans arises). Finally, we could not pace the single cells used for calcium measurements as rapidly as the faster pacing rates in the intact preparations, given that a 2:1 block manifested; this is most likely a consequence of the cell isolation, which is known to prolong APD and thus refractoriness primarily via the reduced density of the potassium channels.

(iii) The ToR-ORd computer model does not spontaneously reduce I_{CaL} in response to NCX blockade, (similarly to [27,58,59]), and the reduction thus had to be added explicitly. While this suggests interesting avenues for further research as discussed above, it is clearly a limitation of existing models. In addition, further research is needed to create models which could manifest all three types of alternans observed in this study ('++', '+−', '+0') dependent on their parametrization, allowing further investigation into the link between CaT and APD alternans.

6. Conclusions

Our experimental work and computational mechanistic modelling and simulation indicate that the NCX blocker ORM-10962 can attenuate alternans in both APD and calcium transient amplitude. This is driven primarily by shifting the intracellular calcium balance to increased sarcoplasmic reticulum loading, reducing SR release refractoriness, thus attenuating alternans.

Funding

This work was supported by grants from the National Research Development and Innovation Office (NKFIH PD-125402 (for NN), FK-129117 (for NN), GINOP-2.3.2-15-2016-00006 and GINOP-2.3.2-15-2016-00012), the LIVE LONGER EFOP-3.6.2-16-2017-00006 project, the János Bolyai Research Scholarship of the Hungarian Academy of Sciences (for NN), the EFOP 3.6.3 VEKOP-16-2017-00009 (for NT), the Hungarian Academy of Sciences, the British Heart Foundation (FS/15/8/3115 for NH and CH/2000004/12801 for DE), Wellcome Trust (100246/Z/12/Z and 214290/Z/18/Z for BR), and by the Orion Pharma (ORM-10962).

Contributions

Study conception: JT; Study design: JT, NN; Experimental data collection: JS, NT, RV, BH; Simulations: JT; Data analysis and visualization: JT, NN; Writing initial manuscript: JT; Critical revisions: All authors; Supervision: NN, BR, AV, NH; Funding acquisition: NN, BR, AV, NH.

Declaration of competing interest

J. Levijoki is employed by Orion Pharma and has been involved in the development of ORM-10962. Other authors have nothing to declare

Appendix A. Supplementary data

Supplementary data to this article can be found online at https://doi.org/10.1016/j.yjmcc.2020.12.015.

References

[1] J. Kimura, S. Miyamae, A. Noma, Identification of sodium-calcium exchange current in single ventricular cells of guinea-pig, J. Physiol. (1987), https://doi.org/10.1113/jphysiol.1987.sp016450.

[2] J.L. Puglisi, R.A. Bassani, J.W.M. Bassani, J.N. Amin, D.M. Bers, Temperature and relative contributions of Ca transport systems in cardiac myocyte relaxation, Am. J. Physiol. Heart Circ. Physiol. (1996) 1772–1778.

[3] J.N. Weiss, A. Garfinkel, H.S. Karagueuzian, P.S. Chen, Z. Qu, Early afterdepolarizations and cardiac arrhythmias, Heart Rhythm. 7 (2010) 1891–1899, https://doi.org/10.1016/j.hrthm.2010.09.017.

[4] S.M. Pogwizd, D.M. Bers, Cellular basis of triggered arrhythmias in heart failure, Trends Cardiovasc. Med. 14 (2004) 61–66, https://doi.org/10.1016/j.tcm.2003.12.002.

[5] X. Wan, M. Cutler, Z. Song, A. Karma, T. Matsuda, A. Baba, D.S. Rosenbaum, New experimental evidence for mechanism of arrhythmogenic membrane potential alternans based on balance of electrogenic INCX/I Ca currents, Heart Rhythm. 9 (2012) 1698–1705, https://doi.org/10.1016/j.hrthm.2012.06.031.

[6] Z. Kohajda, N. Farkas-Morvay, N. Jost, N. Nagy, A. Geramipour, A. Horváth, R. S. Varga, T. Hornyik, C. Corici, K. Acsai, B. Horváth, J. Prorok, B. Ördög, S. Déri, D. Tóth, J. Levijoki, P. Pollesello, T. Koskelainen, L. Otsomaa, A. Tóth, I. Baczkó, I. Leprán, P.P. Nánási, J.G. Papp, A. Varró, L. Virág, The effect of a novel highly selective inhibitor of the sodium/calcium exchanger (NCX) on cardiac arrhythmias in in vitro and in vivo experiments, PLoS One 11 (2016), https://doi.org/10.1371/journal.pone.0166041.

[7] K. Oravecz, A. Kormos, A. Gruber, Z. Márton, Z. Kohajda, L. Mirzaei, N. Jost, J. Levijoki, P. Pollesello, T. Koskelainen, L. Otsomaa, A. Tóth, J.G. Papp, P. P. Nánási, G. Antoons, A. Varró, K. Acsai, N. Nagy, Inotropic effect of NCX inhibition depends on the relative activity of the reverse NCX assessed by a novel inhibitor ORM-10962 on canine ventricular myocytes, Eur. J. Pharmacol. 818 (2018) 278–286, https://doi.org/10.1016/j.ejphar.2017.10.039.

[8] L.D. Wilson, D. Jeyaraj, X. Wan, G.S. Hoeker, T.H. Said, M. Gittinger, K.R. Laurita, D.S. Rosenbaum, Heart failure enhances susceptibility to arrhythmogenic cardiac alternans, Heart Rhythm. 6 (2009) 251–259, https://doi.org/10.1016/j.hrthm.2008.11.008.

[9] S.M. Narayan, M.R. Franz, P. Clopton, E.J. Pruvot, D.E. Krummen, Repolarization alternans reveals vulnerability to human atrial fibrillation, Circulation. 123 (2011) 2922–2930, https://doi.org/10.1161/CIRCULATIONAHA.110.977827.

[10] L.D. Wilson, D.S. Rosenbaum, Mechanisms of arrythmogenic cardiac alternans, Europace. 9 (Suppl. 6) (2007) 77–82, https://doi.org/10.1093/europace/eum210.

[11] J.N. Weiss, A. Karma, Y. Shiferaw, P.S. Chen, A. Garfinkel, Z. Qu, From pulsus to pulseless: the saga of cardiac alternans, Circ. Res. 98 (2006) 1244–1253, https://doi.org/10.1161/01.RES.0000224540.97431.f0.

[12] J. Tomek, G. Hao, M. Tomková, A. Lewis, C. Carr, D.J. Paterson, B. Rodriguez, G. Bub, N. Herring, B-Adrenergic receptor stimulation and alternans in the border zone of a healed infarct: An ex vivo Study and Computational Investigation of Arrhythmogenesis, Front. Physiol. 10 (2019), https://doi.org/10.3389/fphys.2019.00350.

[13] M. Kodama, K. Kato, S. Hirono, Y. Okura, H. Hanawa, T. Yoshida, M. Hayashi, H. Tachikawa, T. Kashimura, K. Watanabe, Y. Aizawa, Linkage between mechanical and electrical alternans in patients with chronic heart failure, J. Cardiovasc. Electrophysiol. 15 (2004) 295–299. http://www.sciencedirect.com/science/article/pii/S1071916401253603%5CnE:%5CArticulos%5CUCL%5CKodama2001.pdf.

[14] M. de Oliveira Antunes, N. Samesima, H.G. Pereira Filho, A.Y. Matsumoto, R. L. Verrier, C.A. Pastore, E. Arteaga-Fernández, C. Mady, Exercise-induced quantitative microvolt T-wave alternans in hypertrophic cardiomyopathy, J. Electrocardiol. 50 (2017) 184–190, https://doi.org/10.1016/j.jelectrocard.2016.10.010.

[15] J. Tomek, B. Rodriguez, G. Bub, J. Heijman, β-adrenergic receptor stimulation inhibits proarrhythmic alternans in post-infarction border zone cardiomyocytes: a computational analysis, Am. J. Physiol. Heart Circ. Physiol. 313 (2017) 338–353, https://doi.org/10.1152/ajpheart.00094.2017.

[16] R. Gardner, L. Wang, B. Lang, J. Cregg, C. Dunbar, W. Woodward, J. Silver, C. Ripplinger, B. Habecker, Targeting protein tyrosine phosphatase sigma after myocardial infarction restores cardiac sympathetic innervation and prevents arrhythmias, Nat. Commun. 6 (2015).

[17] E. Chudin, J. Goldhaber, A. Garfinkel, J. Weiss, B. Kogan, Intracellular Ca2+ dynamics and the stability of ventricular tachycardia, Biophys. J. (1999), https://doi.org/10.1016/S0006-3495(99)77126-2.

[18] M.E. Díaz, S.C. O'Neill, D.A. Eisner, Sarcoplasmic reticulum calcium content fluctuation is the key to cardiac Alternans, Circ. Res. 94 (2004) 650–656, https://doi.org/10.1161/01.RES.0000119923.64774.72.

[19] J.B. Nolasco, R.W. Dahlen, A graphic method for the study of alternation in cardiac action potentials, J.Appl.Physiol. 25 (1968) 191–196.

[20] E.J. Pruvot, R.P. Katra, D.S. Rosenbaum, K.R. Laurita, Role of calcium cycling versus restitution in the mechanism of repolarization Alternans, Circ. Res. 94 (2004) 1083–1090, https://doi.org/10.1161/01.RES.0000125629.72053.95.

[21] J.N. Edwards, L.A. Blatter, Cardiac alternans and intracellular calcium cycling, Clin. Exp. Pharmacol. Physiol. 41 (2014) 524–532, https://doi.org/10.1111/1440-1681.12231.

[22] D.A. Eisner, H.S. Choi, M.E. Díaz, S.C. O'Neill, A.W. Trafford, Integrative analysis of calcium cycling in cardiac muscle, Circ. Res. (2000), https://doi.org/10.1161/01.RES.87.12.1087.

[23] J. Tomek, M. Tomková, X. Zhou, G. Bub, B. Rodriguez, Modulation of cardiac alternans by altered sarcoplasmic reticulum calcium release: a simulation study, Front. Physiol. 9 (2018) 1306, https://doi.org/10.3389/fphys.2018.01306.

[24] J. Tomek, A 'comb' algorithm for accurate detection of calcium transients and action potentials in regularly activating cardiac preparations, BioRxiv. 757294 (2019), https://doi.org/10.1101/757294.

[25] J. Tomek, A. Bueno-Orovio, E. Passini, X. Zhou, A. Minchole, O. Britton, C. Bartolucci, S. Severi, A. Shrier, L. Virag, A. Varro, B. Rodriguez, Development, calibration, and validation of a novel human ventricular myocyte model in health, disease, and drug block, Elife. 8 (2019), e48890, https://doi.org/10.7554/eLife.48890.

[26] E. Grandi, F.S. Pasqualini, D.M. Bers, A novel computational model of the human ventricular action potential and Ca transient, J. Mol. Cell. Cardiol. 48 (2010) 112–121, https://doi.org/10.1016/j.yjmcc.2009.09.019.

[27] K.H.W.J. ten Tusscher, A.V. Panfilov, Alternans and spiral breakup in a human ventricular tissue model, Am. J. Physiol. Heart Circ. Physiol. 291 (2006) H1088–H1100, https://doi.org/10.1152/ajpheart.00109.2006.

[28] J. Heijman, P.G.A. Volders, R.L. Westra, Y. Rudy, Local control of β-adrenergic stimulation: Effects on ventricular myocyte electrophysiology and Ca(2+)-transient, J. Mol. Cell. Cardiol. 50 (2011) 863–871, https://doi.org/10.1016/j.yjmcc.2011.02.007.

[29] E. Passini, O.J. Britton, H.R. Lu, J. Rohrbacher, A.N. Hermans, D.J. Gallacher, R.J. H. Greig, A. Bueno-Orovio, B. Rodriguez, Human in silico drug trials demonstrate higher accuracy than animal models in predicting clinical pro-arrhythmic cardiotoxicity, Front. Physiol. 12 (2017) 668, https://doi.org/10.3389/fphys.2017.00668.

[30] R. Coppini, C. Ferrantini, L. Yao, P. Fan, M. Del Lungo, F. Stillitano, L. Sartiani, B. Tosi, S. Suffredini, C. Tesi, M. Yacoub, I. Olivotto, L. Belardinelli, C. Poggesi, E. Cerbai, A. Mugelli, Late sodium current inhibition reverses electromechanical dysfunction in human hypertrophic cardiomyopathy, Circulation. 127 (2013) 575–584, https://doi.org/10.1161/CIRCULATIONAHA.112.134932.

[31] J.F. Gomez, K. Cardona, L. Romero, J.M. Ferrero, B. Trenor, Electrophysiological and structural remodeling in heart failure modulate arrhythmogenesis. 1D simulation study, PLoS One (2014), https://doi.org/10.1371/journal.pone.0106602.

[32] T.H. Fischer, L.S. Maier, S. Sossalla, The ryanodine receptor leak: how a tattered receptor plunges the failing heart into crisis, Heart Fail. Rev. 18 (2013) 475–483, https://doi.org/10.1007/s10741-012-9339-6.

[33] T.R. Kolstad, J. van den Brink, N. Macquaide, P.K. Lunde, M. Frisk, J.M. Aronsen, E.S. Norden, A. Cataliotti, I. Sjaastad, O.M. Sejersted, A.G. Edwards, G.T. Lines, W. E. Louch, Ryanodine receptor dispersion disrupts Ca 2+ release in failing cardiac myocytes, Elife (2018), https://doi.org/10.7554/eLife.39427.

[34] M. Lindner, M.C. Brandt, H. Sauer, J. Hescheler, T. Böhle, D.J. Beuckelmann, Calcium sparks in human ventricular cardiomyocytes from patients with terminal heart failure, Cell Calcium 31 (2002) 175–182, https://doi.org/10.1054/ceca.2002.0272.

[35] R.H.G. Schwinger, G. Münch, B. Bölck, P. Karczewski, E.G. Krause, E. Erdmann, Reduced Ca2+−sensitivity of SERCA 2a in failing human myocardium due to reduced serin-16 phospholamban phoshorylation, J. Mol. Cell. Cardiol. (1999), https://doi.org/10.1006/jmcc.1998.0897.

[36] J. Pitt-Francis, P. Pathmanathan, M.O. Bernabeu, R. Bordas, J. Cooper, A. G. Fletcher, G.R. Mirams, P. Murray, J.M. Osborne, A. Walter, S.J. Chapman, A. Garny, I.M.M. van Leeuwen, P.K. Maini, B. Rodríguez, S.L. Waters, J. P. Whiteley, H.M. Byrne, D.J. Gavaghan, Chaste: a test-driven approach to software development for biological modelling, Comput. Phys. Commun. 180 (2009) 2452–2471, https://doi.org/10.1016/j.cpc.2009.07.019.

[37] A. Bueno-Orovio, E.M. Cherry, F.H. Fenton, Minimal model for human ventricular action potentials in tissue, J. Theor. Biol. 253 (2008) 544–560, https://doi.org/10.1016/j.jtbi.2008.03.029.

[38] O.J. Britton, A. Bueno-Orovio, K. Van Ammel, H.R. Lu, R. Towart, D.J. Gallacher, B. Rodriguez, Experimentally calibrated population of models predicts and explains intersubject variability in cardiac cellular electrophysiology, Proc. Natl. Acad. Sci. 110 (2013) E2098–E2105, https://doi.org/10.1073/pnas.1304382110.

[39] V. Piacentino, C.R. Weber, X. Chen, J. Weisser-Thomas, K.B. Margulies, D.M. Bers, S.R. Houser, Cellular basis of abnormal calcium transients of failing human ventricular myocytes, Circ. Res. (2003), https://doi.org/10.1161/01.RES.0000062469.83985.9B.

[40] H. Kubo, K.B. Margulies, V. Piacentino, J.P. Gaughan, S.R. Houser, Patients with end-stage congestive heart failure treated with β-adrenergic receptor antagonists have improved ventricular myocyte calcium regulatory protein abundance, Circulation (2001), https://doi.org/10.1161/hc3401.095073.

[41] S. Rohr, J.P. Kucera, A.G. Kléber, Slow conduction in cardiac tissue, I, Circ. Res. 83 (1998) 781–794, https://doi.org/10.1161/01.res.83.8.781.
[42] S. Rohr, J.P. Kucera, Involvement of the calcium inward current in cardiac impulse propagation: induction of unidirectional conduction block by nifedipine and reversal by bay K 8644, Biophys. J. 72 (1997) 754–766, https://doi.org/10.1016/S0006-3495(97)78710-1.
[43] R.M. Shaw, Y. Rudy, Ionic mechanisms of propagation in cardiac tissue: roles of the sodium and L-type calcium currents during reduced excitability and decreased gap junction coupling, Circ. Res. 81 (1997) 727–741, https://doi.org/10.1161/01.RES.81.5.727.
[44] M.L. Koller, S.K.G. Maier, A.R. Gelzer, W.R. Bauer, M. Meesmann, R.F. Gilmour, Altered dynamics of action potential restitution and alternans in humans with structural heart disease, Circulation. 112 (2005) 1542–1548, https://doi.org/10.1161/CIRCULATIONAHA.104.502831.
[45] M.J. Cutler, X. Wan, B.N. Plummer, H. Liu, I. Deschenes, K.R. Laurita, R.J. Hajjar, D.S. Rosenbaum, Targeted sarcoplasmic reticulum Ca2+ ATPase 2a gene delivery to restore electrical stability in the failing heart, Circulation. 126 (2012) 2095–2104, https://doi.org/10.1161/CIRCULATIONAHA.111.071480.
[46] X. Wan, K.R. Laurita, E.J. Pruvot, D.S. Rosenbaum, Molecular correlates of repolarization alternans in cardiac myocytes, J. Mol. Cell. Cardiol. (2005), https://doi.org/10.1016/j.yjmcc.2005.06.004.
[47] M.L. Walker, X. Wan, G.E. Kirsch, D.S. Rosenbaum, Hysteresis Effect implicates calcium cycling as a mechanism of repolarization alternans, Circulation (2003), https://doi.org/10.1161/01.CIR.0000093276.10885.5B.
[48] J. Hüser, Y.G. Wang, K.A. Sheehan, F. Cifuentes, S.L. Lipsius, L.A. Blatter, Functional coupling between glycolysis and excitation-contraction coupling underlies alternans in cat heart cells, J. Physiol. (2000), https://doi.org/10.1111/j.1469-7793.2000.00795.x.
[49] A. Mahajan, Y. Shiferaw, D. Sato, A. Baher, R. Olcese, L.H. Xie, M.J. Yang, P. S. Chen, J.G. Restrepo, A. Karma, A. Garfinkel, Z. Qu, J.N. Weiss, A rabbit ventricular action potential model replicating cardiac dynamics at rapid heart rates, Biophys. J. 94 (2008) 392–410, https://doi.org/10.1529/biophysj.106.98160.
[50] H.R. Ramay, O.Z. Liu, E.A. Sobie, Recovery of cardiac calcium release is controlled by sarcoplasmic reticulum refilling and ryanodine receptor sensitivity, Cardiovasc. Res. 91 (2011) 598–605, https://doi.org/10.1093/cvr/cvr143.
[51] L. Wang, R.C. Myles, N.M. De Jesus, A.K.P. Ohlendorf, D.M. Bers, C.M. Ripplinger, Optical mapping of sarcoplasmic reticulum Ca2+ in the intact heart: ryanodine receptor refractoriness during alternans and fibrillation, Circ. Res. 114 (2014) 1410–1421, https://doi.org/10.1161/CIRCRESAHA.114.302505.
[52] V. Stary, D. Puppala, M. Scherrer-Crosbie, W.H. Dillmann, A.A. Armoundas, SERCA2a upregulation ameliorates cellular alternans induced by metabolic inhibitions, J. Appl. Physiol. 120 (2016) 865–875, https://doi.org/10.1152/japplphysiol.00588.2015.
[53] N. Herring, M. Kalla, D.J. Paterson, The autonomic nervous system and cardiac arrhythmias: current concepts and emerging therapies, Nat. Rev. Cardiol. (2019), https://doi.org/10.1038/s41569-019-0221-2.
[54] A.S. Farkas, K. Acsai, N. Nagy, A. Tóth, F. Fülöp, G. Seprényi, P. Birinyi, P. P. Nánási, T. Forster, M. Csanády, J.G. Papp, A. Varró, A. Farkas, Na+/Ca2+ exchanger inhibition exerts a positive inotropic effect in the rat heart, but fails to influence the contractility of the rabbit heart, Br. J. Pharmacol. (2008), https://doi.org/10.1038/bjp.2008.83.
[55] N. Nagy, A. Kormos, Z. Kohajda, Á. Szebeni, J. Szepesi, P. Pollesello, J. Levijoki, K. Acsai, L. Virág, P.P. Nánási, J.G. Papp, A. Varrō, A. Tōth, Selective Na +/ Ca 2+ exchanger inhibition prevents Ca 2+ overload-induced triggered arrhythmias, Br. J. Pharmacol. (2014), https://doi.org/10.1111/bph.12867.
[56] S. Casini, A.O. Verkerk, M.M.G.J. Van Borren, A.C.G. Van Ginneken, M. W. Veldkamp, J.M.T. De Bakker, H.L. Tan, Intracellular calcium modulation of voltage-gated sodium channels in ventricular myocytes, Cardiovasc. Res. 81 (2009) 72–81, https://doi.org/10.1093/cvr/cvn274.
[57] R. Coronel, M.J. Janse, T. Opthof, A.A. Wilde, P. Taggart, Postrepolarization refractoriness in acute ischemia and after antiarrhythmic drug administration: action potential duration is not always an index of the refractory period, Heart Rhythm. 9 (2012) 977–982, https://doi.org/10.1016/j.hrthm.2012.01.021.
[58] C. Bartolucci, E. Passini, J. Hyttinen, M. Paci, S. Severi, Simulation of the effects of extracellular calcium changes leads to a novel computational model of human ventricular action potential with a revised calcium handling, Front. Physiol. (2020), https://doi.org/10.3389/fphys.2020.00314.
[59] T.R. Shannon, F. Wang, J. Puglisi, C. Weber, D.M. Bers, A mathematical treatment of integrated Ca dynamics within the ventricular myocyte, Biophys. J. 87 (2004) 3351–3371, https://doi.org/10.1529/biophysj.104.047449.
[60] K.E. Brack, R. Narang, J. Winter, G.A. Ng, The mechanical uncoupler blebbistatin is associated with significant electrophysiological effects in the isolated rabbit heart, Exp. Physiol. 98 (2013) 1009–1027, https://doi.org/10.1113/expphysiol.2012.069369.

frontiers in Pharmacology

ORIGINAL RESEARCH
published: 29 January 2020
doi: 10.3389/fphar.2019.01632

Novel Na^+/Ca^{2+} Exchanger Inhibitor ORM-10962 Supports Coupled Function of Funny-Current and Na^+/Ca^{2+} Exchanger in Pacemaking of Rabbit Sinus Node Tissue

Zsófia Kohajda[1,2†], Noémi Tóth[2†], Jozefina Szlovák[2], Axel Loewe[3], Gergő Bitay[2], Péter Gazdag[2], János Prorok[2], Norbert Jost[1,2], Jouko Levijoki[4], Piero Pollesello[4], Julius Gy. Papp[1,2], András Varró[1,2] and Norbert Nagy[1,2]*

[1] MTA-SZTE Research Group of Cardiovascular Pharmacology, Hungarian Academy of Sciences, Szeged, Hungary, [2] Department of Pharmacology and Pharmacotherapy, Faculty of Medicine, University of Szeged, Szeged, Hungary, [3] Institute of Biomedical Engineering, Karlsruhe Institute of Technology (KIT), Karlsruhe, Germany, [4] Orion Pharma, Espoo, Finland

OPEN ACCESS

Edited by:
Esther Pueyo,
University of Zaragoza, Spain

Reviewed by:
Yael Yaniv,
Technion Israel Institute of Technology, Israel
Oliver Monfredi,
University of Virginia, United States
Thomas Hund,
The Ohio State University, United States

***Correspondence:**
András Varró
varro.andras@med.u-szeged.hu

[†]These authors have contributed equally to this work

Specialty section:
This article was submitted to Cardiovascular and Smooth Muscle Pharmacology, a section of the journal Frontiers in Pharmacology

Received: 03 July 2019
Accepted: 13 December 2019
Published: 29 January 2020

Citation:
Kohajda Z, Tóth N, Szlovák J, Loewe A, Bitay G, Gazdag P, Prorok J, Jost N, Levijoki J, Pollesello P, Papp JG, Varró A and Nagy N (2020) Novel Na^+/Ca^{2+} Exchanger Inhibitor ORM-10962 Supports Coupled Function of Funny-Current and Na^+/Ca^{2+} Exchanger in Pacemaking of Rabbit Sinus Node Tissue. Front. Pharmacol. 10:1632. doi: 10.3389/fphar.2019.01632

Background and Purpose: The exact mechanism of spontaneous pacemaking is not fully understood. Recent results suggest tight cooperation between intracellular Ca^{2+} handling and sarcolemmal ion channels. An important player of this crosstalk is the Na^+/Ca^{2+} exchanger (NCX), however, direct pharmacological evidence was unavailable so far because of the lack of a selective inhibitor. We investigated the role of the NCX current in pacemaking and analyzed the functional consequences of the I_f-NCX coupling by applying the novel selective NCX inhibitor ORM-10962 on the sinus node (SAN).

Experimental Approach: Currents were measured by patch-clamp, Ca^{2+}-transients were monitored by fluorescent optical method in rabbit SAN cells. Action potentials (AP) were recorded from rabbit SAN tissue preparations. Mechanistic computational data were obtained using the Yaniv *et al*. SAN model.

Key Results: ORM-10962 (ORM) marginally reduced the SAN pacemaking cycle length with a marked increase in the diastolic Ca^{2+} level as well as the transient amplitude. The bradycardic effect of NCX inhibition was augmented when the funny-current (I_f) was previously inhibited and *vice versa,* the effect of I_f was augmented when the Ca^{2+} handling was suppressed.

Conclusion and Implications: We confirmed the contribution of the NCX current to cardiac pacemaking using a novel NCX inhibitor. Our experimental and modeling data support a close cooperation between I_f and NCX providing an important functional consequence: these currents together establish a strong depolarization capacity providing important safety factor for stable pacemaking. Thus, after individual inhibition of I_f or NCX, excessive bradycardia or instability cannot be expected because each of these currents may compensate for the reduction of the other providing safe and rhythmic SAN pacemaking.

Keywords: Na^+/Ca^{2+} exchanger, funny-current, ORM-10962, pacemaking, sinus-node

INTRODUCTION

Computational modeling as well as experimental results established previously that the normal pacemaker function is not only regulated by the hyperpolarization-activated funny current (I_f) (DiFrancesco, 1981) but is also regulated by the intracellular Ca^{2+} handling (Lakatta and DiFrancesco, 2009; Yaniv et al., 2013a; Yaniv et al., 2015; Sirenko et al., 2016). Lakatta and co-workers suggested that the sinus node (SAN) cells operate by a rhythmic clock-like oscillator system where the sarcoplasmic reticulum serves as a Ca^{2+}-clock, which rhythmically discharges diastolic local Ca^{2+} releases (LCRs), and activates the forward (inward) Na^+/Ca^{2+} exchanger (NCX) current to accelerate the diastolic depolarization and facilitates the membrane-clock (M-clock) (Yaniv et al., 2015). Recent experimental results further suggest that these clocks work tightly coupled since the M-clock regulates the Ca^{2+} influx and efflux while the NCX also regulates the diastolic depolarization forming a coupled-clock system. Therefore, NCX may have crucial importance in the clock-like oscillator system since the NCX-mediated inward current is directly translated to membrane potential changes *via* the operation of forward mode of the exchanger. This hypothesis was repeatedly challenged and the pivotal role of Ca^{2+} clock was questioned by other authors (Noble et al., 2010; Himeno et al., 2011; DiFrancesco and Noble, 2012).

As early as 1983, Irishawa and Morad showed in elegant experiments that full inhibition of I_f current by caesium did not significantly influence SAN spontaneous activity arguing for mechanisms other than I_f (Noma et al., 1983). On the other hand, other studies suggest a fundamental role of the exchanger in normal automaticity. A low-sodium bath solution inhibited spontaneous action potentials (AP) firing in guinea-pig SAN cells *via* suppressing normal function of NCX (Sanders et al., 2006). Other studies reported that depletion of SR store by application of ryanodine markedly disturbed the normal pacemaker activity in rabbit SAN cells (Bogdanov et al., 2001). Mouse genetic models revealed that partial atrial NCX1 knock out (≈90%) caused severe bradycardia and other rhythm disorders (Herrmann et al., 2013), while complete atrial NCX knock-out completely suppressed the atrial depolarization exerting ventricular escape rhythm on the ECG (Groenke et al., 2013). The application of KB-R7943, a non-selective NCX inhibitor, also suppressed spontaneous beating in guinea-pig SAN cells (Sanders et al., 2006) however it has also marked effect on the Ca^{2+}-currents. The supposed crucial role of NCX in the normal pacemaker function of SAN could not be directly investigated experimentally so far due to the lack of a selective NCX inhibitor. Recently, two novel NCX inhibitors were synthesized: ORM-10103 and ORM-10962, both showing improved selectivity without influencing I_{CaL} function (Jost et al., 2013; Kohajda et al., 2016; Oravecz et al., 2017).

Abbreviations: AP, action potential; APD, action potential duration; CL, cycle length; CLV, cycle length variability; DD, diastolic depolarization; DI, diastolic interval; DOF, dofetilide; NCX, sodium-calcium exchanger; I_f, funny-current; IVA, ivabradine; ORM, ORM-10962; RYA, ryanodine; SAN, sinoatrial-node.

In this study we confirmed the contributing role of NCX to spontaneous pacemaking by its direct pharmacological inhibition *via* the novel, selective inhibitor ORM-10962. Our data suggest that a strong crosstalk between I_f and NCX also exists in multicellular level, which was described and discussed by the Lakatta group earlier in single cell level (Yaniv et al., 2015). In addition, however, extending these earlier findings, we show that the effect of individual I_f and NCX inhibition is minimal whereas a combined inhibition acts synergistically, providing an important safety margin for secure spontaneous activity of the SAN.

MATERIALS AND METHODS

Ethical Statement

All experiments were conducted in compliance with the *Guide for the Care and Use of Laboratory Animals* (USA NIH publication No 85-23, revised 1996) and conformed to Directive 2010/63/EU of the European Parliament. The protocols were approved by the Review Board of the Department of Animal Health and Food Control of the Ministry of Agriculture and Rural Development, Hungary (XIII./1211/2012).

Animals

The measurements were performed in right atrial tissue obtained from young New-Zealand white rabbits from both genders weighing 2.0–2.5 kg.

Voltage-Clamp Measurements

Cell Preparations

For measuring I_f pacemaker current, we isolated single cells from the SAN region of rabbit heart by enzymatic dissociation. The animals were sacrificed by concussion after receiving 400 IU/kg heparin intravenously. The chest was opened and the heart was quickly removed and placed into cold (4°C) solution with the following composition (mM): NaCl 135, KCl 4.7, KH_2PO_4 1.2, $MgSO_4$ 1.2, 4-(2-hydroxyethyl)-1-piperazineethanesulfonic acid (HEPES) 10, $NaHCO_3$ 4.4, glucose 10, $CaCl_2$ 1.8, (pH 7.2 with NaOH). The heart was mounted on a modified, 60 cm high Langendorff column and perfused with oxygenated and prewarmed (37°C) solution mentioned above. After washing out of blood (3–5 min) the heart was perfused with nominally Ca-free solution until the heart stopped beating (approx. 3–4 min). The digestion was performed by perfusion with the same solution supplemented with 1.8 mg/ml (260 U/ml) collagenase (type II, Worthington). After 10–12 min, the heart was removed from the cannula. The right atrium was cut and the crista terminalis and SAN region were excised and cut into small strips. Strips were placed into enzyme free solution containing 1 mM $CaCl_2$ and equilibrated at 37°C for 10 min. After 10 min with gentle agitation, the cells were separated by filtering through a nylon mesh. Sedimentation was used for harvesting cells. The supernatant was removed and replaced by HEPES-buffered Tyrode's solution. The cells were stored at room temperature in the Tyrode's solution.

Measurement of Pacemaker Current (Funny Current)

For the measurement of the I_f current, the method of Verkerk et al. (2009) was adapted and applied. The current was recorded in HEPES-buffered Tyrode's solution while the composition of the pipette solution was the following (in mM): KOH 110, KCl 40, K_2ATP 5, $MgCl_2$ 5, EGTA 5, HEPES 10, and GTP 0.1 (pH was adjusted to 7.2 by aspartic acid). The current was activated by hyperpolarizing voltage pulses to −120 mV from a holding potential of −30 mV. The pacemaker current was identified as ivabradine (IVA) sensitive current. The experiments were performed at 37°C.

Fluorescent Optical Measurements

Isolated, spontaneously beating SAN cells were used for measurements. Ca^{2+} transients were measured by Fluo-4 AM fluorescent dye. Isolated cells were loaded with 5 μM dye for 20 min in room temperature in dark. Loaded cells were mounted in a low volume imaging chamber (RC47FSLP, Warner Instruments) and continuously superfused with normal Tyrode solution. Fluorescence measurements were performed on the stage of an Olympus IX 71 inverted fluorescence microscope. The dye was excited at 480 nm and the emitted fluorescence was detected at 535 nm. Optical signals were sampled at 1 kHz and recorded by a photon counting photomultiplier module (Hamamatsu, model H7828). Amplitudes of the Ca^{2+} transients were calculated as differences between systolic and diastolic values. To measure Ca^{2+} changes the cells were damaged by a patch pipette at the end of the experiment to obtain maximal fluorescence (F_{max}). Ca^{2+} was calibrated using the following formula: $K_d(F-F_{min})/(F_{max}-F)$. K_d of the Fluo-4 AM was 335 nM.

Action Potential Measurements With Standard Microelectrode Technique

We have chosen multicellular preparations for action potential measurements for three reasons: 1) all of the ion channels remained intact (current density, kinetics) because of the lack of enzymatic dissociation, thus providing more precise estimates of the ratio between the currents, 2) since the SAN cells are surrounded with atrial cells having a more negative resting membrane potential, the electrotonic coupling may intimately influence the SAN cells. It may have great importance since the I_f current markedly increases as the membrane potential drops to more negative values (Morad and Zhang, 2017), (3) the action potential frequency was very stable with a cycle-length variability lower than 5 ms.

SAN regions obtained from right atria were mounted in a tissue chamber superfused with oxygenated Locke's solution at 37°C. A conventional microelectrode technique was performed as previously described (Kormos et al., 2014; Kohajda et al., 2016; Oravecz et al., 2017). In the case of SAN, the action potentials were empirically found in the right atrium. SAN action potentials were verified by the maximum upstroke speed, which had to be lower than 15 V/s, the resting membrane potential (>−60 mV), and a clear diastolic depolarization (DD). Efforts were made to maintain the same impalement throughout each experiment. If impalement became dislodged, however, electrode adjustment was attempted and, if the action potential characteristics of the re-established impalement deviated by less than 5% from those of the previous measurement, the experiment was continued. When this 5% limit was exceeded, the experiment was terminated and all data were excluded from the analyses.

Action potential durations were measured at 90, 50, and 25% of repolarization. The maximal diastolic potential was defined as the most negative potential reached during the repolarization. The take off potential is the most negative point of the AP upstroke. DD was defined as the interval between the maximal diastolic potential and take off potential. The DD slope was calculated as $\Delta V_m/\Delta t$ between these points. The cycle length was calculated as the peak-to-peak interval between two consecutive APs. The phase 0 depolarization velocity was defined as the maximum of the first derivative of the AP during the upstroke.

Modeling

To complement the experiments, we performed mechanistic computational modeling using the Yaniv *et al*. model of rabbit SAN cells (Yaniv et al., 2013b). The differential equations of the model were solved using a forward Euler scheme. Simulation results were analyzed when the system had converged to a cyclic steady-state.

Statistical Analysis

All data are expressed as mean ± standard error (SEM). Statistical analysis was performed with Student's *t*-test and ANOVA with Bonferroni *post-hoc* test. The results were considered statistically significant when $p < 0.05$. In the case of action potential experiments, all recordings were obtained from different hearts.

Materials

With the exception of ORM-10962 (ORM) (from Orion Pharma, Espoo, Finland), and Fluo-4 AM (Thermo Fisher Scientific, Waltham, MA, USA), all chemicals were purchased from Sigma-Aldrich Fine Chemicals (St. Louis, MO, USA). ORM was dissolved in dimethyl-sulfoxide (DMSO) to obtain a 1 mM stock solution. This stock solution was diluted to reach the desired final concentration (DMSO concentration not exceeding 0.1%) in the bath.

RESULTS

ORM-10962 Has No Effect on Funny Current

Figure 1 shows the measurement of I_f in isolated SAN cells by applying the whole cell configuration of the patch clamp method. The selectivity of ORM on Na^+-, Ca^{2+}-, and major K^+ currents was tested in a previous study from our laboratory (Kohajda et al., 2016). However, its potential effect on the I_f current was not investigated in that previous study. As **Figures 1A**, **C** show a slowly developed current at negative hyperpolarizing membrane potential (from −30 to −120 mV), which was not altered by application of 1 μM ORM (**Figure 1B**). In contrast, it was markedly inhibited by 10 μM IVA (69.3 ± 3.4%), a well known inhibitor of I_f.

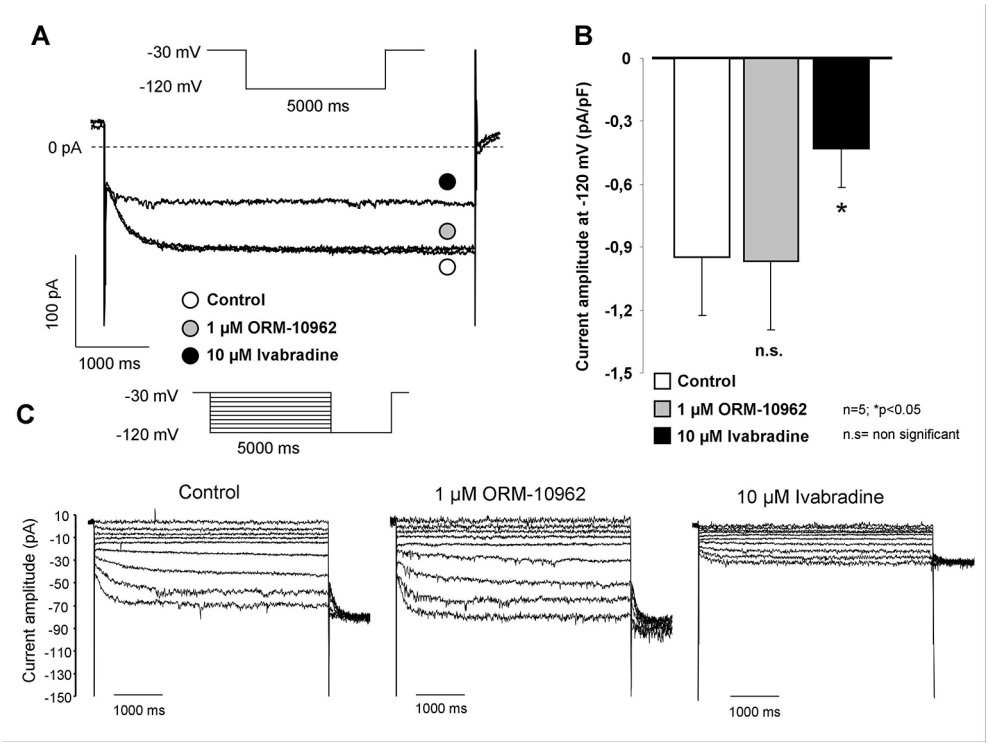

FIGURE 1 | Investigation of the possible effect of ORM-10962 (ORM) on funny current (I_f) in isolated sinus node (SAN) cells. The hyperpolarization activated I_f was elicited by 5,000 ms long rectangle pulse potentials to –120 mV from a holding potential of –30 mV. As representative current traces indicate, the current amplitude after ORM application (gray circle) was identical with the control (open circle). The considerable effect of 10 μM ivabradine (IVA) verified that the elicited current was indeed I_f **(A**, **B)**. Original traces in panel **(C)** represent the absence of ORM effects on current-voltage relationship of I_f by applying hyperpolarization pulses from –120 mV to –30 mV with 10 mV increments.

Na^+/Ca^{2+} Exchanger Inhibition Exerted Moderate Bradycardic Effect on Sinus Node Tissue

Figure 2 summarizes the effect of selective NCX inhibition by ORM on the spontaneous automaticity in SAN. Following application of 1 μM ORM a moderate but significant lengthening effect on the CL was observed (455.6 ± 32 ms *vs.* 493.0 ± 38 ms; Δ = 8.1 ± 1.8% $p < 0.05$, n = 16/16 hearts; **Figures 2A**–**C**) without any influence on the action potential duration (APD) (94.3 ± 6.7 ms *vs.* 96.7 ± 5.9 ms; **Figure 2D**). The slope of the diastolic depolarization phase was significantly reduced after ORM application (15.7 ± 3.1 mV/s *vs.* 10.9 ± 2.8 mV/s; n = 14/14; $p < 0.05$ **Figure 2E**) while the CL variability remained unchanged (7.6 ± 1.2 ms *vs.* 8.1 ± 1.3 ms; **Figure 2F**). The slope of phase 0 AP depolarization was identical during control and ORM experiments (11.2 ± 2.7 V/s *vs.* 12.5 ± 2.3 V/s). The preparations maintained the stable frequency in the time control experiments when DMSO was applied (440 ± 36.1 ms *vs.* 445 ± 37.6; n = 4). In the computational SAN action potential model (Yaniv et al., 2013b), we identified the degree of NCX current suppression required to obtain a similar CL increase as was experimentally measured. Forty-one percent of NCX inhibition was required to obtain 8% CL increase which was equal with the CL change observed experimentally (**Figure 2G**).

Na^+/Ca^{2+} Exchanger Inhibition Slightly Increased the Diastolic Ca^{2+} Level in Isolated Sinus Node Cells

The diastolic Ca^{2+} level increased in isolated SAN cells after ORM treatment (70 ± 11 nM *vs.* 130 ± 24 nM; $p < 0.05$, n = 10; **Figures 3A**, **B**), the effect was similar than was predicted by the Yaniv et al. SAN model (**Figure 3D**). In contrast to the model prediction, we found considerable increase in the transient amplitude (312 ± 37 nM *vs.* 568 ± 85 nM; $p < 0.05$, n = 10 **Figure 3C**), which was nearly doubled (82.1 ± 22%) in response to ORM application compared to the control value.

The Concomitant Application of Ivabradine and ORM-10962 Revealed Coupled Frequency Control Between Funny Current and Na^+/Ca^{2+} Exchanger Measured in Sinus Node Tissue

In the next set of experiments, IVA and ORM were subsequently applied to study a possible coupling between I_f and NCX.

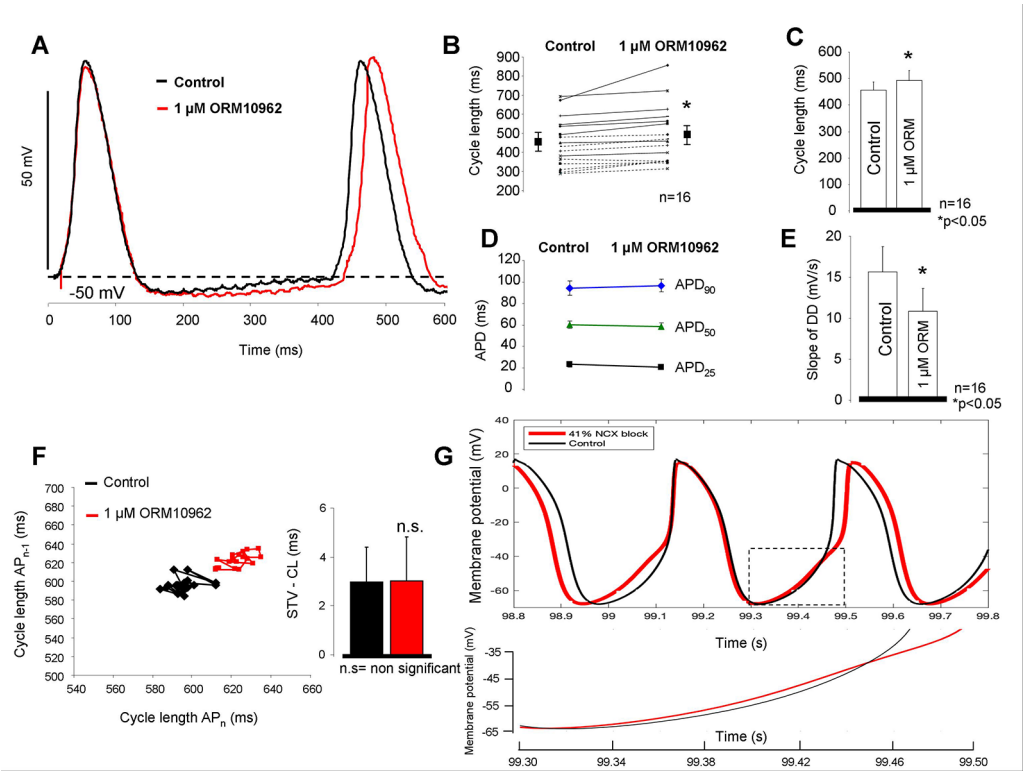

FIGURE 2 | Estimation of the effect of selective Na+/Ca2+ exchanger (NCX) inhibition on sinus node (SAN) tissue. As representative action potential traces **(A)** as well as individual experiments **(B)** and bar graphs **(C)** indicate, application of 1 μM ORM-10962 (ORM) exerted a slight but statistically significant bradycardic effect on SAN tissue. The action potential duration (APD) did not change during the experiment **(D)**, however the slope of the spontaneous depolarization was considerably decreased **(E)**. 30 consecutive cycles were analyzed to estimate the pacing rate variability. Poincaré-plot and bar graphs depict that ORM did not alter the short-term cycle length (CL) variability **(F)**. The Yaniv SAN cell model predicts 41% NCX inhibition to meet with the observed bradycardic effect of 1 μM ORM. The inset illustrates the reduced slope during late diastolic depolarization (DD) when 41% NCX inhibition was applied (red curve) **(G)**.

The effect of 1 μM ORM was substantially larger when I_f was previously inhibited (**Figures 4A**, **B**). Ca^{2+} transient measurements from spontaneously contracting SAN cells showed identical amplitudes (327 ± 23 nM *vs.* 337 ± 42 nM; n = 12) as well as diastolic Ca^{2+} levels (89 ± 22 nM *vs.* 85 ± 13 nM; n = 12) between control and 3 μM IVA (**Figure 4C**). A clear, gradual increase of ORM effect on the CL was observed with combined increasing concentration of IVA (1 μM ORM effect in the presence of 0 μM IVA: 8.1 ± 1.88%; in the presence of 0.5 μM IVA: 9.6 ± 2.3%; in the presence of 3 μM IVA: 17.1 ± 2.5%; **Figure 4D**). The ORM effect in the presence of 0.5 μM IVA did not differ significantly from the control, where 0 μM IVA was applied (8.1 ± 1.88% *versus* 9.6 ± 2.3%). In contrast, ORM effect was significantly larger on the CL in the presence of 3 μM IVA, compared with the control where IVA was not applied (8.1 ± 1.88% *versus* 17.1 ± 2.5%; $p < 0.05$, ANOVA, Bonferroni *post hoc* test). IVA significantly increased the CL both in 0.5 and in 3 μM concentrations ($p < 0.05$, ANOVA, Bonferroni *post hoc* test). In **Figure 4E**, we compare modeling and experimental results. In the Yaniv et al. model, based on a previous study (Bois et al., 1996), I_f inhibition was varied between 0%/20%/60% block (corresponding to 0, 0.5, and 3 μM IVA). Larger, 85% inhibition was only set in the model, since experimental application of 10 μM IVA is not feasible because of the marked I_{Kr} inhibition which can also reduce automaticity. The NCX inhibition was 41% in all cases. As **Figure 4E** shows, the modeling results do not match the experiments quantitatively, however they show a similar tendency (when I_f block increases, the same NCX inhibition causes larger CL prolongation) with markedly steeper correlation.

Figure 4F shows original modeling traces in the presence of 20% (left panel), 60% (middle panel), and 85% (right panel) I_f inhibition when NCX inhibition was 41% in all cases. The action potential modeling demonstrates an increased CL prolongation effect of NCX inhibition as I_f suppression becomes stronger, however, in contrast to the model prediction the steepness of NCX inhibition-induced CL increase was considerable flatter during experiments.

I_{Kr} Inhibition-Induced Bradycardia Did Not Facilitate the Effect of Selective Na^+/Ca^{2+} Exchanger Inhibition on Cycle Length in Sinus Node Tissue

We investigated how bradycardia induced by a mechanism which does not directly involve the inward depolarizing

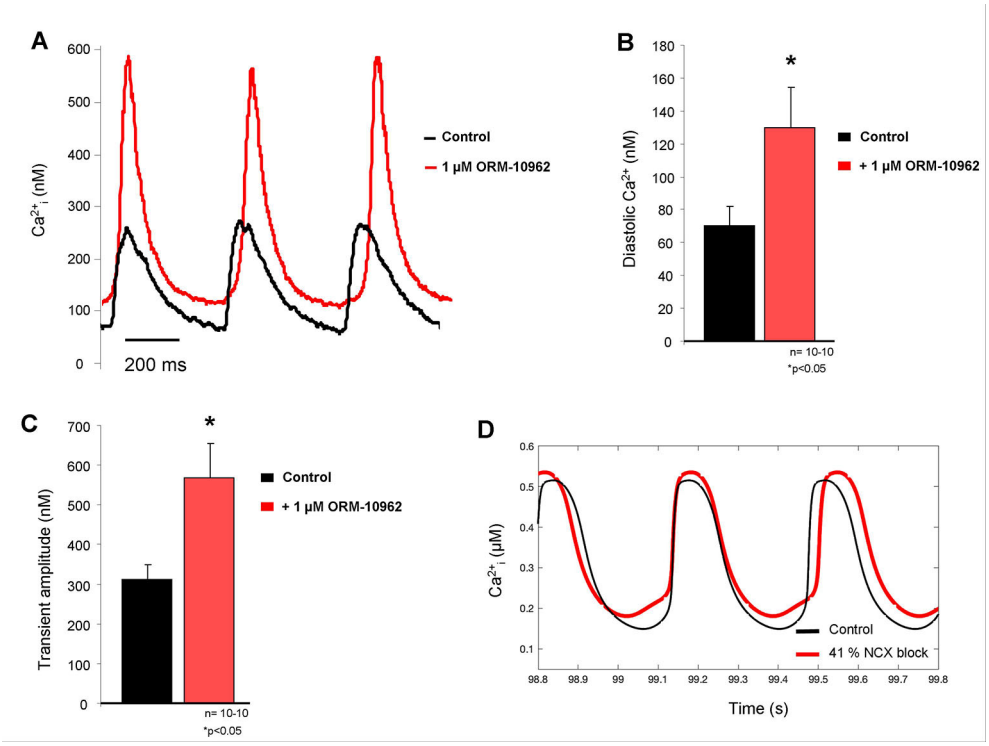

FIGURE 3 | (A) Representative Ca^{2+} transient traces from spontaneously contracting isolated sinus node (SAN) cells under control conditions (black trace) and after 1 µM ORM-10962 (ORM) application (red trace). As original fluorescent data as well as bar graphs indicate, a slight but significant increase of the diastolic Ca^{2+} level **(B)** with increased transient amplitude **(C)** was observed. In line with experimental data, the Yaniv SAN cell model predicted similar diastolic Ca^{2+} gain after 41% Na+/Ca2+ exchanger (NCX) inhibition **(D)**, however the increase of transient amplitude is much more pronounced during the experimental results.

currents (I_f and NCX) would influence the effect of NCX inhibition. Full I_{Kr} block induced by 100 nM dofetilide (DOF) markedly increased the CL of SAN AP (control: 489.3 ± 31 ms → 100 nM dofetilide: 649.1 ± 40.2 ms). This degree of increase of CL was due to the lengthening of APD without changing the DI. The subsequent application of 1 µM ORM exerted a similar effect (1 µM ORM-10962: 679.6 ± 52.6 ms; n = 7/7 hearts; **Figures 5A**, **B**), compared with results obtained after individual administration presented in **Figure 2** (7.2 ± 1.8% *vs.* 8.1 ± 1.8%, **Figure 5F**). It is important that the effect of DOF on CL was nearly similar to 3 µM IVA (32.9 ± 6.7% *vs.* 20.9 ± 4.1%). However, the major difference was that the DOF-mediated increase in CL was practically entirely an APD increase-induced effect (APD_{90}: 94.4 ± 3 ms *vs.* 187 ± 7.1 ms; $p < 0.05$, n = 7; diastolic interval (DI): 338.3 ± 39 ms *vs.* 352.7 ± 44.6 ms, n = 7) while the IVA influenced only the DI without affecting the APD_{90} (**Figures 5C–E**). In contrast, both NCX inhibition by ORM and I_f inhibition by IVA increased the CL due to lengthening of the time of the DI by decreasing its slope. When ORM was applied in combination with DOF the increase of the CL was not additive.

Suppression of Ca^{2+} Increases the Effect of I_f Inhibition on Cycle Length in Sinus Node Tissue

In the next set of experiments, we investigated the potential effect of suppression of SR Ca^{2+} release on the effect of IVA (**Figure 6A**). The aim was to minimize the depolarizing activity of the Ca^{2+} release-induced augmentation of the forward NCX by application of 5 µM ryanodine (RYA) after the control recording. This caused a significant CL prolongation (437.8 ± 20.3 ms *vs.* 499.8 ± 10.4 ms; $p < 0.05$, n = 6/6). The subsequently applied 1 µM ORM-10962 marginally but statistically significantly increased the CL (499.8 ± 10.4 ms *vs.* 520.8 ± 29.9 ms; $p < 0.05$; n = 6/6). However, further 3 µM IVA markedly and significantly augmented the CL of the SAN preparations (520.8 ± 29.9 ms *vs.* 726.6 ± 39.8 ms; $p < 0.05$, n = 6/6; **Figure 6B**). In the **Figure 6C** we compared the IVA effects under normal condition (i.e., in the absence of any other inhibitors—20.9 ± 4.1%) and in the presence of RYA+ORM. As bar graphs in **Figure 6C** show, the IVA exerted markedly larger CL prolongation in the presence of RYA+ORM (42.4 ± 5.7%, $p < 0.05$, Student's T-test).

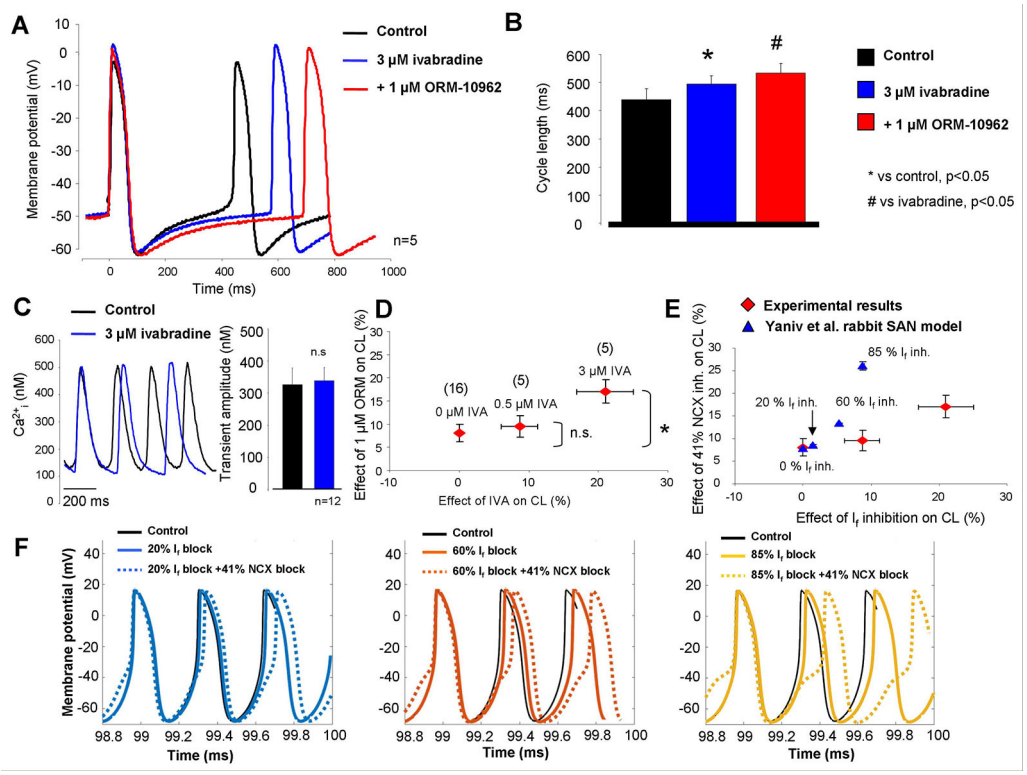

FIGURE 4 | Combined inhibition of Na+/Ca2+ exchanger (NCX) and I_f in sinus node (SAN). As original SAN action potentials and bar graphs report **(A, B)**, 1 µM ORM-10962 (ORM) (red trace) exerted an increased effect after 0.3 µM ivabradine (IVA) pretreatment (blue trace). Panel **(C)** represent Ca^{2+} transients measured from isolated SAN cells under control condition (black trace) and in the presence of 3 µM IVA (blue trace). We found identical Ca^{2+} levels as a result of IVA treatment. In panel **(D)**, the dose dependent effect of IVA (abscissa) on SAN cycle length (CL) was plotted against the effect of consecutive application of 1 µM ORM on CL (ordinate). As was previously described in **Figures 2A–C**, 1 µM ORM has ≈8% effect without IVA. In the presence of 0.5 and 3 µM IVA, the ORM-induced reduction of pacing rate was gradually increased. The numbers in parentheses indicate the corresponding n. The experimental results (red) are compared with the Yaniv SAN cell model (blue) in panel **(E)**. Based on a previous study, 0.5 and 3 µM IVA were represented by 20 and 60% funny current (I_f) inhibition in the presence of constant 41% NCX inhibition. Panel **(F)** represents the modeling results of combined I_f-NCX block. In the three panels, I_f was inhibited by varying degrees (straight lines) and combined with 41% NCX inhibition (dotted lines) yielding an increasing NCX inhibition effect on CL as I_f inhibition increases.

Decrease of $[Ca^{2+}]_O$ Increases the Effect of Funny Current Inhibition on Cycle Length in Sinus Node Tissue

We further tested the coupling between Ca^{2+} handling and I_f on CL control. Reduced $[Ca^{2+}]_o$ (0.9 mM) external solution was selected to achieve this goal since in this concentration, the CL was only slightly reduced (10.3 ± 3.7%). We found that the reduced extracellular Ca^{2+} slightly increased the CL which was further increased after application of 3 µM IVA (control: 469 ± 39.5 ms → 0.9 mM $[Ca^{2+}]_o$: 515.8 ± 40.8 ms → 3 µM IVA: 777 ± 58.7 ms; $p < 0.05$, n = 6/6 hearts, **Figures 7A, B**). We compared again the effects of IVA on the CL under normal condition (i.e., 1.8 $[Ca^{2+}]_o$) and in the presence of low external Ca^{2+} (0.9 mM $[Ca^{2+}]_o$). As bar graphs in **Figure 7C** demonstrates the IVA has markedly improved effect when extracellular Ca^{2+} is low compared with normal Ca^{2+} settings (51.1 ± 5.1% *versus* 20.99 ± 4.1%, $p < 0.05$; Student's t-test). **Figure 7D** represents Ca^{2+} transient measurements from spontaneously contracting isolated cells. We can observe that the application of 0.9 mM $[Ca^{2+}]_o$ significantly decreased the transient amplitude (295 ± 52 nM *vs.* 185 ± 32 nM; $p < 0.05$, n = 8) which may reflect decreased Ca^{2+} influx, SR Ca^{2+} release which may decrease the NCX current and thus attenuate the compensating capacity of NCX. The diastolic Ca^{2+} also significantly decreased (127 ± 33 *vs.* 64 ± 10 nM; $p < 0.05$, n = 8). We addressed this question by using mechanistic modeling (Yaniv et al., 2013b). Left column of **Figure 7E** represents action potentials (upper traces), NCX and I_f current kinetics (middle traces), and global Ca^{2+} transients (lower traces) under normal condition. Upon application of 0.9 mM $[Ca^{2+}]_o$ (right column) the CL slightly reduced, the integral of NCX current under the late phase of DD decreased while the magnitude of I_f current did not changed. The amplitude of the global transient decreased in similar extent as was obtained from SAN cell experiments.

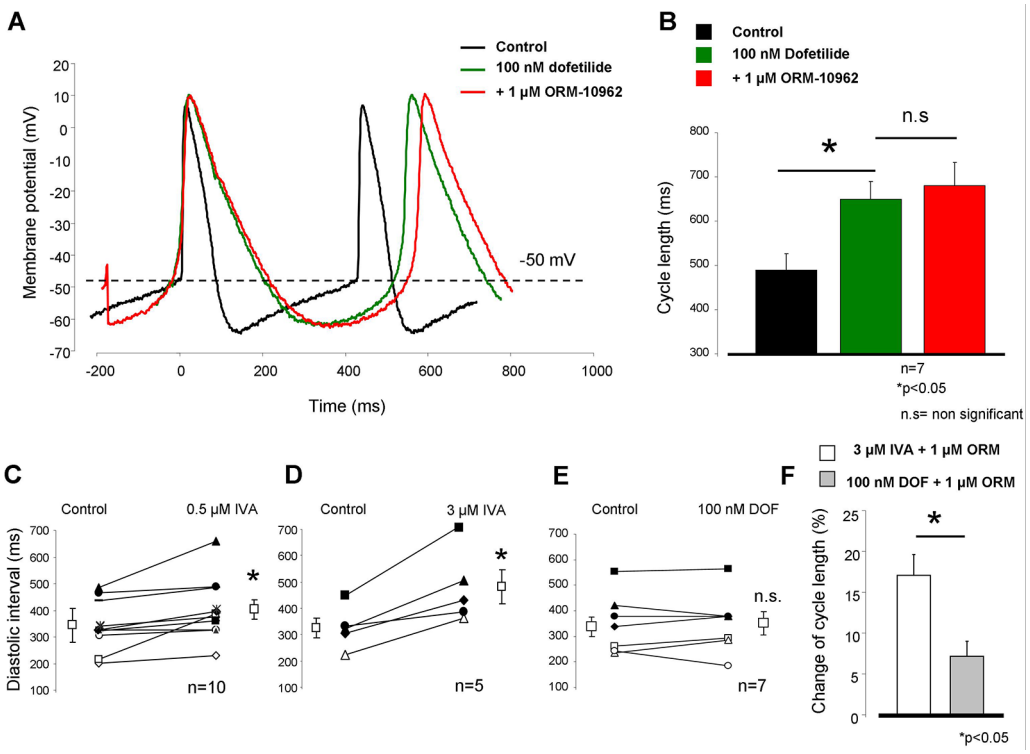

FIGURE 5 | Sinus node (SAN) frequency was decreased by complete I_{Kr} inhibition by 100 nM dofetilide administration. The control cycle length (CL) (black trace) largely increased after dofetilide (green trace). However, the effect of 1 µM ORM-10962 (ORM) did not change compared with the individual effect (red trace, panels **A, B, F)**. The main difference between ivabradine (IVA) and dofetilide (DOF)-induced bradycardia is that 0.5 and 3 µM IVA markedly increased the diastolic interval **(C**, **D)**, which remained unchanged in the case of I_{Kr} inhibition by DOF **(E)**.

Concomitant Inhibition of Na^+/Ca^{2+} Exchanger and Funny Current Increases the Cycle Length Variability in Sinus Node Tissue

The short term CL variability (CLV) was calculated by the analysis of CLs of N = 30 consecutive action potentials by applying the following formula:

$$\mathrm{STV} = \Sigma(\mathrm{CL;i+1} - \mathrm{CL;i}) / \left(n_{beats} x \sqrt{2}\right).$$

One micrometer of ORM-10962 and 3 µM IVA individually prolong the CL without considerable influence on the CL variability (see the area covered in **Figures 8A, B**). The subsequent application of 5 µM RYA (**Figure 8C**, green line) and 5 µM RYA + 1 µM ORM-10962 (**Figure 8C**, red line) showed a tendency to increase the CL variability, however it proved not to be statistically significant. In contrast, additionally adding 3 µM IVA markedly and statistically significantly enhanced the variability parallel with the CL increase, when the Ca^{2+} release and NCX activity were suppressed (**Figure 8C**, blue line). As **Figures 8D**, **E** show, the CL variability exerts similar results as the CL measurements: individual inhibition of NCX (2.53 ± 0.8 ms *vs.* 2.71 ± 0.9 ms; n = 16/16; red line) and I_f (3.6 ± 0.9 ms *vs.* 5.19 ± 0.7 ms; n = 5/5; blue line) or Ca^{2+} handling suppression (3.03 ± 0.87 ms *vs.* 7.0 ± 2.73 ms, n = 7/7; green line) do not alter significantly the CLV while the variability was largely increased if IVA was administrated in the presence of reduced Ca^{2+} cycling activity (7.0 ± 2.73 ms *vs.* 15.29 ± 5.6 ms; orange line).

DISCUSSION

The aim of this study was to verify and estimate the possible contribution of NCX function in SAN automaticity by direct selective pharmacological inhibition. Furthermore, we evaluated the functional consequences of the previously mentioned (Yaniv et al., 2015) I_f-NCX coupling in multicellular tissue level. In this study, we provided evidence for the first time regarding the essential role of NCX in spontaneous automaticity of the SAN by selective pharmacological inhibition. In addition, we described its functional interaction with I_f. This interaction between the DD currents is based on the following experimental results: i) 3 µM IVA has moderate effects on CL (~21%) and CLV (Δ ~ 2 ms), ii) 1 µM ORM has marginal effects on CL (~8%) and no change on CLV, iii) Ca^{2+} cycling suppression by 1 µM ORM + 5 µM RYA has moderate effects on CL (~19%) and CLV (Δ ~ 4 ms), iv) increasing I_f inhibition augments the effect of a

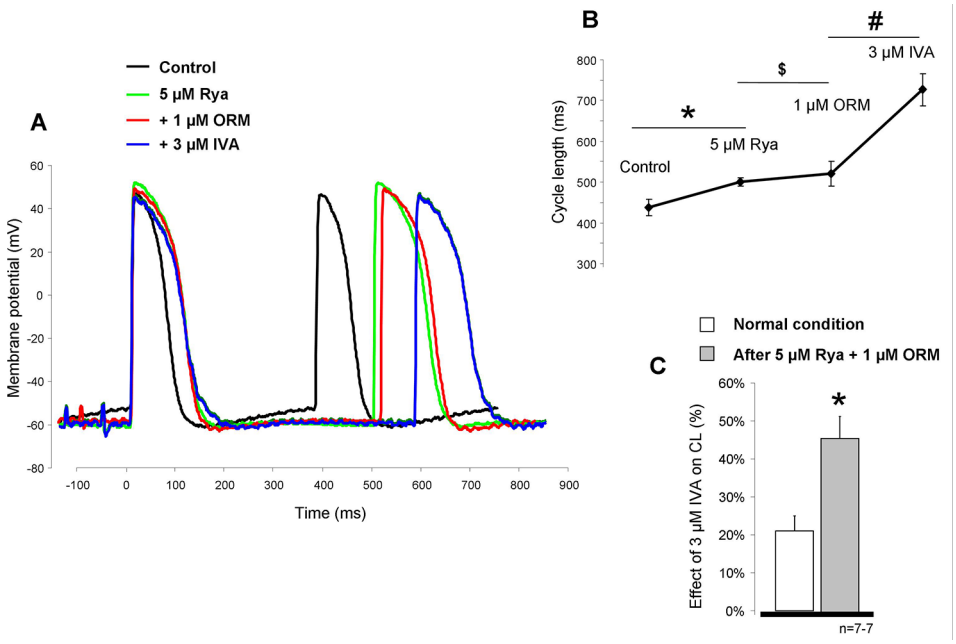

FIGURE 6 | The potential influence of Ca^{2+} handling suppression by 5 μM ryanodine (RYA) (green line) and 1 μM ORM-10962 (red line) on the effect of funny current (I_f) reduction was investigated. As representative curves panel **(A)** and diagram panel **(B)** report, both drugs increased the cycle length (CL) of the action potential. Statistical analysis was achieved by ANOVA. * means RYA compared to control, $ means ORM-10962 (ORM) compared to RYA, and # means ivabradine (IVA) compared to ORM. Comparison of the effect of 3 μM IVA on the CL under normal condition (i.e., without any other inhibitors) and after 5 μM RYA + 1μM ORM shows that the same dose of IVA has markedly increased effect when the contribution of Na+/Ca2+ exchanger (NCX) is reduced by concomitant application of RYA and ORM panel **(C)**.

fixed ORM dose (1 μM) on CL (~ 8 to 17%), v) the effect of 3 uM IVA is enhanced when Ca^{2+} cycling was previously suppressed (from ~ 20 to 42%).

ORM-10962 Does Not Inhibit the Funny Current

The effectiveness and selectivity of ORM-10962, a novel, potent NCX inhibitor was investigated in detail in our previous studies (Kohajda et al., 2016; Oravecz et al., 2017). In these studies, it was shown that ORM inhibited both forward and reverse mode NCX with an IC_{50} values of 55 and 67 nM without changing the I_{Ca}, I_{Na}, I_{K1}, I_{Kr}, I_{Ks}, I_{to}, and $I_{Na}/_K$ pump currents even at high (1 μM) concentrations. However, the I_f current was not investigated. The present study demonstrates that 1 μM ORM did not influence I_f (**Figure 1**) in the presence of high Ca^{2+} buffering, which means that ORM is a suitable tool for the evaluation of NCX in SAN automaticity, however the indirect effects related with ORM-induced Ca^{2+} elevation (without Ca^{2+} buffering) may influence the I_f indirectly (Mattick et al., 2007).

Na^+/Ca^{2+} Exchanger Inhibition Slightly Decreases Sinus Node Firing Rate

We found slight, but statistically significant reduction in the spontaneous firing rate in SAN tissue which is the consequence of the reduced rate of the DD (**Figure 2**). This result is a direct evidence and verification for the contribution of the inward NCX in rhythm generation. Previous studies (Yaniv et al., 2013a; Yaniv et al., 2015) reported that not only the increase of CL, but the parallel increase of pacing variability reports the uncoupling of the I_f-NCX and the destabilization of the DD. Since in our experiments the CL slightly increased while the pacing rate variability did not change, we conclude that the individual NCX inhibition did not cause considerable uncoupling of I_f-NCX.

The rate of forward NCX inhibition by using 1 μM ORM was estimated to ≈90% by applying conventional ramp protocol in the presence of ≈160 nM $[Ca^{2+}]_i$ in canine ventricular myocytes in our previous study (Kohajda et al., 2016). The actual ratio of inhibited NCX which corresponds with the observed CL changes was calculated to 41% by using the Yaniv SAN cell model (Yaniv et al., 2013b). It is important to note, that in our previous study (Oravecz et al., 2017) we have demonstrated that the extent of NCX inhibition (*via* ORM-10962) is decreased when the intracellular Ca^{2+} is intact (i.e., in the presence of Ca^{2+} transient). The underlying mechanism could be asymmetrical block between two modes, autoregulation of the $Ca^{2+}{}_i$ or by preserved inducibility of forward NCX by elevated $Ca^{2+}{}_i$.

Na^+/Ca^{2+} Exchanger Inhibition Markedly Increases the $Ca^{2+}{}_i$ Level

The selective NCX inhibition caused similar diastolic Ca^{2+} changes compared to the Yaniv model predicted, however, in

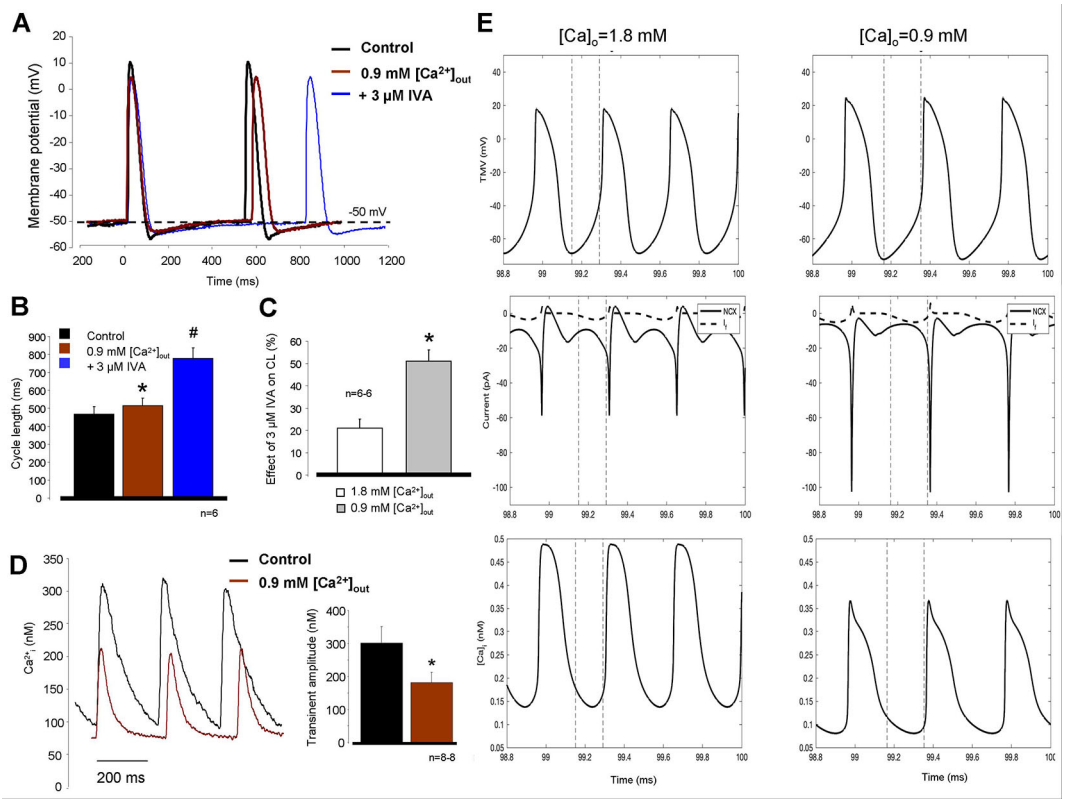

FIGURE 7 | Decreased extracellular Ca^{2+} solution (0.9 mM) was used to suppress the intracellular Ca^{2+} cycling and therefore Na+/Ca2+ exchanger (NCX). The effect of hypocalcemic solution on the cycle length (CL) was marginal (**A, B**, brown trace) however the subsequently applied 3 μM ivabradine (IVA) (blue trace) caused considerable prolongation in the CL. Comparison of the IVA effect in the presence of normal (1.8 mM—white column) *versus* low (0.9 mM—gray column) $CaCl_2$ on panel **(C)** demonstrates nearly doubled effect of IVA on the CL in response of Ca^{2+} reduction **(C)**. * means 0.9 mM $[Ca^{2+}]_o$ compared to control, # means IVA *versus* 0.9 mM $[Ca^{2+}]_o$. Original traces measured from isolated sinus node (SAN) cells in panel **(D)** demonstrate that 0.9 mM $[Ca^{2+}]_o$ (brown trace) significantly decreased the transient amplitude without significant action on diastolic Ca^{2+} levels. **(E)** Modeling simulation of action potentials (upper traces), NCX currents (middle traces, solid lines), I_f currents (middle traces, dashed lines), and global Ca^{2+} transients (lower traces) in the present of normal (1.8 mM), external Ca^{2+} (left column), and 0.9 mM $[Ca^{2+}]_o$ (right column). The results indicate decreased transient amplitude coupled with smaller NCX current in the late diastolic depolarization (DD) with maintained I_f current magnitude in the presence of 0.9 mM $[Ca^{2+}]_o$.

contrast with modeling, we found markedly increased Ca^{2+} transient amplitude which is generally expected after decreased rate of Ca^{2+} extrusion (**Figure 3**). The observed quantitative discrepancy between experiments and modeling may indicate that the extent of NCX inhibition in the experiments could be larger than 41%.

We can speculate that the increasing intracellular Ca^{2+} is known to facilitate the inactivation of the L-type Ca^{2+} current as a part of the autoregulation (Eisner et al., 1998; Eisner et al., 2000). The gain of the $[Ca^{2+}]_i$ may indirectly shortens the CL which means two parallel, counteracting effect of selective NCX inhibition: the inhibition of the inward NCX current may reduce the actual frequency by suppressing its contribution in the DD, however it is partially compensated for the CL abbreviating effect of increased $[Ca^{2+}]_i$. Furthermore, the I_f may also contribute in the limitation of the ORM effect: i) a theoretical possibility exists that ORM-induced Ca^{2+} elevation may increase the I_f, however this was ruled out by a previous work (Zaza et al., 1991). ii) It was reported that SAN myocytes express Ca^{2+}-activated adenylate cyclase isoform, which might raise cAMP (and I_f) in response to NCX blockade (Mattick et al., 2007).

The Moderate Bradycardic Effect of Na^+/Ca^{2+} Exchanger Inhibition May Be Explained by Funny Current-Na^+/Ca^{2+} Exchanger Coupling

However, one may speculate after considering the crucial role of NCX in the coupled-clock theory, why the NCX inhibition-induced "bradycardia" exerted a relatively low influence. Using genetic mouse models Gao *et al.* claimed that partial ablation of NCX (≈70–80%) using an αMHC-inducible "Cre" transgenic line, has also a slight effect on the baseline spontaneous AP firing frequency (Gao et al., 2013). In line with this, it was found that even a small NCX fraction is able to generate sufficient inward current to provide appropriate depolarization current which is

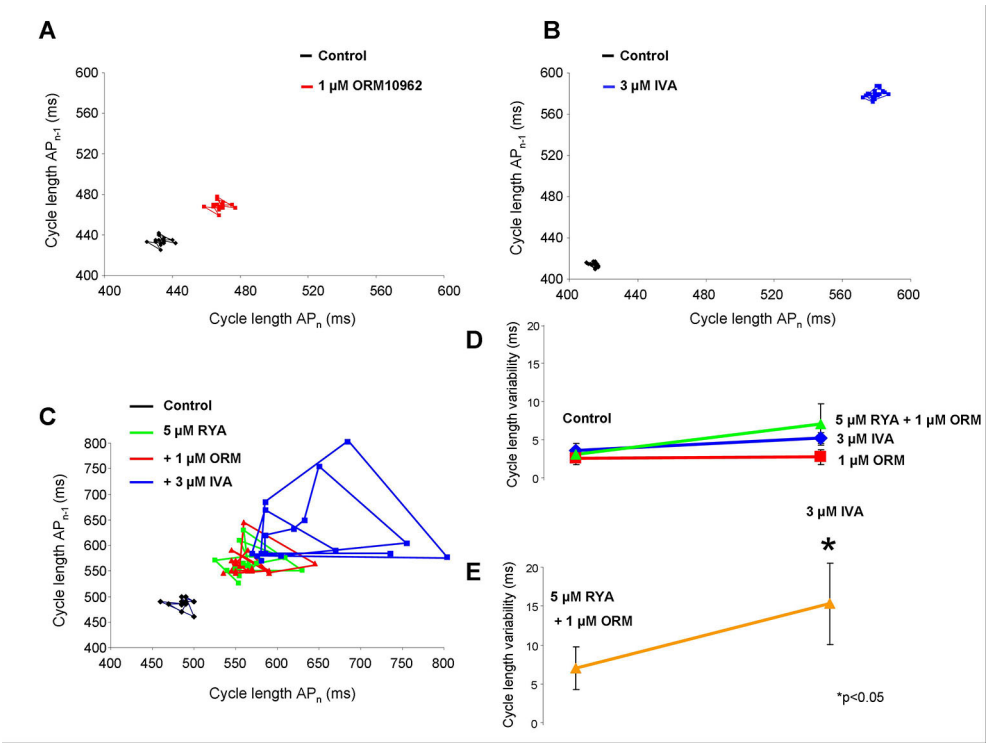

FIGURE 8 | The effect of suppression of diastolic depolarization (DD) currents [Na+/Ca2+ exchanger (NCX) and I_f] on short time cycle length (CL) variability. When 1 μM ORM-10962 panel **(A)** or 3 μM ivabradine (IVA) panel **(B)** were applied, the variability did not change significantly. Instead, the CL was prolonged. Comparison of the effect of 1 μM ORM-10962 (ORM) (red line), 5 μM ryanodine (RYA) (blue line), and 5 μM RYA + 1 μM ORM (green line) on the CL variability shows that these compound do not change the variability significantly panel **(D)**. In contrast IVA administration after the application of RYA+ORM caused considerably increased variability panel **(E)** as the Poincaré-plot (panel **C,** blue line) shows.

able to maintain normal SAN cell activity (Groenke et al., 2013). Our and these previous results highlight the possibility that a functional coupling between I_f and NCX represents a potency to compensate for the NCX inhibition-induced reduction of the pacing frequency.

In accordance with this theory our and previous results indicate a relatively moderate effect of IVA on the CL when it is administrated at 3 μM (**Figure 4A**) or at 10 μM (Yaniv et al., 2012). At the same time, caesium was unable to stop SAN beating even though it has a large effect on I_f (Noma et al., 1983). These inconsistent results can be explained by the voltage-dependent block of IVA or caesium (DiFrancesco, 1995), or by proposing an insulator function of the I_f to protect the SAN cells from the strong negative electrical sink of the connected atrial tissue (Morad and Zhang, 2017). However, a functional coupling between I_f and NCX (Bois et al., 1996; Lakatta et al., 2010; Yaniv et al., 2013a) providing redundant pacemaking systems could also explain—or at least contribute to—the observed results. This phenomenon, which could be very similar to the repolarization reserve (Biliczki et al., 2002; Herrmann et al., 2007; Lengyel et al., 2007; Nagy et al., 2009), may be also able to reduce the effects of the individual inhibition of NCX or I_f explaining the relatively small extent of IVA or NCX effects.

Indeed, we found that the effect of 1 μM ORM gradually increased as the rate of I_f block was enhanced (**Figure 4**). In line with this, the Yaniv model provided similar but steeper tendency, when we represented the 0.5, 1, and 3 μM IVA doses by 20, 60, and 80% I_f block based on previous results (Bois et al., 1996). While 10 μM IVA was not used experimentally due to selectivity problems, 85% I_f inhibition could be computed in the Yaniv model. The detailed modeling results are depicted in **Figures 4E, F**. Consistent with experimental results, the effect of 41% NCX inhibition on CL is increased as I_f inhibition becomes stronger. However, the modeling predicts a much steeper increase in the CL in the presence of enhancing I_f block. The underlying mechanism of this discrepancy could be the markedly higher Ca^{2+} increase measured during experiments which could limit the bradycardic effect of NCX inhibition. A previous study reported a decreased SR Ca^{2+} content after I_f inhibition by IVA (Yaniv et al., 2013a) demonstrating an indirect suppression of NCX during I_f inhibition. Our Ca^{2+} measurements (**Figure 4C**) indicate unchanged Ca^{2+} release after application of IVA, which may indicate that the underlying mechanism of increased ORM effect may be rather related with the increased sensitivity of DD when it is already inhibited by the I_f block.

I_{Kr} Inhibition Mediated Bradycardia Does Not Alter the Effect of Na^+/Ca^{2+} Exchanger Inhibition

It is possible to decelerate spontaneous frequency without major direct influence on I_f or NCX. The SAN rate was reduced by 100% I_{Kr} block (**Figure 5**) in which the developed decrease in the firing rate was mainly achieved by APD prolongation without or minimal change in diastolic interval—instead of I_f block, which markedly increases the diastolic interval without effect on APD. This also means that despite the bradycardia, I_f is intact during these experiments. In line with this, NCX inhibition provided a similar effect to the one which was experienced when NCX was inhibited individually in **Figure 2**. This observation could be explained by an I_f dependent compensation of NCX reduction. At the same time it also means that the mechanism of the bradycardia is important regarding the effect of NCX inhibition. It seems possible that I_f mediated bradycardia and concomitant increase in diastolic interval may be important in the I_f-NCX interaction.

Suppression of Ca^{2+}_i Augments the Effect of Funny Current Inhibition

Assuming that a mutual interaction between I_f and NCX exists, this crosstalk should work in the opposite direction as well, i.e., a disturbance in the Ca^{2+} cycling should affect I_f. The suppression of the Ca^{2+} handling by the subsequent application of ryanodine and ORM together caused ≈20% increase in the CL in line with previous results (Bucchi et al., 2003). Under this condition, the effect of 3 μM IVA was considerably larger compared with normal settings (≈45% *vs.* 20%, see **Figure 6C**). In line with this, we found similar augmentation of IVA effect (21% *vs.* 51%) when Ca^{2+} handling was suppressed by low extracellular Ca^{2+} (**Figure 7**). Experimental as well as modeling simulations suppose that the Ca^{2+} handling and thus the NCX current suppression decreases the flux of the depolarizing NCX current, increases the length of DD, thus, the suppressed net current underlying the DD provides improved effect for I_f inhibition.

Funny Current-Na^+/Ca^{2+} Exchanger Coupling Controls Cycle Length Variability

Previous studies (Yaniv et al., 2013a; Yaniv et al., 2015) reported that the I_f-NCX coupling not only controls the current CL but it may have a crucial role in maintaining the normal rhythm of the SAN. Therefore, the increase of the CL variability could be a further indicator of the integrity of I_f-NCX axis appearing after a considerable CL increase reporting significant I_f-NCX uncoupling. Our results support this assumption indicating that after individual inhibition of I_f or NCX, not only the excessive CL increase is restricted but the SAN rhythm is also maintained. However, when both of I_f and NCX are suppressed, besides the marked CL increase, a perturbation in the rhythm also appeared indicating the exhausted capacity of the I_f-NCX to depolarize the membrane during the DD (**Figure 8**). Since we could not reach complete inhibition of I_f and NCX in our experiments, we cannot estimate precisely the relative importance of these currents in the normal SAN rhythm. However, it seems possible that these currents contribute in the "depolarization reserve" (Herrmann et al., 2007) not only to the control of the current CL but also to the maintenance of the normal pacing rhythm as a consequence of the strong depolarizing of the I_f-NCX crosstalk.

Proposed Mechanism

We suggest that the observed NCX-I_f interplay is the consequence of the increased susceptibility of DD to any intervention when the DD was previously inhibited by another compound (Rocchetti et al., 2000; Zaza and Lombardi, 2001; Monfredi et al., 2014). This means that the bradycardic effect of NCX inhibition is larger when I_f was previously inhibited (independently from the Ca^{2+} handling). *Vice versa*, when the NCX was previously suppressed (as a consequence of reduced Ca^{2+} release) the decreased DD current density is more sensitive to changes, which increases the bradycardic effect of IVA.

CONCLUSION

In the present study, we provide direct pharmacological evidence regarding the role of NCX in pacemaker mechanism by its selective inhibition with the novel, highly selective compound ORM-10962. We found that individual inhibitions of NCX or I_f cause only moderate bradycardia and rhythm disturbance. However, combined suppression of these currents acted synergistically and supports the hypothesis of mutual crosstalk between NCX and I_f in SAN even in multicellular tissue having important functional consequences. This means that individual inhibition of DD currents may have moderated effect on CL and variability under normal conditions because the underlying currents may be able to compensate each other. This important crosstalk may provide a considerable safety margin for SAN pacemaking.

STUDY LIMITATIONS

Our study has three important limitations. 1) The action potentials measured in our experiments do not represent the characteristics of the core SAN cells. These cells are much more "follower" cells, having AP waveforms largely influenced by the cell-to-cell coupling. 2) The applied inhibitors (IVA, ORM, RYA) are not able to cause complete block of ion channels in the applied concentrations. Therefore, the described phenomena indicate only partial effects and not able to estimate the absolute contribution of NCX during the DD. 3) Since our aim was to explore ion current cooperation, our results represent ion channel function independent from the autonomic nervous system. The activation of the sympathetic or parasympathetic nervous system—or modulation of the β_1/M_2 receptors—intimately changes the cAMP, PKA, CaMKII levels which have effects on the DD currents, therefore the discussed I_f-NCX coupling cannot be directly extrapolated to *in vivo* systems. The ion current crosstalk characterization during intact autonomic control requires further experiments.

DATA AVAILABILITY STATEMENT

All datasets generated for this study are included in the article/supplementary material.

ETHICS STATEMENT

The animal study was reviewed and approved by Munkahelyi Állatkísérleti Bizottság (MÁB).

AUTHOR CONTRIBUTIONS

ZK performed ion current measurements and data analysis. NT performed fluorescent optical measurements, action potential measurements and data analysis. JS performed ion current measurements and data analysis. AL performed the computational modeling and data analysis, contributed to conception of the study as well as manuscript preparation and funding for the computational study. PG performed ion current measurements, GB and JP performed action potential measurements. NJ organized the database and ensured the financial support of the study. JL and PP contributed to the development of ORM-10962. JGYP contributed to manuscript preparation, AV and NN ensured the financial support of the study, contributed conception and design of the study, data analysis and visualization, and manuscript preparation. All authors contributed to manuscript revision, read and approved the submitted version.

FUNDING

This work was supported by grants from the National Research Development and Innovation Office (NKFIH PD-125402 (for NN), FK-129117 (for NN), GINOP-2.3.2-15-2016-00006, the LIVE LONGER EFOP-3.6.2-16-2017-00006 project, the János Bolyai Research Scholarship of the Hungarian Academy of Sciences (for NN), the UNKP-18-4-SZTE-76 New National Excellence Program of the Ministry for Innovation and Technology (for NN), the EFOP 3.6.3 VEKOP-16-2017-00009 (for NT), the Hungarian Academy of Sciences and by the Orion Pharma (ORM-10962).

ACKNOWLEDGMENTS

We are grateful to Prof. Dr. David Eisner (University of Manchester, UK) for his help and suggestions for the manuscript. We gratefully acknowledge financial support by the Deutsche Forschungsgemeinschaft (DFG, German Research Foundation) – Project-ID 258734477 – SFB 1173 (to AL). The publication of this study was supported by the University of Szeged Open Access Fund (4309).

REFERENCES

Biliczki, P., Virag, L., Iost, N., Papp, J. G., and Varro, A. (2002). Interaction of different potassium channels in cardiac repolarization in dog ventricular preparations: role of repolarization reserve. *Br. J. Pharmacol.* 137 (3), 361–368. doi: 10.1038/sj.bjp.0704881

Bogdanov, K. Y., Vinogradova, T. M., and Lakatta, E. G. (2001). Sinoatrial nodal cell ryanodine receptor and $Na(^{+})$-$Ca(^{2+})$ exchanger: molecular partners in pacemaker regulation. *Circ. Res.* 88 (12), 1254–1258. doi: 10.1161/hh1201.092095

Bois, P., Bescond, J., Renaudon, B., and Lenfant, J. (1996). Mode of action of bradycardic agent, S 16257, on ionic currents of rabbit sinoatrial node cells. *Br. J. Pharmacol.* 118 (4), 1051–1057. doi: 10.1111/j.1476-5381.1996.tb15505.x

Bucchi, A., Baruscotti, M., Robinson, R. B., and DiFrancesco, D. (2003). I(f)-dependent modulation of pacemaker rate mediated by cAMP in the presence of ryanodine in rabbit sino-atrial node cells. *J. Mol. Cell Cardiol.* 35 (8), 905–913. doi: 10.1016/s0022-2828(03)00150-0

DiFrancesco, D., and Noble, D. (2012). The funny current has a major pacemaking role in the sinus node. *Heart Rhythm.* 9 (2), 299–301. doi: 10.1016/j.hrthm.2011.09.021

DiFrancesco, D. (1981). A new interpretation of the pace-maker current in calf Purkinje fibres. *J. Physiol.* 314, 359–376. doi: 10.1113/JPHYSIOL.1981.SP013713

DiFrancesco, D. (1995). Cesium and the pacemaker current. *J. Cardiovasc. Electrophysiol.* 6 (12), 1152–1155.

Eisner, D. A., Trafford, A. W., Diaz, M. E., Overend, C. L., and O'Neill, S. C. (1998). The control of Ca release from the cardiac sarcoplasmic reticulum: regulation versus autoregulation. *Cardiovasc. Res.* 38 (3), 589–604. doi: 10.1016/s6363(98)00062-5

Eisner, D. A., Choi, H. S., Diaz, M. E., O'Neill, S. C., and Trafford, A. W. (2000). Integrative analysis of calcium cycling in cardiac muscle. *Circ. Res.* 87 (12), 1087–1094. doi: 10.1161/01.res.87.12.1087

Gao, Z., Rasmussen, T. P., Li, Y., Kutschke, W., Koval, O. M., Wu, Y., et al. (2013). Genetic inhibition of Na^{+}-Ca^{2+} exchanger current disables fight or flight sinoatrial node activity without affecting resting heart rate. *Circ. Res.* 112 (2), 309–317. doi: 10.1161/CIRCRESAHA.111.300193

Groenke, S., Larson, E. D., Alber, S., Zhang, R., Lamp, S. T., Ren, X., et al. (2013). Complete atrial-specific knockout of sodium-calcium exchange eliminates sinoatrial node pacemaker activity. *PloS One* 8 (11), e81633. doi: 10.1371/journal.pone.0081633

Herrmann, S., Stieber, J., Stockl, G., Hofmann, F., and Ludwig, A. (2007). HCN4 provides a 'depolarization reserve' and is not required for heart rate acceleration in mice. *EMBO J.* 26 (21), 4423–4432. doi: 10.1038/sj.emboj.7601868

Herrmann, S., Lipp, P., Wiesen, K., Stieber, J., Nguyen, H., Kaiser, E., et al. (2013). The cardiac sodium-calcium exchanger NCX1 is a key player in the initiation and maintenance of a stable heart rhythm. *Cardiovasc. Res.* 99 (4), 780–788. doi: 10.1093/cvr/cvt154

Himeno, Y., Toyoda, F., Satoh, H., Amano, A., Cha, C. Y., Matsuura, H., et al. (2011). Minor contribution of cytosolic Ca2+ transients to the pacemaker rhythm in guinea pig sinoatrial node cells. *Am. J. Physiol. Heart Circ. Physiol.* 300 (1), H251–H261. doi: 10.1152/ajpheart.00764.2010

Jost, N., Nagy, N., Corici, C., Kohajda, Z., Horvath, A., Acsai, K., et al. (2013). ORM-10103, a novel specific inhibitor of the Na+/Ca2+ exchanger, decreases early and delayed afterdepolarizations in the canine heart. *Br. J. Pharmacol.* 170 (4), 768–778. doi: 10.1111/bph.12228

Kohajda, Z., Farkas-Morvay, N., Jost, N., Nagy, N., Geramipour, A., Horvath, A., et al. (2016). The effect of a novel highly selective inhibitor of the Sodium/Calcium exchanger (NCX) on cardiac arrhythmias in In Vitro and In Vivo experiments. *PloS One* 11 (11), e0166041. doi: 10.1371/journal.pone.0166041

Kormos, A., Nagy, N., Acsai, K., Vaczi, K., Agoston, S., Pollesello, P., et al. (2014). Efficacy of selective NCX inhibition by ORM-10103 during simulated ischemia/reperfusion. *Eur. J. Pharmacol.* 740, 539–551. doi: 10.1016/j.ejphar.2014.06.033

Lakatta, E. G., and DiFrancesco, D. (2009). What keeps us ticking: a funny current, a calcium clock, or both? *J. Mol. Cell Cardiol.* 47 (2), 157–170. doi: 10.1016/j.yjmcc.2009.03.022

Lakatta, E. G., Maltsev, V. A., and Vinogradova, T. M. (2010). A coupled system of intracellular Ca^{2+} clocks and surface membrane voltage clocks controls the timekeeping mechanism of the heart's pacemaker. *Circ. Res.* 106 (4), 659–673. doi: 10.1161/CIRCRESAHA.109.206078

Lengyel, C., Varro, A., Tabori, K., Papp, J. G., and Baczko, I. (2007). Combined pharmacological block of I(Kr) and I(Ks) increases short-term QT interval variability and provokes torsades de pointes. *Br. J. Pharmacol.* 151 (7), 941–951. doi: 10.1038/sj.bjp.0707297

Mattick, P., Parrington, J., Odia, E., Simpson, A., Collins, T., and Terrar, D. (2007). Ca^{2+}-stimulated adenylyl cyclase isoform AC1 is preferentially expressed in guinea-pig sino-atrial node cells and modulates the I(f) pacemaker current. *J.7 Physiol.* 582 (Pt 3), 1195–1203. doi: 10.1113/jphysiol.2007.133439

Monfredi, O., Lyashkov, A. E., Johnsen, A. B., Inada, S., Schneider, H., Wang, R., et al. (2014). Biophysical characterization of the underappreciated and important relationship between heart rate variability and heart rate. *Hypertension* 64 (6), 1334–1343. doi: 10.1161/HYPERTENSIONAHA.114.03782

Morad, M., and Zhang, X. H. (2017). Mechanisms of spontaneous pacing: sinoatrial nodal cells, neonatal cardiomyocytes, and human stem cell derived cardiomyocytes. *Can. J. Physiol. Pharmacol.* 95 (10), 1100–1107. doi: 10.1139/cjpp-2016-0743

Nagy, N., Szuts, V., Horvath, Z., Seprenyi, G., Farkas, A. S., Acsai, K., et al. (2009). Does small-conductance calcium-activated potassium channel contribute to cardiac repolarization? *J. Mol. Cell Cardiol.* 47 (5), 656–663. doi: 10.1016/j.yjmcc.2009.07.019

Noble, D., Noble, P. J., and Fink, M. (2010). Competing oscillators in cardiac pacemaking: historical background. *Circ. Res.* 106 (12), 1791–1797. doi: 10.1161/CIRCRESAHA.110.218875

Noma, A., Morad, M., and Irisawa, H. (1983). Does the "pacemaker current" generate the diastolic depolarization in the rabbit SA node cells? *Pflugers Arch.* 397 (3), 190–194. doi: 10.1007/bf00584356

Oravecz, K., Kormos, A., Gruber, A., Marton, Z., Kohajda, Z., Mirzaei, L., et al. (2017). Inotropic effect of NCX inhibition depends on the relative activity of the reverse NCX assessed by a novel inhibitor ORM-10962 on canine ventricular myocytes. *Eur. J. Pharmacol.* 818, 278–286. doi: 10.1016/j.ejphar.2017.10.039

Rocchetti, M., Malfatto, G., Lombardi, F., and Zaza, A. (2000). Role of the input/output relation of sinoatrial myocytes in cholinergic modulation of heart rate variability. *J. Cardiovasc. Electrophysiol.* 11 (5), 522–530. doi: 10.1111/j.1540-8167.2000.tb00005.x

Sanders, L., Rakovic, S., Lowe, M., Mattick, P. A., and Terrar, D. A. (2006). Fundamental importance of Na+-Ca2+ exchange for the pacemaking mechanism in guinea-pig sino-atrial node. *J. Physiol.* 571 (Pt 3), 639–649. doi: 10.1113/jphysiol.2005.100305

Sirenko, S. G., Maltsev, V. A., Yaniv, Y., Bychkov, R., Yaeger, D., Vinogradova, T., et al. (2016). Electrochemical Na+ and Ca2+ gradients drive coupled-clock regulation of automaticity of isolated rabbit sinoatrial nodal pacemaker cells. *Am. J. Physiol. Heart Circ. Physiol.* 311 (1), H251–H267. doi: 10.1152/ajpheart.00667.2015

Verkerk, A. O., den Ruijter, H. M., Bourier, J., Boukens, B. J., Brouwer, I. A., Wilders, R., et al. (2009). Dietary fish oil reduces pacemaker current and heart rate in rabbit. *Heart Rhythm.* 6 (10), 1485–1492. doi: 10.1016/j.hrthm.2009.07.024

Yaniv, Y., Maltsev, V. A., Ziman, B. D., Spurgeon, H. A., and Lakatta, E. G. (2012). The "funny" current (I(f)) inhibition by ivabradine at membrane potentials encompassing spontaneous depolarization in pacemaker cells. *Molecules* 17 (7), 8241–8254.

Yaniv, Y., Sirenko, S., Ziman, B. D., Spurgeon, H. A., Maltsev, V. A., and Lakatta, E. G. (2013a). New evidence for coupled clock regulation of the normal automaticity of sinoatrial nodal pacemaker cells: bradycardic effects of ivabradine are linked to suppression of intracellular Ca(2)(+) cycling. *J. Mol. Cell Cardiol.* 62, 80–89. doi: 10.1016/j.yjmcc.2013.04.026

Yaniv, Y., Stern, M. D., Lakatta, E. G., and Maltsev, V. A. (2013b). Mechanisms of beat-to-beat regulation of cardiac pacemaker cell function by Ca(2)(+) cycling dynamics. *Biophys. J.* 105 (7), 1551–1561. doi: 10.1016/j.bpj.2013.08.024

Yaniv, Y., Lakatta, E. G., and Maltsev, V. A. (2015). From two competing oscillators to one coupled-clock pacemaker cell system. *Front. Physiol.* 6, 28. doi: 10.3389/fphys.2015.00028

Zaza, A., and Lombardi, F. (2001). Autonomic indexes based on the analysis of heart rate variability: a view from the sinus node. *Cardiovasc. Res.* 50 (3), 434–442. doi: 10.1016/s0008-6363(01)00240-1

Zaza, A., Maccaferri, G., Mangoni, M., and DiFrancesco, D. (1991). Intracellular calcium does not directly modulate cardiac pacemaker (if) channels. *Pflugers Arch.* 419 (6), 662–664. doi: 10.1007/BF00370312

Conflict of Interest: PP and JL are employed by Orion Pharma, which has been involved in the development of ORM-10962.

The remaining authors declare that the research was conducted in the absence of any commercial or financial relationships that could be construed as a potential conflict of interest.

NRC Research Press

ARTICLE

Muscarinic agonists inhibit the ATP-dependent potassium current and suppress the ventricle–Purkinje action potential dispersion[1]

Tibor Magyar, Tamás Árpádffy-Lovas, Bence Pászti, Noémi Tóth, Jozefina Szlovák, Péter Gazdag, Zsófia Kohajda, András Gyökeres, Balázs Györe, Zsolt Gurabi, Norbert Jost, László Virág, Julius Gy. Papp, Norbert Nagy, and István Koncz

Abstract: Activation of the parasympathetic nervous system has been reported to have an antiarrhythmic role during ischemia–reperfusion injury by decreasing the arrhythmia triggers. Furthermore, it was reported that the parasympathetic neurotransmitter acetylcholine is able to modulate the ATP-dependent potassium current ($I_{K\text{-}ATP}$), a crucial current activated during hypoxia. However, the possible significance of this current modulation in the antiarrhythmic mechanism is not fully clarified. Action potentials were measured using the conventional microelectrode technique from canine left ventricular papillary muscle and free-running Purkinje fibers, under normal and hypoxic conditions. Ionic currents were measured using the whole-cell configuration of the patch-clamp method. Acetylcholine at 5 μmol/L did not influence the action potential duration (APD) either in Purkinje fibers or in papillary muscle preparations. In contrast, it significantly lengthened the APD and suppressed the Purkinje–ventricle APD dispersion when it was administered after 5 μmol/L pinacidil application. Carbachol at 3 μmol/L reduced the pinacidil-activated $I_{K\text{-}ATP}$ under voltage-clamp conditions. Acetylcholine lengthened the ventricular action potential under simulated ischemia condition. In this study, we found that acetylcholine inhibits the $I_{K\text{-}ATP}$ and thus suppresses the ventricle–Purkinje APD dispersion. We conclude that parasympathetic tone may reduce the arrhythmogenic substrate exerting a complex antiarrhythmic mechanism during hypoxic conditions.

Key words: acetylcholine, Purkinje fibers, papillary muscles, hypoxia.

Résumé : On a rapporté que l'activation du système nerveux parasympathique joue un rôle antiarythmique pendant l'ischémie reperfusion par l'inhibition des déclencheurs des arythmies. En outre, on a rapporté que l'acétylcholine, neurotransmetteur parasympathique, est en mesure de moduler le courant potassique ATP dépendant ($I_{K\text{-}ATP}$), un courant essentiel qui est activé pendant l'hypoxie. Cependant, la signification éventuelle de la modulation de ce courant dans le mode d'action antiarythmique n'a pas été entièrement clarifié. Nous avons mesuré des potentiels d'action à l'aide de la technique de microélectrode classique dans le muscle papillaire et des fibres de Purkinje libres de ventricule gauche, en situations normale et hypoxique chez le chien. Nous avons mesuré les courants ioniques à l'aide de la configuration sur cellules entières de la méthode de « patch clamp ». L'acétylcholine à 5 μmol/L n'avait pas d'influence sur la durée du potentiel d'action (DPA), tant dans les préparations de fibres de Purkinje que dans le muscle papillaire. Cependant, elle entraînait un allongement de la DPA et une inhibition complète de la dispersion de la DPA entre le Purkinje et le muscle quand elle était administrée après l'administration de pinacidil à 5 μmol/L. Le carbachol à 3 μmol/L entraînait une diminution du courant $I_{K\text{-}ATP}$ activé par le pinacidil sous clampage du voltage. L'acétylcholine entraînait un allongement de la DPA ventriculaire en situation d'ischémie reperfusion. Dans cette étude, nous avons observé que l'acétylcholine entraîne une inhibition du courant $I_{K\text{-}ATP}$ et conséquemment une inhibition complète de la dispersion de la DPA entre le muscle et le Purkinje. Nous en arrivons à la conclusion que le tonus parasympathique pourrait permettre d'atténuer le substrat arythmogène exerçant un mode d'action antiarythmique complexe en situation d'hypoxie. [Traduit par la Rédaction]

Mots-clés : acétylcholine, fibres de Purkinje, muscles papillaires, hypoxie.

Received 13 July 2020. Accepted 16 November 2020.

T. Magyar,* T. Árpádffy-Lovas,* B. Pászti, N. Tóth, J. Szlovák, P. Gazdag, A. Gyökeres, Z. Gurabi, and I. Koncz.† Department of Pharmacology and Pharmacotherapy, Faculty of Medicine, University of Szeged, Szeged, Hungary.

Z. Kohajda. MTA-SZTE Research Group of Cardiovascular Pharmacology, Hungarian Academy of Sciences, Szeged, Hungary.

B. Györe. Faculty of Dentistry, University of Szeged, Hungary.

N. Jost. Department of Pharmacology and Pharmacotherapy, Faculty of Medicine, University of Szeged, Szeged, Hungary; MTA-SZTE Research Group of Cardiovascular Pharmacology, Hungarian Academy of Sciences, Szeged, Hungary; Department of Pharmacology and Pharmacotherapy, Interdisciplinary Excellence Centre, University of Szeged, Szeged, Hungary.

L. Virág. Department of Pharmacology and Pharmacotherapy, Faculty of Medicine, University of Szeged, Szeged, Hungary; Department of Pharmacology and Pharmacotherapy, Interdisciplinary Excellence Centre, University of Szeged, Szeged, Hungary.

J.Gy. Papp and N. Nagy.† Department of Pharmacology and Pharmacotherapy, Faculty of Medicine, University of Szeged, Szeged, Hungary; MTA-SZTE Research Group of Cardiovascular Pharmacology, Hungarian Academy of Sciences, Szeged, Hungary.

Corresponding author: István Koncz (email: koncz.istvan@med.u-szeged.hu).

*Shared first authorship.

†Shared senior authorship.

[1]This paper is part of a special issue of selected papers from the joint North American/European IACS 2019.

Introduction

The parasympathetic nervous system has a crucial role in controlling the actual heart rate and impulse propagation by influencing the sinoatrial and atrioventricular nodes (Higgins et al. 1973). The parasympathetic nerve endings operate by releasing acetylcholine that acts on M_2 receptors, activating several intracellular signaling routes, and ultimately influencing the cardiac ion channels (Harvey and Belevych 2003). Even though the parasympathetic nervous system primarily innervates the supraventricular areas of the heart, there are certain important ion channels in the ventricular muscle that are known to be influenced by the release of acetylcholine. It has previously been reported that the inward rectifier potassium current (I_{K1}; Koumi et al. 1995) and the slow component of the delayed rectifier potassium current (I_{Ks}; Pappano and Carmeliet 1979) are inhibited, whereas ATP-dependent potassium current ($I_{K\text{-}ATP}$) and acetylcholine-activated inward-rectifying potassium current ($I_{K\text{-}ACh}$) are activated by acetylcholine via G proteins (Terzic et al. 1994; Ito et al. 1994; Kim et al. 1997).

The importance of these effects of acetylcholine is underpinned by the fact that the activation of $I_{K\text{-}ATP}$ channels is well known during hypoxia and ischemia, situations in which the duration of the action potential is shortened (Weiss and Venkatesh 1993). Furthermore, it was reported that vagal activation is also facilitated under ischemia–reperfusion (Recordati et al. 1971). This vagal activation during hypoxia could be antiarrhythmic, since it was reported that increased parasympathetic tone reduces the catecholaminergic-induced early and delayed afterdepolarizations (arrhythmia triggers) (Song et al. 1992) and reduces the incidence of ventricular fibrillation (Zuanetti et al. 1987; Collins and Billman 1989). However, the underlying mechanism of the antiarrhythmic effect of M_2-receptor activation is not fully clarified.

Arrhythmias may develop when an arrhythmogenic substrate (e.g., dispersion of repolarization) and arrhythmia triggers (e.g., early and delayed afterdepolarizations) simultaneously exist in the heart. The arrhythmogenic substrate could be prominent at Purkinje–ventricle connections because of the relatively weak electrotonic coupling due to a low number of gap junctions (Varró and Baczkó 2010). As a consequence of the different pharmacological susceptibility of Purkinje fibers and ventricular muscles (Baláti et al. 1998); the activation of $I_{K\text{-}ATP}$ may modulate the Purkinje and ventricular action potential duration (APD) to different extents, and the developed APD dispersion may contribute to the onset of arrhythmias.

The objective of this study was to investigate the possible effect of acetylcholine on the $I_{K\text{-}ATP}$ and on the $I_{K\text{-}ATP}$-mediated APD dispersion under normal and hypoxic conditions.

We also studied the effect of acetylcholine and cilostazol on pharmacological Purkinje fiber models of the early repolarization syndrome. These findings are available as Supplementary Material[2].

Methods

Human tissues

Non-diseased human hearts that were unusable for transplantation (based on logistical, not patient-related considerations) were obtained from organ donors. Before cardiac explanation, organ donor patients did not receive any medication except dobutamine, furosemide, and plasma expanders. The investigations conform to the principles outlined in the *Declaration of Helsinki* of the World Medical Association. All experimental protocols were approved by the Scientific and Research Ethical Committee of the Medical Scientific Board at the Hungarian Ministry of Health (ETT-TUKEB), under ethical approval No. 4991-0/2010-1018EKU (339/PI/010). Human cardiac tissue was stored in cardioplegic solution at 4 °C for 4–8 h.

Animals

All experiments using canine cardiac preparations were carried out in compliance with the principles of the *Guide for the Care and Use of Laboratory Animals* (USA NIH publication N. 85-23, revised 1996) and conformed to Directive 2010/63/EU of the European Parliament. The protocols have been approved by the Ethical Committee for the Protection of Animals in Research of the University of Szeged, Szeged, Hungary (approval No. I-74-24-2017) and by the Department of Animal Health and Food Control of the Ministry of Agriculture and Rural Development (authority approval No. XIII/3331/2017).

Conventional microelectrode technique

Ventricular (papillary or trabecular) muscles were obtained from the right ventricle of canine hearts. Free-running Purkinje fibers were identified as false tendons and isolated from both ventricles of human and canine hearts. Canine hearts were removed through a right lateral thoracotomy from anesthetized (thiopental 30 mg/kg i.v.) mongrel dogs of either sex weighing 10–15 kg. At impalement, Purkinje fibers were observed under a surgical microscope (Zeiss OPMI PRO). The preparations were placed in Locke's solution and allowed to equilibrate for at least 2 h while superfused (flow rate 4–5 mL/min) also with Locke's solution containing (in mmol/L) NaCl 120, KCl 4, $CaCl_2$ 2, $MgCl_2$ 1, $NaHCO_3$ 22, and glucose 11. The pH of this solution was 7.40–7.45 when gassed with 95% O_2 and 5% CO_2 at 37 °C. In the experiments in which the effects of tissue hypoxia were examined, we changed the gas mixture to 95% N_2 and 5% CO_2, pH remained at 7.40–7.45. All experiments were performed at 37 °C. During the equilibration period, preparations were stimulated at a basic cycle length of 500 ms. Electrical pulses of 0.5–2 ms in duration at twice the diastolic threshold in intensity (S_1) were delivered to the preparations through bipolar platinum electrodes. Transmembrane potentials were recorded using glass capillary microelectrodes filled with 3 mol/L KCl (tip resistance: 5 to 15 MΩ). The microelectrodes were coupled through an Ag–AgCl junction to the input of a high-impedance, capacitance-neutralizing amplifier (Experimetria 2011). Intracellular recordings were displayed on a storage oscilloscope (Hitachi V-555) and led to a computer system (APES) designed for on-line determination of the following parameters: resting membrane potential, action potential amplitude, APD at 10%–90% repolarization, and the maximum rate of rise of the action potential upstroke (V_{max}). Control recordings were obtained after an equilibration period. The compounds used in all experiments were purchased from Sigma/Merck.

Cell isolation

Ventricular myocytes were enzymatically dissociated from the left ventricle of dog hearts. Canine hearts were removed through a right lateral thoracotomy from anesthetized (thiopental 30 mg/kg i.v.) mongrel dogs of either sex weighing 10–15 kg. Cardiac myocytes were isolated from the left ventricle, containing an arterial branch through which the segment was perfused on a Langendorff apparatus with solutions in the following sequence: normal Tyrode's solution (containing in mmol/L 144 NaCl, 0.4 NaH_2PO_4, 4 KCl, 0.53 $MgSO_4$, 1.8 $CaCl_2$, 5.5 glucose, 5 HEPES, pH 7.4 adjusted with NaOH) for 10 min, Ca^{2+}-free Tyrode's solution for 10 min, and Ca^{2+}-free Tyrode's solution containing collagenase (Worthington type II, 0.66 mg/mL). To the final perfusion solution, protease (type XIV, 0.12 mg/mL) was added at the 15 and the 30 min timepoints for digestion.

[2]Supplementary data are available with the article at https://doi.org/10.1139/cjpp-2020-0408.

Fig. 1. Representative traces of Purkinje fiber (PF) (A, B) and ventricular muscle (VM) preparations (C, D); 5 μmol/L acetylcholine (red dotted lines) alone caused no changes in either preparation type (A, C), whereas it caused significant prolongation when applied cumulatively after 5 μmol/L pinacidil (B, D, pinacidil effect represented as blue dashed lines). Bars in panel E represent the values of APD_{90} in each treatment group, from top to bottom corresponding to the traces A to D. Abbreviations under bars: C, control; P, pinacidil, A, acetylcholine. The pacing cycle length was 500 ms. Values are mean ± standard error; *, # denote a significant difference at $p < 0.05$ by RM-ANOVA followed by Bonferroni's post-hoc test. [Colour online.]

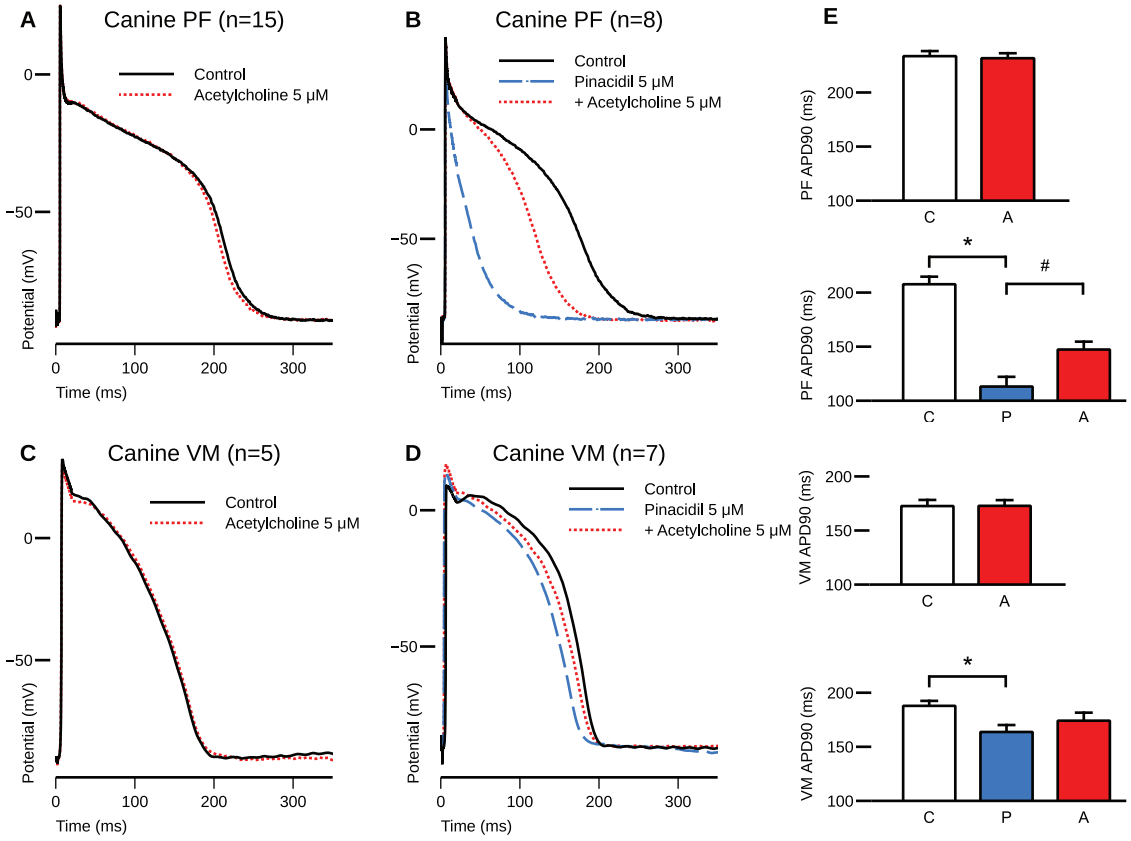

Measurement of ionic currents

One drop of cell suspension was placed in a transparent recording chamber mounted on the stage of an inverted microscope (Olympus IX51, Tokyo, Japan), and individual myocytes were allowed to settle and adhere to the chamber bottom for at least 5–10 min before superfusion was initiated and maintained by gravity. Only rod-shaped cells with clear striations were used. HEPES-buffered Tyrode's solution (composition in mmol/L: NaCl 144, NaH_2PO_4 0.4, KCl 4.0, $CaCl_2$ 1.8, $MgSO_4$ 0.53, glucose 5.5, and HEPES 5.0, at pH of 7.4) was used as the normal superfusate. During the measurement of $I_{K\text{-}ATP}$, 1 μmol/L nisoldipine was added to the bath solution to block L-type Ca^{2+} channel (I_{CaL}), rapidly activating delayed rectifier K^+ channel (I_{Kr}) was blocked by 0.1 μmol/L dofetilide, and I_{Ks} was blocked by 0.5 μmol/L HMR-1556. Micropipettes were fabricated from borosilicate glass capillaries (Science Products GmbH, Hofheim, Germany), using a P-97 Flaming/Brown micropipette puller (Sutter Co., Novato, California, USA), and had a resistance of 1.5–2.5 MΩ when filled with pipette solution. The membrane currents were recorded with Axopatch-200B amplifiers (Molecular Devices, Sunnyvale, California, USA) by applying the whole-cell configuration of the patch-clamp technique. The membrane currents were digitized with an 250 kHz analogue-to-digital converter (Digidata 1440A; Molecular Devices, Sunnyvale, California, USA) under software control (pClamp 8 and pClamp 10; Molecular Devices, Sunnyvale, California, USA). The composition of the pipette solution (in mmol/L) was as follows: KOH 110, KCl 40, K_2ATP 5, $MgCl_2$ 5, EGTA 5, HEPES 10, and GTP 0.1 (pH was adjusted to 7.2 by aspartic acid).

Statistical analysis

Results are expressed as mean ± standard error of the mean (SE). Normality of distributions was verified using the Shapiro–Wilk test, and homogeneity of variances was verified using Bartlett's test in each treatment group. Statistical comparisons were made using analysis of variance (ANOVA) for repeated measurements, followed by Bonferroni's post-hoc test. Differences were considered significant when p was <0.05.

Results

Acetylcholine lengthened the APD after pinacidil-mediated action potential shortening

Canine Purkinje fibers and ventricular papillary muscles were paced at a 500 ms cycle length. In canine Purkinje fibers (PFs; $n = 15$), acetylcholine (5 μmol/L) did not affect the repolarization (233.6 ± 4.7 ms to 231.7 ± 4.6 ms; Figs. 1A and 1E). In contrast, in canine Purkinje fibers (n = 8), the $I_{K\text{-}ATP}$ activator pinacidil, applied in a 5 μmol/L concentration, significantly abbreviated the APD_{90} (207.7 ± 7.0 ms versus 113.1 ± 9.1 ms, $p <$ 0.05) values. After steady state was reached, acetylcholine was administered. Within 3 min, acetylcholine prolonged the APD_{90} to 147.3 ± 7.4 ms, partially reversing the effects of pinacidil (Figs. 1B and 1E; $p < 0.05$).

Fig. 2. Pinacidil (5 μmol/L) increased the action potential duration (APD) dispersion (indicated by ΔAPD_{90} in percentages, and in ms above the bars) between Purkinje fiber (PF) and ventricular muscle (VM) preparations, whereas acetylcholine (5 μmol/L), when applied after pinacidil, decreased dispersion. The pacing cycle length was 500 ms. [Colour online.]

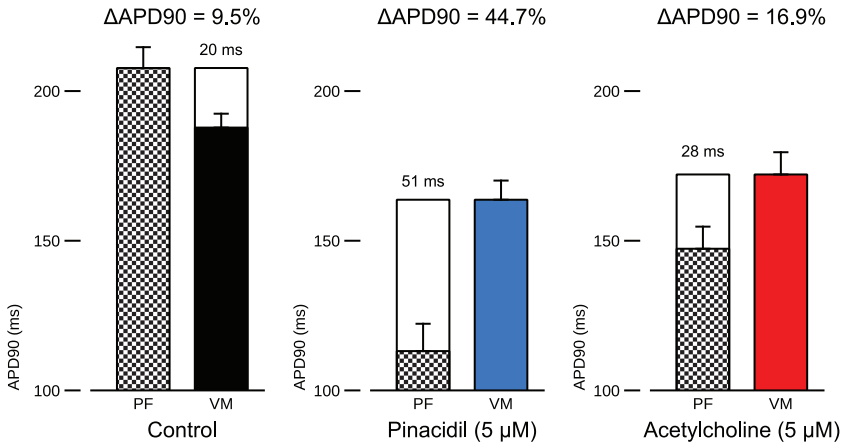

Similarly, as observed in Purkinje fibers, 5 μmol/L acetylcholine alone failed to influence the APD of the ventricular muscle (APD_{90}: 172.6 ± 5.7 ms versus 172.8 ± 5.3 ms; Fig. 1C). Pinacidil (n = 5; 5 μmol/L) pretreatment significantly abbreviated the APD_{90} value (187.9 ± 4.5 ms versus 163.7 ± 6.4 ms, $p < 0.05$), similarly to the effects observed in the case of Purkinje fibers. After a period of 30 min, sufficient to reach a steady state, acetylcholine was added to the superfusate. Within 4 min, acetylcholine (5 μmol/L) prolonged APD_{90} to 172.1 ± 7.4 ms ($p < 0.05$), thus, partially reversing the effects of pinacidil (Figs. 1D and 1E).

Acetylcholine decreased the calculated APD dispersion between Purkinje fibers and ventricular muscles

The changes in the difference between the APD_{90} values of Purkinje fibers and ventricular muscles can be used to infer the effects of pinacidil and acetylcholine on the dispersion between these cardiac tissue types (Fig. 2). The control APD_{90} dispersion (9.5%, 20 ms) was significantly increased upon 5 μmol/L pinacidil application (44.7%, 51 ms). On the other hand, subsequently applied 5 μmol/L acetylcholine markedly decreased the repolarization heterogeneity (16.9%, 28 ms; $p < 0.05$).

Carbachol decreased the pinacidil-induced current activation

During ionic current measurements, voltage ramps were used from a holding potential of −90 mV. Membrane potential was hyperpolarized to −120 mV, and then was slowly (over 36 s) depolarized to 60 mV. Ionic currents were analyzed and compared at 0 and +30 mV. We found that carbachol did not change the control current when it was applied *without* pinacidil (0 mV control: 0.20 ± 0.2 pA/pF versus 3 μmol/L carbachol: 0.32 ± 0.2 pA/pF, n = 6; +30 mV control: 0.55 ± 0.4 pA/pF versus 3 μmol/L carbachol: 0.74 ± 0.3 pA/pF, n = 6) (Fig. 3B). In contrast, when 5 μmol/L pinacidil was applied first, subsequently employed carbachol significantly reduced the current at both voltages (0 mV control: 0.24 ± 0.2 pA/pF → 5 μmol/L pinacidil: 2.03 ± 0.3 pA/pF → 3 μmol/L carbachol: 1.51 ± 0.4 pA/pF, n = 8, $p < 0.05$; +30 mV control: 0.78 ± 0.6 pA/pF → 5 μmol/L pinacidil: 3.17 ± 0.3 pA/pF → 3 μmol/L carbachol: 2.26 ± 0.3 pA/pF, n = 8, $p < 0.05$) (Fig. 3C).

These measurements were carried out with acetylcholine as well. However, we found carbachol to be more stable during the applied long voltage protocol.

Acetylcholine restored the APD after hypoxia-induced action potential shortening

Simulated hypoxia, achieved by gassing the solution with N_2 and CO_2 instead of O_2 and CO_2, resulted in a significant abbreviation of APD_{90} from 181.4 ± 5.7 to 135.0 ± 8.6 ms ($p < 0.05$) (Figs. 4A and 4B), and a decrease in amplitude (103.7 ± 2.8 versus 92 ± 3.5 mV). The maximum rate of depolarization was also decreased (185.8 ± 15.8 versus 156.1 ± 20.6 V/s). When applied during hypoxia, 5 μmol/L acetylcholine caused a significant APD_{90} prolongation to 164.4 ± 4.4 ms, partially reversing the effect of hypoxia on the repolarization. AMP returned to a normal range (102.1 ± 1.6 mV), while V_{max} remained at 156.0 ± 16.1 V/s.

Acetylcholine caused a slight abbreviation in human Purkinje fibers

In human Purkinje fibers (n = 2), 5 μmol/L acetylcholine caused a slight abbreviation of APD_{90}, from 269.0 ± 28.4 to 251.6 ± 42.85 ms, and APD_{50}, from 184.4 ± 20.0 to 173.3 ± 27.1 ms, without affecting other characteristics of the action potential (Fig. 5).

Discussion

In this study we investigated the electrophysiological effects of muscarinic agonists on the $I_{K\text{-}ATP}$ current. We found that (*i*) under normal conditions acetylcholine did not influence the APD. (*ii*) In contrast, when $I_{K\text{-}ATP}$ was pharmacologically activated by pinacidil, subsequently applied acetylcholine lengthened the APD as well as (*iii*) reduced the pinacidil-induced Purkinje–ventricle APD dispersion. (*iv*) In line with this, carbachol inhibited the $I_{K\text{-}ATP}$ that was previously activated by pinacidil. (*v*) Acetylcholine increased the APD after hypoxia-induced action potential shortening.

Acetylcholine inhibits the $I_{K\text{-}ATP}$ in canine ventricular myocytes

It is well known that acetylcholine shortens the atrial APD and has been implicated in atrial fibrillation (Nakayama et al. 1968). Acetylcholine directly affects the GIRK1/4 or Kir3.1 and (or) Kir3.4 channels (Nobles et al. 2018; Corey and Clapham 1998); encoded by *KCNJ3* and *KCNJ4* genes (Kurachi 1995). These channels are largely expressed in atrial, sinoatrial and atrioventricular nodal cells (Navarro-Polanco et al. 2013). At the same time, previous studies (Terzic et al. 1994; Ito et al. 1994) claimed that acetylcholine activates the $I_{K\text{-}ATP}$ channels, even though the physiological consequences of this effect on the action potential were not clarified.

Fig. 3. Effect of carbachol on $I_{K\text{-}ATP}$. Ionic currents were measured under a slow voltage ramp protocol (panel A) between –120 mV and 60 mV. The currents were analyzed at 0 and 30 mV. Panel B demonstrates original representative current traces (left) and bar graphs (right) where 3 μmol/L carbachol (dotted line) failed to influence the control current analyzed at 0 mV. Inset shows identical current fractions between –3 mV and 45 mV (indicated by dashed rectangle). Current traces in panel C, as well as in the inset, illustrate large increase of the membrane current after application of 5 μmol/L pinacidil (blue dashed line) that was inhibited by the subsequently applied 3 μmol/L carbachol (red dotted line). In bar graphs (right), an asterisk (*) denotes significant change between control (left column) and pinacidil (middle column), and a hash tag (#) indicates significant change between pinacidil (middle column) and carbachol (right column). [Colour online.]

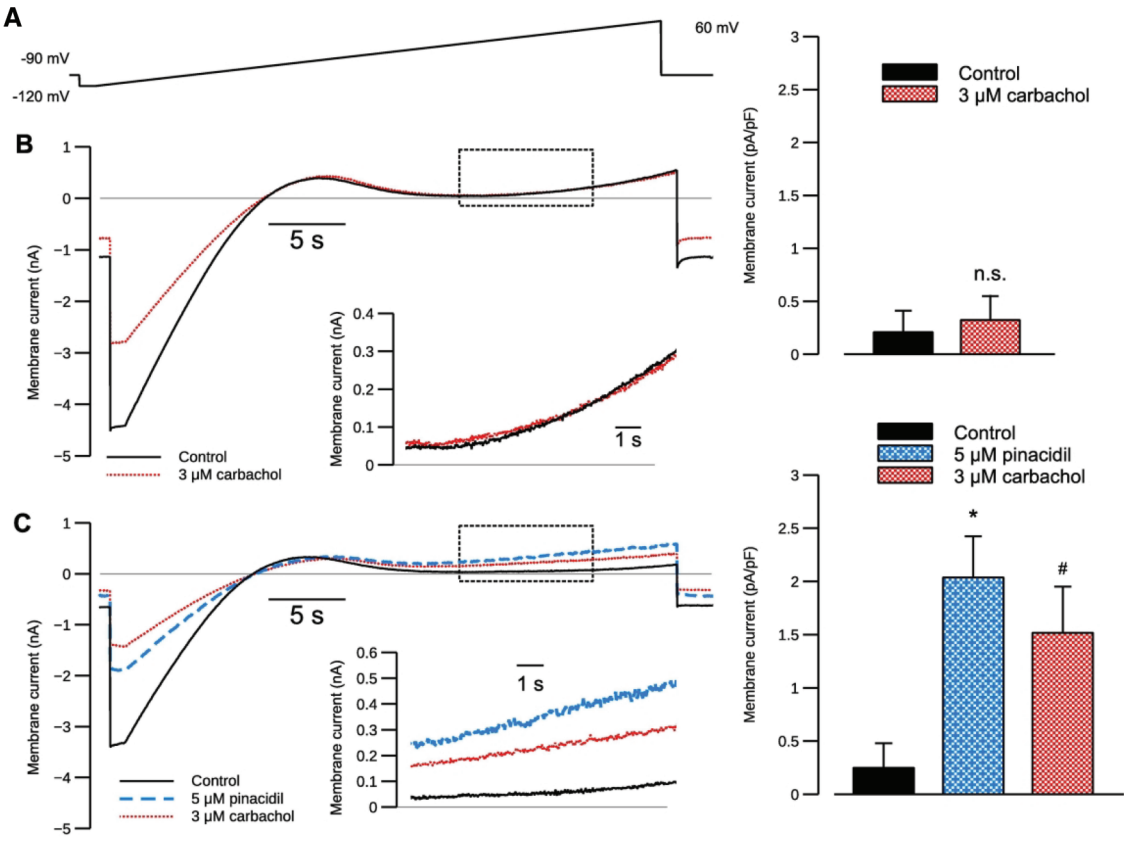

Fig. 4. Representative action potential trace (A) showing that hypoxic conditions caused significant action potential duration (APD) abbreviation and decreased mean diastolic potential and amplitude in canine ventricular preparations (blue dashed line), whereas acetylcholine (5 μmol/L) caused a significant prolongation in APD (red dotted line). Values of APD_{90} are represented as bars (B). Abbreviations under bars: C, control; H, hypoxia; A, acetylcholine. The pacing cycle length was 500 ms. Values are mean ± standard error; *, # denotes a significant difference at $p < 0.05$ by RM-ANOVA followed by Bonferroni's post-hoc test. [Colour online.]

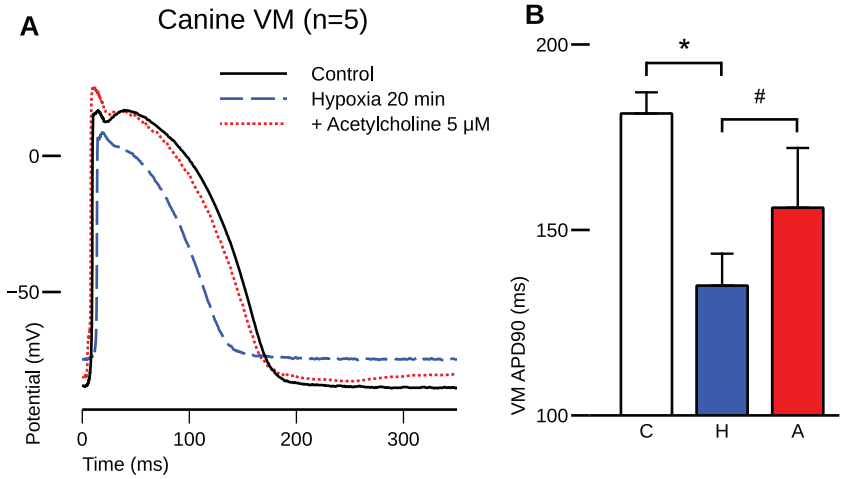

Fig. 5. Representative action potential showing the effect of acetylcholine (5 μmol/L, red dotted line) on a Purkinje fiber taken from a human donor heart (A). Values of APD_{90} are represented as bars (B). Abbreviations under bars: C, control; A, acetylcholine. The pacing cycle length was 500 ms. Values are mean ± standard error. [Colour online.]

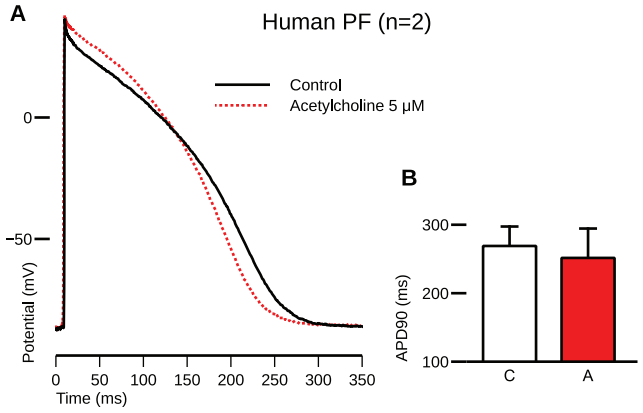

The $I_{K\text{-}ATP}$ ATP-sensitive potassium channels comprise heterooctamers consisting of four inward rectifying potassium channel pore-forming subunits (Kir6.1 or Kir6.2, encoded by *KCNJ8* and *KCNJ11* genes, respectively) and four ATP-binding cassette protein sulfonylurea receptors (SUR1 or SUR2, encoded by *ABCC8* and *ABCC9* genes, respectively; Inagaki et al. 1995). An important feature of the $I_{K\text{-}ATP}$ is its closed state under physiological intracellular ATP levels (i.e., under normoxia) and its activation by metabolic stress, when the ratio of ATP/ADP is decreased, e.g., during myocardial ischemia (Deutsch et al. 1991).

Activation of the sarcolemmal $I_{K\text{-}ATP}$ during myocardial ischemia shortens the action potential of various cardiac tissues to different extents, thus, it may promote APD dispersion and re-entry type arrhythmias (Janse and Wit 1989). Accordingly, several investigations found $I_{K\text{-}ATP}$ activation to be pro-arrhythmic (Chi et al. 1990), suggesting that sarcolemmal $I_{K\text{-}ATP}$ inhibition may prevent arrhythmias induced by myocardial ischemia and ischemia–reperfusion (Billman et al. 1998; Englert et al. 2003; Vajda et al. 2007).

In our experiments under normal conditions, we found no effect of carbachol on the membrane current (Fig. 3), and similarly, acetylcholine failed to influence the ventricular and Purkinje APDs (Figs. 1A and 1C). The observed discrepancy between our and previous results, in which an activation of $I_{K\text{-}ATP}$ was described upon acetylcholine administration (Terzic et al. 1994; Ito et al. 1994; Kim et al. 1997), could be the consequence of the species difference and the distinct experimental conditions.

In contrast, an important and, to the best of our knowledge, previously not published result of our study is that carbachol is able to suppress the pinacidil-activated $I_{K\text{-}ATP}$. As a consequence, in parallel tissue action potential experiments, acetylcholine lengthened the APD as long as it was previously shortened by the application of pinacidil, a $I_{K\text{-}ATP}$ activator. Since $I_{K\text{-}ATP}$ activation could be arrhythmogenic (Chi et al. 1990) by causing an increase in the APD dispersion, this effect of acetylcholine raises the possibility of a novel antiarrhythmic mechanism of the previously described antiarrhythmic effect of parasympathetic activation during hypoxia (Song et al. 1992; Zuanetti et al. 1987; Collins and Billman 1989).

Our experiments conducted under hypoxic conditions provided similar results (i.e., acetylcholine lengthened the hypoxia-induced shortened ventricular action potential; Fig. 4). Even though tissue hypoxia is a complex phenomenon (Carmeliet 1999), during which several factors change simultaneously (e.g., Ca^{2+}_i, Na^{+}_i, pH, conductance of gap junctions, membrane potential), it is feasible that $I_{K\text{-}ATP}$ activation, as a response to ATP depletion, is an important factor in the observed action potential shortening. Since acetylcholine lengthened the action potential under hypoxic conditions, we suggest $I_{K\text{-}ATP}$ inhibition as a possible underlying mechanism.

Acetylcholine decreased the pinacidil-induced ventricle–Purkinje APD dispersion

Free-running Purkinje fibers connect to the ventricular muscle on a small surface area, providing a relatively large-resistance coupling (Tranum-Jensen et al. 1991) and a large sink for current flow that favors conduction blocks more than other parts of the healthy myocardium. Also, due to the weaker electrotonic coupling, the dispersion of repolarization here can be greater than in other areas (Martinez et al. 2018), causing the Purkinje–ventricle APD ratio to have critical importance in arrhythmia generation. In our experiments, we found significantly greater shortening in Purkinje fibers caused by pinacidil, which could be the consequence of the generally weaker repolarization reserve that makes the Purkinje action potential more susceptible to any pharmacological interventions (Varró et al. 2000; Baláti et al. 1998). Similarly, acetylcholine exerted larger lengthening in the Purkinje fibers, probably by the same action that ultimately led to reduced ventricle–Purkinje APD dispersion. The reduction of the ventricle–Purkinje fiber APD dispersion could suppress the arrhythmogenic substrate, providing a narrower vulnerable period for a critically timed extrasystole to trigger a life-threatening arrhythmia under hypoxic conditions.

Proposed mechanism

Since inhibition of the K-ATP channels is possible by blocking various PKA-mediated pathways (Tinker et al. 2018), we suggest that the decrease of cAMP levels caused by the activation of cardiac muscarinic receptors using acetylcholine or carbachol was the factor that decreased the density of the $I_{K\text{-}ATP}$ current in patch-clamp measurements, leading to the subsequent prolongation observed in APDs.

Conclusions

We found that muscarinic agonists inhibit the $I_{K\text{-}ATP}$. Therefore, during $I_{K\text{-}ATP}$-mediated action potential shortening, acetylcholine causes asymmetrical action potential lengthening between ventricular muscle and Purkinje fiber that leads to reduced APD dispersion.

These results suggest that beyond suppressing the catecholaminergic-induced arrhythmogenic triggers (Song et al. 1992), the parasympathetic tone may also be able to reduce the arrhythmogenic substrate under hypoxic conditions.

There are some limitations to our study. (*i*) In our experiments, the ventricular and Purkinje fiber action potentials were measured from electrically uncoupled tissue samples. (*ii*) The presented effects were attributed to the M_2 muscarinic receptor; nevertheless, the exact level of contribution of other receptor subtypes was not addressed. To achieve this, further studies are needed, utilizing specific agonist and antagonist drugs.

Acknowledgements

We are grateful to Dr. Károly Acsai for his valuable contribution in performing statistical comparisons. This work was supported by grants from the National Research, Development and Innovation Office — NKFIH PD-116011 (for IK), FK-129117 (for NN), and the ÚNKP-18-4, ÚNKP-19-4 and ÚNKP-20-5-SZTE-165 New National Excellence Program of the Ministry for Innovation and Technology (for IK and NN), the János Bolyai Research Scholarship of the Hungarian Academy of Sciences (for NN) and EFOP-3.6.2-16-2017-00006 (LIVE LONGER) and EFOP 3.6.3-VEKOP-16-2017-00009

and Ministry of Human Capacities, Hungary grant 20391-3/2018/FEKUSTRAT, and the University of Szeged.

References

Baláti, B., Varró, A., and Papp, J.G. 1998. Comparison of the cellular electrophysiological characteristics of canine left ventricular epicardium, M cells, endocardium and Purkinje fibers. Acta Physiol. Scand. **164**(2): 181–190. doi:10.1046/j.1365-201X.1998.00416.x. PMID:9805105.

Billman, G.E., Englert, H.C., and Schölkens, B.A. 1998. HMR 1883, a novel cardioselective inhibitor of the ATP-sensitive potassium channel. Part II: Effects on susceptibility to ventricular fibrillation induced by myocardial ischemia in conscious dogs. J. Pharmacol. Exp. Ther. **286**(3): 1465–1473. PMID:9732412.

Carmeliet, E. 1999. Cardiac ionic currents and acute ischemia: from channels to arrhythmias. Physiol. Rev. **79**(3): 917–1017. doi:10.1152/physrev.1999.79.3.917. PMID:10390520.

Chi, L., Uprichard, A.C., and Lucchesi, B.R. 1990. Profibrillatory actions of pinacidil in a conscious canine model of sudden coronary death. J. Cardiovascular Pharmacol. **15**(3): 452–464. doi:10.1097/00005344-199003000-00016. PMID:1691370.

Collins, M.N., and Billman, G.E. 1989. Autonomic response to coronary occlusion in animals susceptible to ventricular fibrillation. Am. J. Physiol. **257**(6 Pt. 2): H1886–1894. doi:10.1152/ajpheart.1989.257.6.H1886. PMID:2603974.

Corey, S., and Clapham, D.E. 1998. Identification of native atrial G-protein-regulated inwardly rectifying K+ (GIRK4) channel homomultimers. J. Biol. Chem. **273**(42): 27499–27504. doi:10.1074/jbc.273.42.27499. PMID:9765280.

Deutsch, N., Klitzner, T.S., Lamp, S.T., and Weiss, J.N. 1991. Activation of cardiac ATP-sensitive K+ current during hypoxia: correlation with tissue ATP levels. Am. J. Physiol. **261**(3 Pt. 2): H671–676. doi:10.1152/ajpheart.1991.261.3.H671. PMID:1909501.

Englert, H.C., Heitsch, H., Gerlach, U., and Knieps, S. 2003. Blockers of the ATP-sensitive potassium channel SUR2A/Kir6.2: a new approach to prevent sudden cardiac death. Curr. Med. Chem. Cardiovasc. Hematol. Agents. **1**(3): 253–271. doi:10.2174/1568016033477423. PMID:15326916.

Harvey, R.D., and Belevych, A.E. 2003. Muscarinic regulation of cardiac ion channels. Br. J. Pharmacol. **139**(6): 1074–1084. doi:10.1038/sj.bjp.0705338. PMID:12871825.

Higgins, C.B., Vatner, S.F., and Braunwald, E. 1973. Parasympathetic control of the heart. Pharmacol. Rev. **25**(1): 119–155. PMID:4348231.

Inagaki, N., Gonoi, T., Clement, J.P., Namba, N., Inazawa, J., Gonzalez, G., et al. 1995. Reconstitution of IKATP: An inward rectifier subunit plus the sulfonylurea receptor. Science, **270**(5239): 1166–1170. doi:10.1126/science.270.5239.1166. PMID:7502040.

Ito, H., Vereecke, J., and Carmeliet, E. 1994. Mode of regulation by G protein of the ATP-sensitive K+ channel in guinea-pig ventricular cell membrane. J. Physiol. **478**(Pt. 1): 101–107. doi:10.1113/jphysiol.1994.sp020233. PMID:7965825.

Janse, M.J., and Wit, A.L. 1989. Electrophysiological mechanisms of ventricular arrhythmias resulting from myocardial ischemia and infarction. Physiol. Rev. **69**(4): 1049–1169. doi:10.1152/physrev.1989.69.4.1049. PMID:2678165.

Kim, D., Watson, M., and Indyk, V. 1997. ATP-dependent regulation of a G protein-coupled K+ channel (GIRK1/GIRK4) expressed in oocytes. Am. J. Physiol. **272**(1 Pt. 2): H195–206. doi:10.1152/ajpheart.1997.272.1.H195. PMID:9038938.

Koumi, S., Wasserstrom, J.A., and Ten Eick, R.E. 1995. Beta-adrenergic and cholinergic modulation of the inwardly rectifying K+ current in guinea-pig ventricular myocytes. J. Physiol. **486** (Pt. 3): 647–659. doi:10.1113/jphysiol.1995.sp020841. PMID:7473226.

Kurachi, Y. 1995. G protein regulation of cardiac muscarinic potassium channel. Am. J. Physiol. **269**(4 Pt. 1): C821–C830. doi:10.1152/ajpcell.1995.269.4.C821. PMID:7485449.

Martinez, M.E., Walton, R.D., Bayer, J.D., Haïssaguerre, M., Vigmond, E.J., Hocini, M., and Bernus, O. 2018. Role of the Purkinje-muscle junction on the ventricular repolarization heterogeneity in the healthy and ischemic ovine ventricular myocardium. Front. Physiol. **9**: 718. doi:10.3389/fpls.2018.00718. PMID:29962961.

Nakayama, K., Suzuki, Y., and Hashimoto, K. 1968. Sustained atrial fibrillation by acetylcholine infusion into the sinus node artery. Tohoku J. Exp. Med. **96**(4): 333–339. doi:10.1620/tjem.96.333. PMID:5720457.

Navarro-Polanco, R.A., Aréchiga-Figueroa, I.A., Salazar-Fajardo, P.D., Benavides-Haro, D.E., Rodríguez-Elías, J.C., Sachse, F.B., et al. 2013. Voltage sensitivity of M_2 muscarinic receptors underlies the delayed rectifier-like activation of ACh-gated K(+) current by choline in feline atrial myocytes. J. Physiol. **591**(17): 4273–4286. doi:10.1113/jphysiol.2013.255166. PMID:23652593.

Nobles, M., Montaigne, D., Sebastian, S., Birnbaumer, L., and Tinker, A. 2018. Differential effects of inhibitory G protein isoforms on G protein-gated inwardly rectifying K+ currents in adult murine atria. Am. J. Physiol. Cell Physiol. **314**(5): C616–C626. doi:10.1152/ajpcell.00271.2016.

Pappano, A.J., and Carmeliet, E.E. 1979. Epinephrine and the pacemaking mechanism at plateau potentials in sheep cardiac Purkinje fibers. Pflugers Arch. **382**(1): 17–26. doi:10.1007/BF00585899. PMID:574937.

Recordati, G., Schwartz, P.J., Pagani, M., Malliani, A., and Brown, A.M. 1971. Activation of cardiac vagal receptors during myocardial ischemia. Experientia, **27**(12): 1423–1424. doi:10.1007/BF02154267. PMID:5144849.

Song, Y., Thedford, S., Lerman, B.B., and Belardinelli, L. 1992. Adenosine-sensitive afterdepolarizations and triggered activity in guinea pig ventricular myocytes. Circ. Res. **70**(4): 743–753. doi:10.1161/01.RES.70.4.743. PMID:1551200.

Terzic, A., Tung, R.T., Inanobe, A., Katada, T., and Kurachi, Y. 1994. G proteins activate ATP-sensitive K+ channels by antagonizing ATP-dependent gating. Neuron, **12**(4): 885–893. doi:10.1016/0896-6273(94)90340-9. PMID:8161458.

Tinker, A., Aziz, Q., Li, Y., and Specterman, M. 2018. ATP-sensitive potassium channels and their physiological and pathophysiological roles. Compr. Physiol. **8**(4): 1463–1511. doi:10.1002/cphy.c170048. PMID:30215858.

Tranum-Jensen, J., Wilde, A.A., Vermeulen, J.T., and Janse, M.J. 1991. Morphology of electrophysiologically identified junctions between Purkinje fibers and ventricular muscle in rabbit and pig hearts. Circ. Res. **69**(2): 429–437. doi:10.1161/01.RES.69.2.429. PMID:1860183.

Vajda, S., Baczkó, I., and Leprán, I. 2007. Selective cardiac plasma-membrane K(ATP) channel inhibition is defibrillatory and improves survival during acute myocardial ischemia and reperfusion. Eur. J. Pharmacol. **577**(1–3): 115–123. doi:10.1016/j.ejphar.2007.08.016. PMID:17904545.

Varró, A., and Baczkó, I. 2010. Possible mechanisms of sudden cardiac death in top athletes: a basic cardiac electrophysiological point of view. Pflugers Arch. **460**(1): 31–40. doi:10.1007/s00424-010-0798-0. PMID:20186549.

Varró, A., Baláti, B., Iost, N., Takács, J., Virág, L., Lathrop, D.A., et al. 2000. The role of the delayed rectifier component IKs in dog ventricular muscle and Purkinje fibre repolarization. J. Physiol. **523**(Pt 1): 67–81. doi:10.1111/j.1469-7793.2000.00067.x. PMID:10675203.

Weiss, J.N., and Venkatesh, N. 1993. Metabolic regulation of cardiac ATP-sensitive K+ channels. Cardiovasc. Drugs Ther. **7**(Suppl. 3): 499–505. doi:10.1007/BF00877614. PMID:8251419.

Zuanetti, G., De Ferrari, G.M., Priori, S.G., and Schwartz, P.J. 1987. Protective effect of vagal stimulation on reperfusion arrhythmias in cats. Circ. Res. **61**(3): 429–435. doi:10.1161/01.RES.61.3.429. PMID:3621502.